[redacted]

TU Delft

Delft University of Technology

Faculty of Civil Engineering
Department Hydraulic Engineering

Laboratory observations of the velocity field in the entrance of a tidal harbor and the exchange of heat between harbor and river.

E.J. Langendoen

report no. 5-90

This research is supported by the Netherlands Technology Foundation (STW)

1990

Hydromechanics Section
Hydraulic and Geotechnical Engineering Division
Department of Civil Engineering
Delft University of Technology
Delft, The Netherlands

Contents

1. Introduction

Many harbors in the world suffer from siltation of their basins and in many cases removal of the deposited sediment leads to high costs. This siltation results from a net transport of sediment to the harbor caused by the water motion in the harbor entrance. The water motion is very complex and of a three-dimensional nature. Three main mechanisms of exchange of water through the harbor entrance can be distinguished: (1) exchange in consequence of a velocity difference between the flow along the mouth of the harbor and the resulting gyres in the harbor entrance, (2) a net transport caused by withdrawal and discharge of water, from and to the harbor basin respectively, or by variations in the water level of the adjacent water body (e.g. sea, estuary or river), and (3) exchange in consequence of a density difference (generally related to differences in salinity) between water in the harbor and the adjacent water body.

Mechanisms (1) and (2) have been examined in a physical model in the Laboratory of Fluid Mechanics of the Department of Civil Engineering of the Delft University of Technology. The influence of mechanism (3) on the exchange between harbor and adjacent water body has been examined, simultaneously with mechanisms (1) and (2), in the Tidal Flume of Delft Hydraulics. The adjacent water body was a tidal river in both studies. The research at the Delft University of Technology is discussed in this report. The reader is referred to [5] regarding the research at Delft Hydraulics.

The main goal of the research was to generate a data set by which the three-dimensional numerical model "Trisula" ([2]) can be tested for flows in harbor entrances. This model then can be used to design harbor entrances so as to minimize the cost of maintenance dredging. Furthermore, our insight into the interactions between the mechanisms was to be enlarged.

The experimental procedure is described in section 2. Measurements of depth averaged flow patterns are discussed in section 3, and the variation over the water column of the velocity field is considered in section 4. The exchange of heat between harbor and river is discussed in section 5. Finally some conclusions follow in section 6.

2. Experimental Procedure

2.1 Introduction

The exchange of matter (e.g. sediment, constituents or water) between a harbor and a fresh water tidal river is governed by the first two flow mechanisms mentioned in the introduction: (1) gyres in the harbor entrance driven by the flow in the river, and (2) a net flow caused by water level variations in the river. The exchange of water then is a function of the geometry of the harbor entrance and the dimensionless parameters $\hat{u}T/B$, B/L, h/B and $\hat{h}/h$, see for example [7]. Here $\hat{u}$ is the amplitude of the tidal current velocity, T the tidal period, B the width of the harbor, L the length of the harbor, h the water depth and $\hat{h}$ the amplitude of the variation in time of the tide level. See Fig. 2.1 for a definition sketch. The geometry of the harbor entrance can be expressed by the dimensionless parameter B_e/B and the angle α at which the harbor entrance is oriented with respect to the river axis. Here B_e is the entrance width. The influence of these parameters on the exchange of water between harbor and river and the flow pattern in the entrance has been studied in a physical model. Other aspects of the entrance geometry can also be significant, such as the steepness of the sidewalls of the entrance and the position of a narrowed entrance relative to the harbor basin, but these aspects have not been dealt with in this study.

The model consists of a basin, area 4×2 m^2, in which harbor entrances of various geometries can be built, and an adjacent straight flume, length 18 m and width 1 m, representing a river in which a uniform time-varying (tidal) current is generated, see Fig. 2.2. The bottom of the model is horizontal and the sidewalls are vertical. The flow in the flume is generated by a constant water supply and an adjustable sharp-crested weir at each end of the flume. Five geometries of the harbor have been considered, see Fig. 2.3. Table 1 lists the experiments made and the values of the dimensionless parameters for the five model harbors. The mean water depth was 0.11 m in all experiments.

As can be noticed in Table 1, eight experiments were made without tide level changes and one experiment was made with tide level changes. Two different procedures were used to generate a tidal flow with and without water level changes. In the experiments without water level changes the weirs followed the same program with a phase difference of half a tidal period to produce a sinusoidal tidal current. To generate both a sinusoidal tidal current and a sinusoidal variation in the tide level only one weir moved, while the other was fixed. Consequently, a difference in the amplitudes of the tidal current velocity existed in both experiments.

If the model harbors are supposed to represent a harbor of width 200 m and depth 20 m, which is the

Table 1 Values of the dimensionless parameters for the five model harbors

	exp. no.	$\frac{\hat{u}T}{B}\cdot\frac{B_e}{B}$	$\frac{B}{L}$	$\frac{h}{B}$	$\frac{\hat{h}}{h}$	$\frac{B_e}{B}$	α
Harbor 1	1A	95	1	0.11	0	1	90
	1B	190					
	1C	380					
Harbor 2	2A	95	0.5	0.11	0	1	90
	2B	190					
	2C	380					
Harbor 3	3	95	1	0.11	0	0.5	90
Harbor 4	4	190	1	0.11	0	1	45
Harbor 5	5	140 high tide 115 low tide	0.5	0.11	0.18	1	90

size of a typical basin in the Rotterdam harbor area, the length and depth scales are of the order 200. Using conventional Froude law scaling to obtain the velocity scale would yield a maximum Reynolds number in the model harbors of 2750, assuming a maximum water velocity in the field of 1 m/s. To maintain a turbulent flow in the model harbors the Froude number criterion was dropped, moreover free surface deformations are not important here. Scaling according to the Reynolds number criterion would yield a maximum Froude number in the flume of 170. As a compromise a velocity scale of 2.5 was chosen. The related maximum Reynolds number in the model harbors was about 15000 and the maximum Froude number in the flume 0.36. This requirement was met, for the experiments without tidal water level variations, by supplying a constant flow rate of 65 ℓ/s at each end of the flume, and varying the discharge over the weirs between ca. 24 ℓ/s and 106 ℓ/s. As a result, the amplitude of the flow rate in the flume was 41 ℓ/s ($\hat{u}$ = 0.37 m/s).

A characteristic time scale of the tide, t_t, is its tidal period T. The time scale of the flow in the harbor entrance (the development of a gyre), t_g, is proportional to $L_g B/\hat{u}B_e$, with L_g the length of the primary gyre. This time scale is based on experiments in steady flow by Booij [1]. It can be assumed that the length of the gyre is proportional to the width of the harbor, if the ratio of the width and the length of the harbor is not much larger than 1 and the ratio of the water depth and the entrance width is not much smaller than 0.01

or 0.02. The ratio t_t/t_g - $\hat{u}TB_e/B^2$ which then results, should be equal in the field and the experimental model. For a diurnal tide the model period would become 590 s. To speed up the experiments a little, a period of 500 s was selected. The influence of the period has been examined in model harbors (1) and (2) where also periods of 250 s and 1000 s have been studied.

In experiment (5) the discharge in the flume varied from 36 ℓ/s ($\hat{u}$ = 0.28 m/s) at high tide to 21 ℓ/s ($\hat{u}$ = 0.23 m/s) at low tide. Figure 2.4 shows the discharges and the water level elevations in the river in front of the harbor for both the experiments with and without tide level changes.

2.2 Instrumentation and measuring-programme

Depth averaged velocities, distributions in the water column of time-mean velocities and the exchange of heat between harbor and river were measured to determine the influence of the various parameters, listed in Table 1, on the flow pattern in the harbor entrance and the exchange of water between harbor and river.

The depth averaged velocities were determined using cylindrical floats (diameter 1.0 cm) that drew about 10.5 cm. The movements of the floats were recorded on video. Images were digitized on a micro-computer each 0.25 s, and the positions of the floats were determined. Velocities were obtained by time-differencing. The accuracy is approximately 1.0 cm/s.

The time-mean velocity distributions in the water column were determined by means of an electromagnetic flow meter (EFM). The EFM employs Faraday's Induction Law for measurement of the velocity of a conductive fluid moving through a magnetic field. This field is generated by a pulsed current through a small coil inside the body of the sensor. Two pairs of diametrically opposed platinum electrodes sense the voltages produced by the flow past the sensor. The sensor has been designed in such a way that these voltages are proportional to the magnitude of the two horizontal velocity components parallel to the planes of the electrodes. The sensor, an ellipsoid (height 11 mm and diameter 33 mm), is connected to a rod (diameter 10 mm) with a maximum immersion length of 85 cm. The size of the measuring-volume is of the order of the size of the probe. The measuring-range is from 0 to 1.0 m/s. The accuracy is 1% of full scale.

The exchange of mass between harbor and river is caused by advection due to the mean flow and turbulence. To examine the combined effect of advection and turbulent diffusion, the water in the harbor was heated by approximately 2 degrees centigrade by mixing it with hot water when the current in the river was near maximum. This water was sprayed into the water inside the harbor so as to obtain a horizontally and vertically uniform temperature distribution while disturbing the flow as little as possible. The hot water was dyed so that the degree of mixing could be observed by eye. Subsequent time histories of temperature were measured using thermistors. The response time of the thermistors is 0.8 s and the accuracy 0.15 degree centigrade.

In experiments 1A, 1C, 2A and 2C only depth averaged velocities were determined. In experiment 1B depth averaged velocities as well as velocity distributions in the water column and the exchange of heat between harbor and river were determined. The measurements with the EFM were made at the locations shown in Fig. 2.5.a at 1.5, 4, 6 and 8 cm above the bottom. The velocities were determined for a complete tidal cycle. The locations of the temperature measurements are shown in Fig. 2.5.b. Temperatures were obtained at 2, 5 and 9 cm above the bottom.

In experiment 2B the velocity distributions in the water column were determined only at maximum current in the river by fixing both weirs so that a steady flow was generated in the river. This is acceptable because, as will be discussed in sections three and four, the flow in the harbor is quasi-steady during maximum current in the river. Velocities were measured at the locations shown in Fig. 2.6.a at 2, 3, 4, 5, 6, 7, 8 and 9 cm above the bottom. Furthermore, depth averaged velocities and the exchange of heat between harbor and river were determined. The locations of the temperature measurements (at 3 and 8 cm above the bottom) are shown in Fig. 2.6.b.

In experiments 3 and 4 measurements were made similar to those in experiment 2. The locations of the measurements with the EFM and the temperature measurements are shown in Fig. 2.7 (experiment 3) and Fig. 2.8 (experiment 4) respectively.

In experiment 5 only the velocity distributions in the water column were determined for an entire tidal cycle. The locations of the measurements (at 2, 4 and 6 cm above the bottom) are shown in Fig. 2.9.

The measurements with the EFM in model harbors (1) and (5) were done for two cycles. A sample frequency of 1 Hz was used. The instantaneous velocities were phase-averaged first, after which a triangular filter with a width of 20 s was used to smooth the signal. A sample duration of 300 s and a sample frequency of 1 Hz were used for the measurements with the EFM in model harbors (2), (3) and (4). The instantaneous velocities were integrated in time to obtain the time-mean velocities.

Because the measuring technique used to measure time histories of temperature comprises some uncertainties the experiments were repeated three or four times.

3. Depth averaged flow patterns

3.1 Introduction

In this section only the depth averaged flow patterns in model harbors (2), (3) and (4) are discussed. The variation of the depth averaged flow pattern in model harbor (1) during a tidal cycle was discussed in [4].

Briefly, it was concluded that the phenomena which occurred in the harbor entrance around and after slack water may be important for the exchange of matter between harbor and river. Large lumps of water from the river were exchanged with water from the harbor. This convective exchange was much larger than the exchange around maximum current in the river, when there is only a turbulent transport through the mixing layer at the transition between harbor and river. The progress of the phenomena after slack water (for example the development of a new gyre) depended on the parameter $\hat{u}TB_e/B^2$, when observing the flow patterns in the harbor at equal phases, t/T where t = time, of the tide. Decreasing this parameter caused an increase of the phase difference between the development of the gyre and the accelerating flow in the river.

The depth averaged flow patterns in model harbors (2), (3) and (4) bear resemblance to those in model harbor (1). However, the influence of the geometries of the harbor and the entrance can be observed in the flow patterns, as is shown in sections 3.2 to 3.4.

3.2 Depth averaged flow patterns in model harbor (2)

The influence of the parameter $\hat{u}TB_e/B^2$ on the flow pattern in the entrance was studied as in the experiments in model harbor (1) by varying the magnitude of the period. In model harbor (1) a period larger than 250 s was necessary to obtain a quasi-steady flow in the harbor at maximum current in the river. It can be expected that a period of 250 s will certainly be too small to obtain a quasi-steady flow in model harbor (2), because the time, t_g, the flow pattern in the harbor needs to adapt to the flow in the river is proportional to the length of the primary gyre in the harbor (page 3).

Observed flow patterns for a period of 500 s are shown in Figures 3.1 to 3.4 at various times. A second, counter rotating gyre exists at the back of the harbor around maximum current (Fig. 3.1.a). This gyre spans the width of the harbor, and its breadth gradually increases from about 0.25 m at maximum current to 0.5 m during slack water. The flow near the entrance at slack water, see Fig. 3.2.a, resembles that in harbor (1). The primary gyre moves to the river, but not to the same extent as in model harbor (1). The old primary gyre is broken into two parts, one part is transported with the flow in the river and the other is pushed to the back of the harbor by the developing new gyre. At this moment three gyres are present in the harbor, see Fig. 3.3.a. The old primary gyre decays (Fig. 3.3.b). However, the flow pattern that arises cannot endure because the new gyre and the old secondary gyre have a coinciding direction of rotation. The old secondary gyre then is assimilated by the new gyre, see Fig. 3.4.a. As a result, the length to width ratio of the gyre is approximately two, which, according to a previous study of Booij [1] is impossible in steady flow. Booij stated that if the length to width ratio of the gyre is higher than 1.7 a secondary gyre will arise. Here the new secondary gyre comes into existence just at the next maximum current in the river, see Fig. 3.4.b.

The observed depth averaged flow patterns for a period of 250 s are shown in Figures 3.5 to 3.7. The flow patterns just before and at slack water, Figs. 3.5.a and b, agree quite well with those for a period of 500 s. However, the water velocities in the gyre are somewhat larger than those for a period of 500 s. The gyre has less time to adapt itself to the decelerating flow in the river for a smaller period.

The flow patterns after slack water differ from those at the same phase with a period of 500 s. Compare for this purpose Fig. 3.6.a with Fig. 3.3.a, both for t/T = 0.6. The phase difference between the flow in the river and the developing new gyre is larger for a period of 250 s. However, the development of the new gyre is approximately equally fast. This is shown in Figures 3.6.b (T = 250 s) and 3.3.a (T = 500 s), both for t/t_g = 18.5 with t the time after slack water.

Figures 3.7.a and b show that at maximum current the counter rotating secondary gyre has not come into existence yet. Thus, a quasi-steady flow is not obtained for a period of 250 s in model harbor (2).

The observed depth averaged flow patterns in experiment 2C (T = 1000 s) are shown in Figures 3.8 to 3.10. The flow pattern around slack water, Fig. 3.8.a, is similar to that for a period of 500 s. However, the water velocities in the gyre are somewhat smaller. It can be observed that the old primary gyre has vanished at t/T = 0.62 for a period of 1000 s, see Fig. 3.9.b. For the period of 500 s the primary gyre vanished approximately at t/T = 0.7.

The phase difference between the flow in the river and the developing new gyre is smaller for a period of 1000 s than for a period of 500 s. However, the development of the gyre is equally fast. Compare for this purpose the flow patterns when t/t_g = 29.6, with t the time after slack water, Fig. 3.3.b for a period of 500 s and Fig. 3.9.a for a period of 1000 s.

The secondary gyre comes into existence before maximum current, see Fig. 3.10.b.

From these measurements it can be concluded that a period of at least 500 s is needed to obtain a quasi-steady flow in model harbor (2) at maximum current in the river. The rate of the development of the new primary gyre seems to be independent of the tidal period.

3.3 Depth averaged flow patterns in model harbor (3)

The observed depth averaged flow patterns in model harbor (3) are shown in Figures 3.11 to 3.14. In harbor (3) a single gyre, see Fig. 3.11.a, as observed in model harbor (1) exists around maximum current. However, the water velocities are less by approximately 40 per cent. At slack water the gyre remains completely within the harbor, see Fig. 3.12.a. As a result, the exchange of water between harbor and river will be smaller at slack water than in model harbors (1) and (2).

The new gyre initially grows mainly in a direction parallel to the river, see Fig. 3.12.b, and the old gyre is more long-lived than that in harbor (1) (experiment 1B), see Figures 3.13.a and b. This is partly due to the small exchange at slack water through which the gyre can persist almost unchanged and partly due to a smaller entrance width.

In experiment 1B quasi-steady flow in the harbor was obtained at $t/T \approx 0.7$, while in harbor (3) this occurs at $t/T \approx 0.75$, just around maximum current. In model harbor (1) a period slightly higher than 250 s was sufficient to obtain a quasi-steady flow in the harbor at maximum current, while in model harbor (3) with half the entrance width the period must be at least 500 s to obtain a quasi-steady flow in the harbor at maximum current. This was to be expected because the time the harbor flow needs to adapt to the flow in the river is inversely proportional to the entrance width (page 3).

3.4 Depth averaged flow patterns in model harbor (4)

The observed depth averaged flow patterns in model harbor (4) are shown in Figures 3.15 to 3.20. When the flow in the river is from left to right at maximum current, a large gyre, almost occupying the entire harbor area, and a small gyre in the right bottom corner of the harbor are present in the harbor, see Fig. 3.15.a. The water velocities in the gyre are as large as the water velocities in the gyre in experiment 1B at maximum current.

During slack water the same phenomena are observed as in the previous experiments. The gyre moves into the river and is broken into two parts, one part that is advected with the flow in the river and the other part that is pushed to the back of the harbor, see Figures 3.15.b and 3.16.a. Furthermore, it is observed that the gyre in the right bottom corner of the harbor increases in size. After slack water three gyres are present in the harbor. In contrast with the previous experiments the old gyre does not decay, see Figures 3.16.a to 3.18.a. Only the sizes of the gyres are changing. For example, the gyre in the right bottom corner of the harbor becomes very small. The water velocities in the primary gyre are approximately 50 per cent of those at the previous maximum current.

The differences in the sizes of the gyres and the water velocities in the gyres are probably caused by the geometry of the downstream sidewall of the entrance. The angle between the downstream wall of the entrance and the river has a marked influence on the velocities in the gyre and the size of the gyre. A small angle was found to imply large velocities in the gyre and a large size of the gyre. Booij [1] found a decrease in the velocities of 40 per cent for an angle of 135 degrees with respect to those for an angle of 90 degrees.

At the next slack water the primary gyre moves into the river again and after slack water a new large gyre comes into existence. The old primary gyre decays quite fast compared to experiments 1B and 2C. It has vanished approximately at $t/T = 0.1$, see Fig. 3.19.a, compared to $t/T \approx 0.12$ for experiments 1B and 2C.

4. Velocity distribution in the water column

4.1 Introduction

In section three it was observed that the flow patterns in the harbor consisted of one or more gyres. The flow in the gyre is highly curved, as a consequence of which a secondary flow exists in the gyre. This secondary flow was already observed by Rohr in 1934 [6]. The secondary current consists of the velocity component normal to the direction of the depth averaged velocity. The secondary current results in a flow direction towards the center of the gyre near the bottom, and a flow direction opposite near the free surface. The secondary current is important for the sediment transport in the harbor. Small sediment particles will spiral towards the center of the gyre and deposit because of the small water velocities.

The secondary current can also be important for the development of secondary gyres in the harbor. This can possibly account for the fact that depth averaged numerical models can hardly predict secondary gyres.

To examine the depth dependence of the velocity field measurements were made in all model harbors.

4.2 Model harbor (1)

Figure 4.1 shows the flow patterns at four levels for experiment 1B at t = 375 s (maximum current). Two notable processes can be observed. Firstly, a secondary current with the velocities directed towards the center of the gyre at 1.5 cm above the bottom, and a flow in opposite direction near the free surface occurs. The angle between the flow direction near the bottom and the flow direction near the surface is about 20 degrees. The ratio of the maximum velocities of the secondary current and the main flow, v_s/U, varies between 0.14 and 0.18 at 0.10 m from the harbor sidewalls.

Secondly, the near-bottom velocities close to the downstream sidewall normal to the river are clearly larger (approximately 50 per cent) than those higher in the water column. This phenomenon commences when the new gyre has moved towards the downstream sidewall of the harbor, and it proceeds almost until the next slack water, see Figures 4.2 to 4.5. The velocity near the bottom at the measurement location closest to the stagnation point is very small compared to the water velocities higher in the water column. Moreover, until maximum current, the flow at this measurement location is, near the bottom, towards the river. It seems that this outflow of fluid near the bottom is replaced by high-momentum fluid from the mixing layer between harbor and river. Figure 4.6 shows the velocity distribution in the water column at t = 375 s at a location 0.1 m from the downstream harbor sidewall and 0.4 m into the harbor.

The same phenomenon was observed in the experiments made at Delft Hydraulics [5], both with stratified flow and unstratified flow in the river. Especially in the experiments with stratified flow, where the salt could be used also as tracer, it was observed that, near the stagnation point, fresh water entering the harbor from the river was flowing towards the bottom.

Figure 4.7 shows some time histories of depth averaged velocities at four verticals in the harbor and one vertical in the river. It can be observed that around maximum current the water velocities in the gyre remain fairly constant. A quasi-steady flow is established in the harbor. The energy supplied by the main flow to the flow in the gyre is balanced by the friction at the bottom and at the sidewalls of the harbor. The velocity difference between the flow in the river and the flow in the harbor decreases after maximum current. This will influence the turbulent exchange of mass between harbor and river (see section 5).

4.3 Model harbors (2), (3) and (4)

In model harbors (2), (3) and (4) velocity distributions in the water column were measured only at maximum current in the river, see Figures 4.8 to 4.11. To this end a steady flow was generated in the river as is discussed in section 2.2.

Figure 4.8 shows that in model harbor (2) the same processes occur as in model harbor (1). The velocity distribution at vertical 1 shows the presence of a secondary current and larger water velocities near the bottom than higher in the water column. The ratio of the maximum velocities of the secondary current and the main flow is approximately 0.23. The water velocities near the bottom, at vertical 1, are about 50 per cent larger than those higher in the water column.

The velocity distribution at vertical 2 has been measured to detect whether the secondary gyre is possibly driven by the secondary current. However, despite the steady flow in the river, the flow in the mixing layer between the primary and secondary gyre is unsteady. The sizes of the primary and secondary gyres are constantly changing. Consequently, the shear layer moves a little up and down. Because the velocity distribution at vertical 2 is measured only once, it is difficult to identify whether vertical 2 is situated at the center line (time-averaged) of the mixing layer. As a result, rather inaccurate results are obtained at vertical 2 and to a less extent also at verticals 3 and 4. A secondary current cannot be observed at these verticals.

The ratio between the maximum water velocities in the primary gyre and the secondary gyre is about 0.3, which is equal to the ratio between the velocity in the river and that in the primary gyre [1, 3].

In model harbor (3), analogous to model harbors (1) and (2), the water velocities near the bottom close to the stagnation point are larger, about 35 per cent, than those higher in the water column (see Fig. 4.9). The secondary current is weak and can be observed only at verticals 3 and 4 ($v_s/U \approx 0.05$).

Larger water velocities near the bottom close to the stagnation point are observed in model harbor (4) as well, both when the flow in the river is from left to right (t = 125 s, Fig. 4.10) and when the flow in the river is from right to left (t = 375 s, Fig. 4.11). At t = 125 s the velocities near the bottom are approximately 20 per cent larger, and at t = 375 s approximately 50 per cent larger than those higher in the water column.

At t = 125 s the ratio v_s/U is 0.07 at vertical 2 and 0.22 at vertical 3. At t = 375 s the ratio v_s/U is 0.22 at vertical 1 and 0.09 at vertical 2.

4.4 Model harbor (5)

The results obtained from the measurements in model harbor (5) bear resemblance to the results obtained at Delft Hydraulics [5]. The results show a clear difference between the flow patterns at high and low tides. At high tide (t = 125 s, Fig. 4.12) the flow pattern in the entrance is similar to that in experiment 2B. A large primary gyre is present in the harbor entrance, as is to be expected. The two processes observed at maximum current in the previous experiments are notable too. Near the bottom the flow in the gyre is directed towards the center of the gyre and half-way down the water column (6 cm above the bottom) the flow in the gyre is directed away from the center of the gyre. At the downstream sidewall of the harbor entrance the water velocity near the bottom is larger than higher in the water column.

At low tide (t = 375 s, Fig. 4.13) the flow pattern in the entrance is rather indeterminate and the velocities are low. Although the influence of filling or emptying of the basin at low tide is negligible, a gyre in the entrance cannot be observed. In the research at Delft Hydraulics a gyre did exist in the entrance at low tide. However, the shape of the gyre was somewhat irregular. This was probably due to the emptying of the harbor basin preceding low tide which hindered the development of the gyre.

At slack water after high tide (t = 250 s, see Fig. 4.14), when the net flow through the entrance due to the emptying of the basin is at its maximum, it can be observed that the gyre moves into the river.

At slack water after low tide (t = 500 s, see Fig. 4.15), when the net flow through the entrance due to the filling of the basin is at its maximum, the gyre remains in the harbor. The filling of the basin prevents the gyre from moving into the river.

Figures 4.16 to 4.18 show that the development of the new gyre after ebb slack tide is faster in experiment 5 than in experiment 2B. Thus, the result of the filling of the basin is an acceleration of the evolution of the new gyre. Booij [1] found that withdrawal of water at the back of the harbor, which is comparable to a filling of the basin due to a rise of the tide, results in larger velocities in the gyre and a slightly faster development of the gyre. Discharge of water at the back of the harbor, comparable to an emptying of the basin, results in smaller velocities in the gyre and a slower development of the gyre.

The new gyre after flood slack tide starts to develop at the back of the harbor entrance only at t = 425 s, see Figure 4.19. From t = 450 s to t = 500 s the water velocities in the gyre and the shape of the gyre hardly change.

5. Exchange of heat between harbor and river

5.1 Introduction

Heated water is used as a tracer to examine the exchange of mass between harbor and river. As will be derived below the heat transport through the entrance of the harbor can be determined from the progress in time of the mean temperature of the harbor water.

The balance equation for internal energy is given by

$$\rho \frac{\partial}{\partial t} E_{int} + \rho u_i \frac{\partial}{\partial x_i} E_{int} = \frac{\partial}{\partial x_i}\left(\kappa \frac{\partial \theta}{\partial x_i}\right) - p \frac{\partial u_i}{\partial x_i} + \mu \left[\frac{\partial u_j}{\partial x_i}\left(\frac{\partial u_j}{\partial x_i} + \frac{\partial u_i}{\partial x_j}\right) - \frac{2}{3}\left(\frac{\partial u_i}{\partial x_i}\right)^2\right] \tag{5.1}$$

which equation is nothing else but the first law of thermodynamics. Here ρ is the mass density, E_{int} the internal energy per unit mass, u_i the velocity component in x_i direction, κ the heat conductivity, θ the temperature, p the pressure and μ the dynamic viscosity. For an incompressible fluid and $E_{int} = c\theta$, where c is the specific heat, the heat balance reduces to

$$\rho \frac{\partial}{\partial t}(c\theta) + \rho u_i \frac{\partial}{\partial x_i}(c\theta) = \frac{\partial}{\partial x_i}\left(\kappa \frac{\partial \theta}{\partial x_i}\right) + \mu \frac{\partial u_j}{\partial x_i}\left(\frac{\partial u_j}{\partial x_i} + \frac{\partial u_i}{\partial x_j}\right) \tag{5.2}$$

Assuming a constant specific heat in space and time, and neglecting the effects of molecular conduction and dissipation the heat balance becomes

$$\rho c \frac{\partial \theta}{\partial t} + \rho c u_i \frac{\partial \theta}{\partial x_i} = 0 \tag{5.3}$$

The heat flux through the harbor entrance can be determined by applying equation (5.3) to the harbor volume, V_H, which leads to

$$\int_{V_H} \rho c \frac{\partial \theta}{\partial t} dV + \int_{V_H} \rho c u_i \frac{\partial \theta}{\partial x_i} dV = 0 \tag{5.4}$$

Applying to this equation Green's theorem and assuming that the volume of water in the harbor is constant in time, yields

$$\rho c \frac{\partial}{\partial t} \int_{V_H} \theta \, dV - \rho c \int_{V_H} \theta \frac{\partial u_i}{\partial x_i} dV + \rho c \int_S \theta u_n \, dS = 0 \tag{5.5}$$

where u_n is the velocity in n direction normal to the boundaries (S) of the harbor. For an incompressible fluid and assuming that the free surface is fixed in time and horizontal, and the heat losses at the closed boundaries and the free surface are negligible, equation (5.5) becomes

$$\rho c \frac{\partial}{\partial t} \int_{V_H} \theta \, dV + \rho c \int_{\text{entrance}} \theta u_n \, dS = 0 \tag{5.6}$$

The heat transport Q_θ (both convective and diffusive) through the entrance therefore can be determined from

$$Q_\theta(t) = \rho c \int_{\text{entrance}} \theta u_n \, dS = -\rho c \frac{\partial}{\partial t} \int_{V_H} \theta \, dV = -\rho c V_H \frac{d\bar{\theta}}{dt} \tag{5.7}$$

where $\bar{\theta}$ is the volume-averaged temperature of the water in the harbor. Substitution of $\theta = \theta_0 + \theta_e$, where θ_0 is the temperature of the river water and θ_e the excess temperature with respect to the river water, in equation (5.7) yields for the heat transport

$$Q_\theta(t) = -\rho c V_H \frac{d}{dt}\left(\bar{\theta}_0 + \bar{\theta}_e\right) = -\rho c V_H \left(\frac{d\bar{\theta}_0}{dt} + \frac{d\bar{\theta}_e}{dt}\right) = -\rho c V_H \frac{d\bar{\theta}_e}{dt} \tag{5.8}$$

where it has been assumed that the variation in time of the mean temperature of the river water is much smaller than the variation in time of the mean excess temperature of the water in the harbor with respect to the river water. Henceforth the subscript e will be omitted.

A normalized heat transport, λ, is defined according to

$$\lambda(t) = \frac{Q_\theta(t)}{\rho c A \hat{u} \bar{\theta}(t)} = -\frac{V_H \frac{d\bar{\theta}}{dt}}{A \hat{u} \bar{\theta}(t)} \tag{5.9}$$

where A is the area of cross-section of the harbor entrance and $\hat{u}$ the amplitude of the water velocity in the river.

5.2 Results

The thermistor measurements were used to obtain $\bar{\theta}(t)$. This signal was low-pass filtered and numerically differentiated with respect to time.

Figures 5.1 to 5.6 show the time histories of $\lambda(t)$ for model harbors (1), (2), (3) and (4). The progress of λ for the various harbor geometries can be explained from the flow pattern in the harbor entrance and the geometry of the harbor.

For model harbor (1) the large peaks around slack water evidently result from the pronounced advective exchange which then occurs. The gyre is moving into the river and guides, by its rotation, river water into the harbor. See also Photo 1. The second peak is lower than the first, since water that is less easily exchanged remains in the harbor after the first slack water.

The dip in λ after slack water results from the fact that the new gyre has not yet developed. The new gyre is moving towards the downstream sidewall of the harbor. As a consequence of which only new water, with the same temperature as the river water, is present near the entrance and the exchange of heat is low. This can be observed in Photo 2.

The subsequent rise is caused by the arrival at the entrance of warmer water, the remnants of the old primary gyre, from the back of the harbor, which is advected by the new gyre.

The gradual decrease in λ during the quasi-steady phase, when diffusion governs the exchange process, is caused by the decreasing velocity difference between the flow in the river and the flow in the gyre. As a result, the turbulence generated in the mixing layer at the transition from harbor to river will also decrease and consequently the turbulent exchange does so too.

The first peak for harbor (2) is lower than that for harbor (1), since the secondary gyre does not contribute to the exchange process. However, the second peak is relatively high because more old water is present near the entrance.

The increase in λ, starting at t = 300 s is caused by the arrival of the remnants of the old primary gyre at the entrance, see Photo 3. When the developing new gyre spans the entire width of the harbor, see Photo 4, λ is constant for some time. The sudden increase at $t \approx 370$ s is caused by the arrival of the remnants of the old secondary gyre at the entrance, see Photo 5.

The peaks at slack water in the case of harbor (3) are low, since the gyre does not move into the river, see Photo 6. However, λ is quite large between the slack periods. The temperature gradient in the entrance of the harbor is larger because less heat is exchanged during slack water.

There is a distinct difference in the progress of λ between both maximum currents in the case of harbor (4). This depends on the orientation of the harbor entrance (see also section 3.4) with respect to the river flow direction as can be observed in the behavior and the shape of the mixing layer at the transition from harbor to river. When the flow in the river is from left to right (Photo 7) the mixing layer is rather wide with large vortices. It was observed that the mixing layer at the harbor entrance was not stable, but was swaying in and out, producing a large exchange of water between harbor and river. When the flow in the river is from right to left (Photo 8) the mixing layer is thin with small vortices, giving a much smaller exchange of water between harbor and river.

The tide averaged values of λ are 0.019 for harbor (1), 0.022 for harbor (2), 0.023 for harbor (3), and 0.020 for harbor (4), respectively. These values are remarkably close to each other, although the flow conditions are rather different. The value of λ in steady-flow conditions ($\hat{u}$ now being the constant water velocity in the river) is about 0.032 (Booij [1]), which is also about the value near maximum current in the present experiments.

6. Summary and conclusions

The research that has been presented in this report is a part of an ongoing study on the siltation of tidal harbors. The study deals with the water motion in the harbor entrance, which motion causes the siltation. As yet, too little is known about this complicated time-dependent water motion.

The data obtained during the research will be used to calibrate the 3-D numerical model Trisula, so that this model can be used as a tool to predict the water motion in a harbor entrance. With the present knowledge of the transport of cohesive sediments, a better prediction of the siltation of a particular harbor entrance will then be possible.

Experiments have been performed in a physical model at the Laboratory of Fluid Mechanics of the Delft University of Technology. In these experiments the influences, on the flow patterns in the harbor entrance and the exchange of heat between harbor and river, of the geometries of the harbor and the harbor entrance, the tidal period and tidal water level changes were examined.

Measurements of the time-dependent velocity and temperature fields were made in five model harbors. In the experiments without tidal water level changes three harbors had their length axes perpendicular to the length axis of the river, namely (1) a square harbor of 1 m^2, (2) a rectangular harbor of 1×2 m^2 and (3) a square harbor of 1 m^2 with a narrowed entrance of 0.5 m; one harbor, (4), of 1 m^2 and an entrance width of 1 m had its length axis at an angle of 45 degrees to the length axis of the flume. In the experiment with tidal water level changes a rectangular harbor, (5), with an entrance width of 1 m and a storage area of 8 m^2 had its length axis perpendicular to the length axis of the river.

It can be concluded that:

- details of circulating flows and gyres depend markedly on the geometry of the harbor.
- the progress of the phenomena after slack water in model harbor (2), that is the development of a new primary gyre, does not seem to depend on the tidal period. As a consequence, the phase difference between the development of the gyre and the accelerating flow in the river increases as the period decreases.
- the flow pattern in the harbor is highly influenced by the orientation of the harbor entrance. An explanation for this phenomenon is deficient at the moment.
- in the model harbors, except harbor (3), a quite strong secondary current is present in the gyre. The maximum velocity in the secondary current is on the average 15 per cent of the main flow. This means that a three-dimensional numerical model will be necessary to simulate the flow pattern in the harbor correctly.
- close to the downstream sidewall, in all model harbors, larger water velocities (20 to 50 per cent larger) were observed near the bottom than higher in the water column. Near the bed high-momentum fluid from

the mixing layer between harbor and river appears to be transported into the harbor.

- tidal water level changes cause an acceleration in the development of the new gyre towards high tide. Towards low tide the development of the new gyre is hindered by the emptying of the basin.
- in harbors (1), (2) and (4) a large increase in advective exchange takes place around slack water. The influence of turbulence seems to be of secondary importance during this phase of the tide.
- a narrowed entrance highly reduces the exchange of mass between harbor and river at slack water.
- if the flow pattern in the harbor comprises various gyres, in this research harbor (2), the normalized exchange will be less because the secondary, tertiary, etc. gyres do not contribute to the exchange process.
- when the current in the river is around maximum, the flow is quasi-steady for a quite large duration. The exchange then takes place through the mixing layer between river and harbor, that is, it is caused by turbulent motions only.
- although during slack water a less refined turbulence model is sufficient in a numerical model, the modeling of turbulence is important during the quasi-steady phase of the tide, especially when the geometry of the entrance is more complex (e.g. harbor (4)).

References

[1] Booij, R., "Measurements of the exchange between river and harbor.", (in Dutch), Report no. 9-86 (1986), Delft University of Technology.

[2] Delft Hydraulics, "Trisula manual.", 3 volumes.

[3] Dursthoff, W., "On the qualitative exchange of water between river and harbor.", (in German), Mitteilungen des Franzius-Instituts für Grund- und Wasserbau der Technischen Universität Hannover, 1970, heft 34, pp. 194-368.

[4] Langendoen, E.J., "Laboratory observations and calculations of the depth averaged flow patterns in a square harbor on a tidal river.", Report no. 8-89, Delft University of Technology.

[5] Langendoen, E.J. & Karelse, M., "Laboratory observations of velocity and density fields in the entrance of a harbor on a stratified tidal river.", Report no. 1-90, Delft University of Technology.

[6] Rohr, F., "The movement of water and sediment in river and sea harbors.", (in German), Untersuchungen aus dem Flußbaulaboratorium der Technischen Hochschule zu Karlsruhe, Verlag von R. Oldenburg, München und Berlin, 1934.

[7] Westrich, B., "Water exchange in confined basins induced by unsteady main stream currents.", Proc. IAHR Congress on Hydraulic Engineering for Improved Water Management, 1977, Baden Baden, Vol. 2, pp. 461-468.

Notation

A	area of cross-section of the harbor entrance
B	width of the harbor
B_e	width of the harbor entrance
c	specific heat
E_{int}	internal energy
h	water depth
$\hat{h}$	amplitude of the vertical tide
L	length of the harbor
L_g	length of the gyre
p	pressure
Q_θ	heat transport
S	surface
T	tidal period
t	time
t_g	time scale of the development of the gyre
t_t	time scale of the tide
U	velocity in the flow direction
$\hat{u}$	amplitude of the tidal current velocity
u_i	velocity component
V_H	harbor volume
v_s	velocity of the secondary current
x_i	coordinate
α	angle between the harbor and river axes
κ	heat conductivity
λ	normalized heat transport
μ	dynamic viscosity

Appendix A
Data File Description

This appendix describes the format under which the basic data files have been stored and the means by which they can be retrieved. Also, an explanation of any unusual aspects of particular data file structures is provided to help in any data retrieval effort. All files are available on floppy disks.

The coordinate system used to mark the locations of the measuring-points is right-handed and has its origin at the center of the harbor entrance. The abscissa x is directed parallel and the ordinate y normal to the river axis. y is negative in the harbor. The vertical coordinate z is directed upward and is zero at the bottom. The velocity component u is in x-direction and the velocity component v in y-direction.

Depth averaged flow patterns

The x and y coordinates and the velocity components u and v of the floats are stored at specific times. The files with the stored data are text files. The naming procedure used to distinguish the data files is nnn.exp, with nnn the time and exp the experiment number. Table A-1 lists all the data files that are available. The first record of each file contains the time (real), the subsequent records contain, in order, the x coordinate, the y coordinate, and the velocity components u and v of a float (all reals). The last record of the file contains the number 10000 to mark the end of the file.

Table A-1 Data files for the depth averaged flow patterns

Harbor 1			Harbor 2			Harbor 3	Harbor 4
250 s	500 s	1000 s	250 s	500 s	1000 s		
000.1A	000.1B	000.1C	070.2A	140.2B	400.2C	000.3	000.4
005.1A	005.1B	010.1C	075.2A	150.2B	420.2C	010.3	010.4
010.1A	010.1B	020.1C	080.2A	160.2B	440.2C	020.3	020.4
015.1A	015.1B	030.1C	085.2A	170.2B	460.2C	030.3	030.4
020.1A	020.1B	040.1C	090.2A	180.2B	480.2C	040.3	040.4
025.1A	025.1B	050.1C	095.2A	190.2B	500.2C	050.3	050.4
030.1A	030.1B	060.1C	100.2A	200.2B	520.2C	060.3	060.4
035.1A	035.1B	070.1C	105.2A	210.2B	540.2C	070.3	070.4
040.1A	040.1B	080.1C	110.2A	220.2B	560.2C	080.3	080.4
045.1A	045.1B	090.1C	115.2A	230.2B	580.2C	090.3	090.4
050.1A	135.1B	100.1C	120.2A	240.2B	600.2C	100.3	100.4

Table A-1 (continued)

Harbor 1			Harbor 2			Harbor 3	Harbor 4
250 s	500 s	1000 s	250 s	500 s	1000 s		
055.1A	140.1B	110.1C	125.2A	250.2B	620.2C	110.3	110.4
060.1A	145.1B	120.1C	130.2A	260.2B	640.2C	120.3	120.4
065.1A	150.1B	130.1C	135.2A	270.2B	660.2C	130.3	130.4
070.1A	155.1B	140.1C	140.2A	280.2B	680.2C	140.3	200.4
075.1A	160.1B	460.1C	145.2A	290.2B	700.2C	150.3	210.4
080.1A	165.1B	470.1C	150.2A	300.2B	720.2C	390.3	220.4
085.1A	170.1B	480.1C	155.2A	310.2B	740.2C	400.3	230.4
090.1A	175.1B	490.1C	160.2A	320.2B	760.2C	410.3	240.4
095.1A	180.1B	500.1C	165.2A	330.2B	780.2C	420.3	250.4
100.1A	185.1B	510.1C	170.2A	340.2B	800.2C	430.3	260.4
105.1A	190.1B	520.1C	175.2A	350.2B		440.3	270.4
110.1A	195.1B	530.1C	180.2A	360.2B		450.3	280.4
115.1A	200.1B	540.1C	185.2A	370.2B		460.3	290.4
120.1A	205.1B	550.1C	190.2A	380.2B		470.3	300.4
125.1A	210.1B	560.1C	195.2A	390.2B		480.3	310.4
130.1A	215.1B	570.1C	200.2A	400.2B		490.3	320.4
135.1A	220.1B	580.1C					330.4
140.1A	225.1B	590.1C					340.4
195.1A	230.1B	600.1C					350.4
200.1A	235.1B	610.1C					360.4
205.1A	240.1B	620.1C					370.4
210.1A	245.1B	630.1C					380.4
215.1A	250.1B	640.1C					450.4
220.1A	255.1B	650.1C					460.4
225.1A	260.1B	660.1C					470.4
230.1A	265.1B	670.1C					480.4
235.1A	270.1B	680.1C					490.4
240.1A	275.1B	690.1C					
245.1A	280.1B	760.1C					
	285.1B	770.1C					
	290.1B	780.1C					
	295.1B	790.1C					
	300.1B	800.1C					
	305.1B	810.1C					
	310.1B	820.1C					
	315.1B	830.1C					
	320.1B	840.1C					
	325.1B	850.1C					
	330.1B	860.1C					
	335.1B	870.1C					
	340.1B	880.1C					

Table A-1 (continued)

Harbor 1			Harbor 2			Harbor 3	Harbor 4
250 s	500 s	1000 s	250 s	500 s	1000 s		
	345.1B	890.1C					
	350.1B	900.1C					
	355.1B	910.1C					
	360.1B	920.1C					
	365.1B	930.1C					
	490.1B	940.1C					
	495.1B	950.1C					
		960.1C					
		970.1C					
		980.1C					
		990.1C					

Measurements with the electromagnetic flow meter

The results of the measurements made with the electromagnetic flow meter in model harbor 1 are stored in the files HARBOR1.BIN and HAR1BC.BIN, and the results of the measurements in model harbor 5 in the files HARBOR5.BIN and HAR5BC.BIN. The files HARBOR1.BIN and HARBOR5.BIN contain the water velocities in the harbor entrance and the water velocities in the section of the river in front of the harbor. The files HAR1BC.BIN and HAR5BC.BIN contain the boundary conditions needed for the calibration of a numerical model. All files are binary files. The files HARBOR1.BIN and HAR1BC.BIN have a record length of 4020 bytes and the files HARBOR5.BIN and HAR5BC.BIN have a record length of 820 bytes. The water velocities are stored every second for model harbor 1 and every 5 seconds for model harbor 5, beginning at t = 0 s (slack water).

The file HARBOR1.BIN contains 184 records and HAR1BC.BIN 32 records. Each record can be read by, for example, the FORTRAN instruction: READ(unit) X,Y,Z,(U(I),V(I),I=1,501), where X, Y and Z are REAL*4 variables indicating the coordinates of the measurement location, and U and V are REAL*4 arrays of dimension 501 containing the velocity components.

The file HARBOR5.BIN contains 85 records and HAR5BC.BIN 25 records. The first record of each file contains the water elevation in the river in front of the harbor. The water depth can be calculated by adding the mean water depth, 0.11 m, to the water elevations. This record can be read by, for example, the FORTRAN instruction: READ(unit) (H(I),I=1,101), where H is a REAL*4 array of dimension 101 containing the water level elevation. The record is completed with spaces to make direct accessing of the file possible. Subsequent records can be read by the FORTRAN instruction: READ(unit) X,Y,Z,(U(I),V(I),I=1, 101), where X, Y and Z are REAL*4 variables indicating the coordinates of the measurement location, and U and V are REAL*4 arrays of dimension 101 containing the velocity components.

Temperature measurements

The excess temperature field, with respect to the temperature of the river, at different levels above the bottom, in the various harbor entrances is stored in the files TEMP1.BIN (harbor 1), TEMP2.BIN (harbor 2), TEMP3.BIN (harbor 3), and TEMP4A.BIN and TEMP4B.BIN (harbor 4). All files are binary files with a record length of 4996 bytes. The first record of each file contains the following information: a string of 150 bytes (indicating among others the harbor type), two REAL*4 values, namely the time of the first temperature sample and the time interval between the temperature samples, and an INTEGER*2 value representing the number of samples. The record is completed with spaces to make direct accessing of the file possible. All subsequent records contain data that can be read by the FORTRAN instruction: READ(unit) X,Y,Z,(T(I),I=1,IAANT), where X, Y and Z are REAL*4 variables indicating the coordinates of the measurement location. T is a REAL*4 array of dimension IAANT containing the excess temperatures with IAANT the number of samples.

Figures

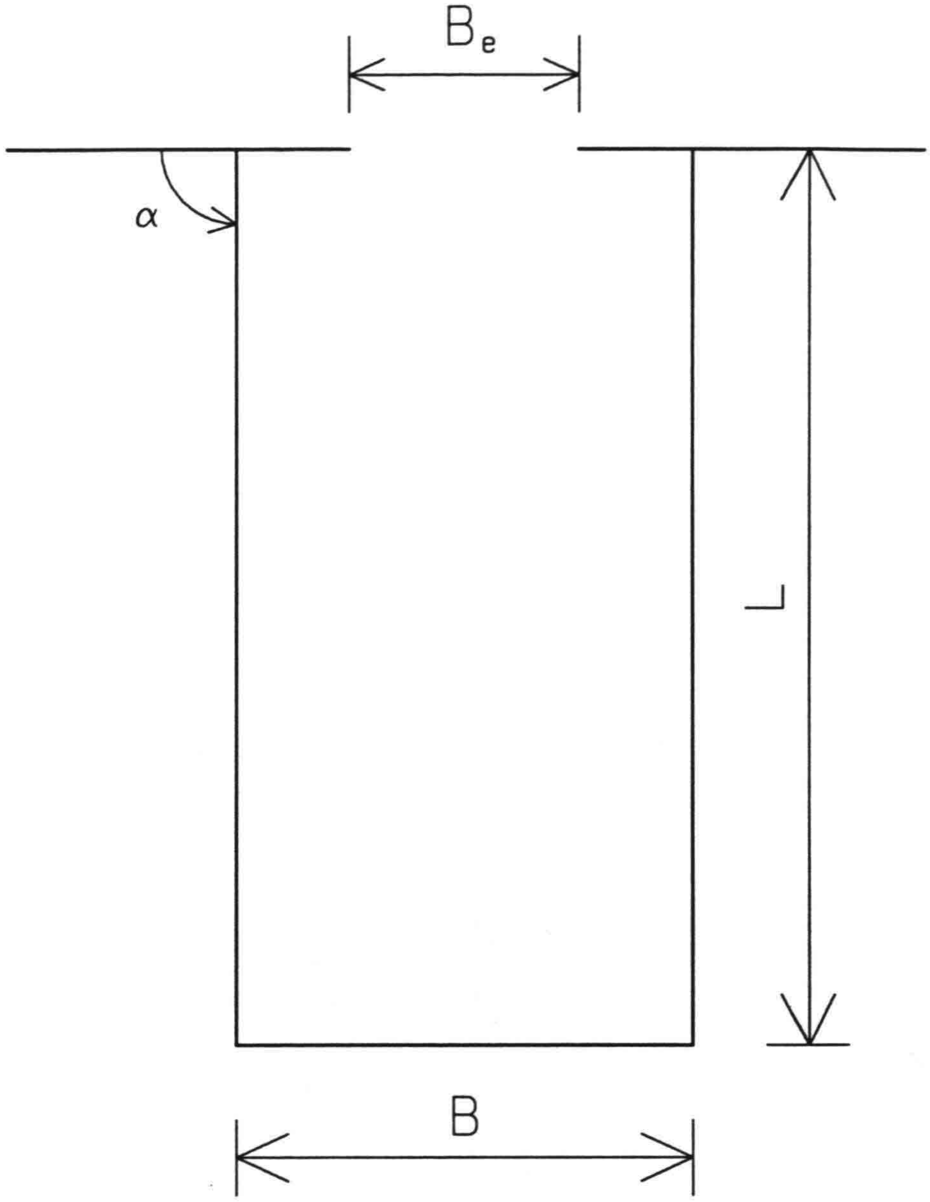

Definition sketch

Delft University of Technology

Fig. 2.1

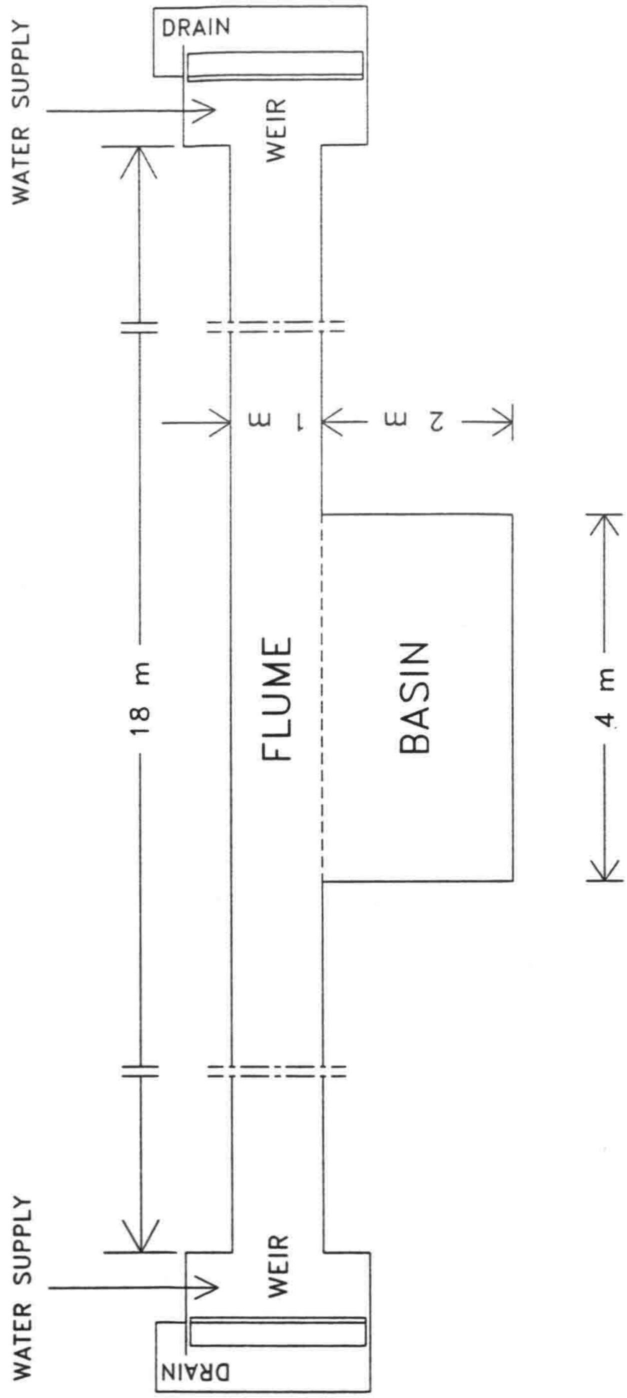

Physical model

Delft University of Technology

Fig. 2.2

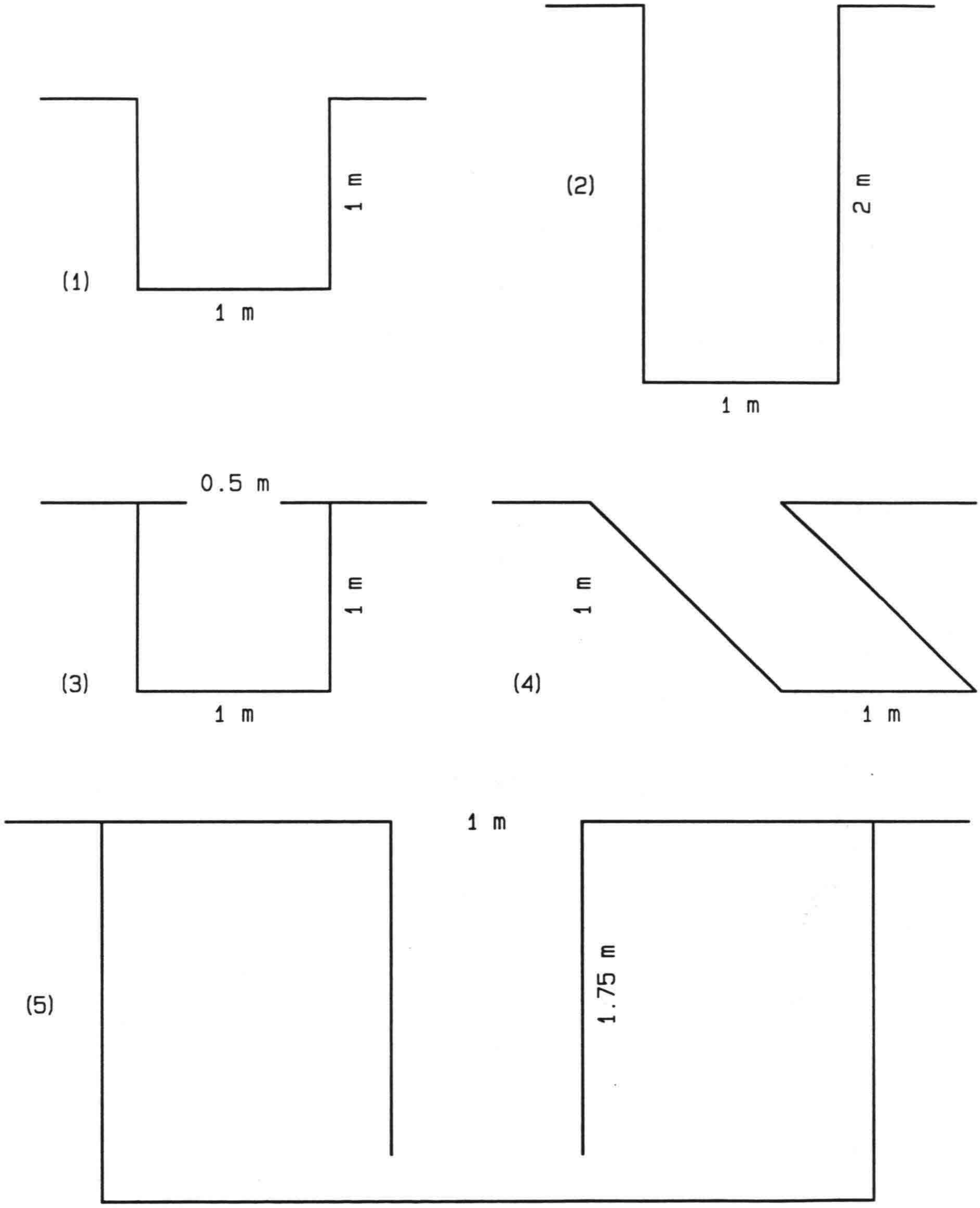

Top view of model harbors

Delft University of Technology

Fig. 2.3

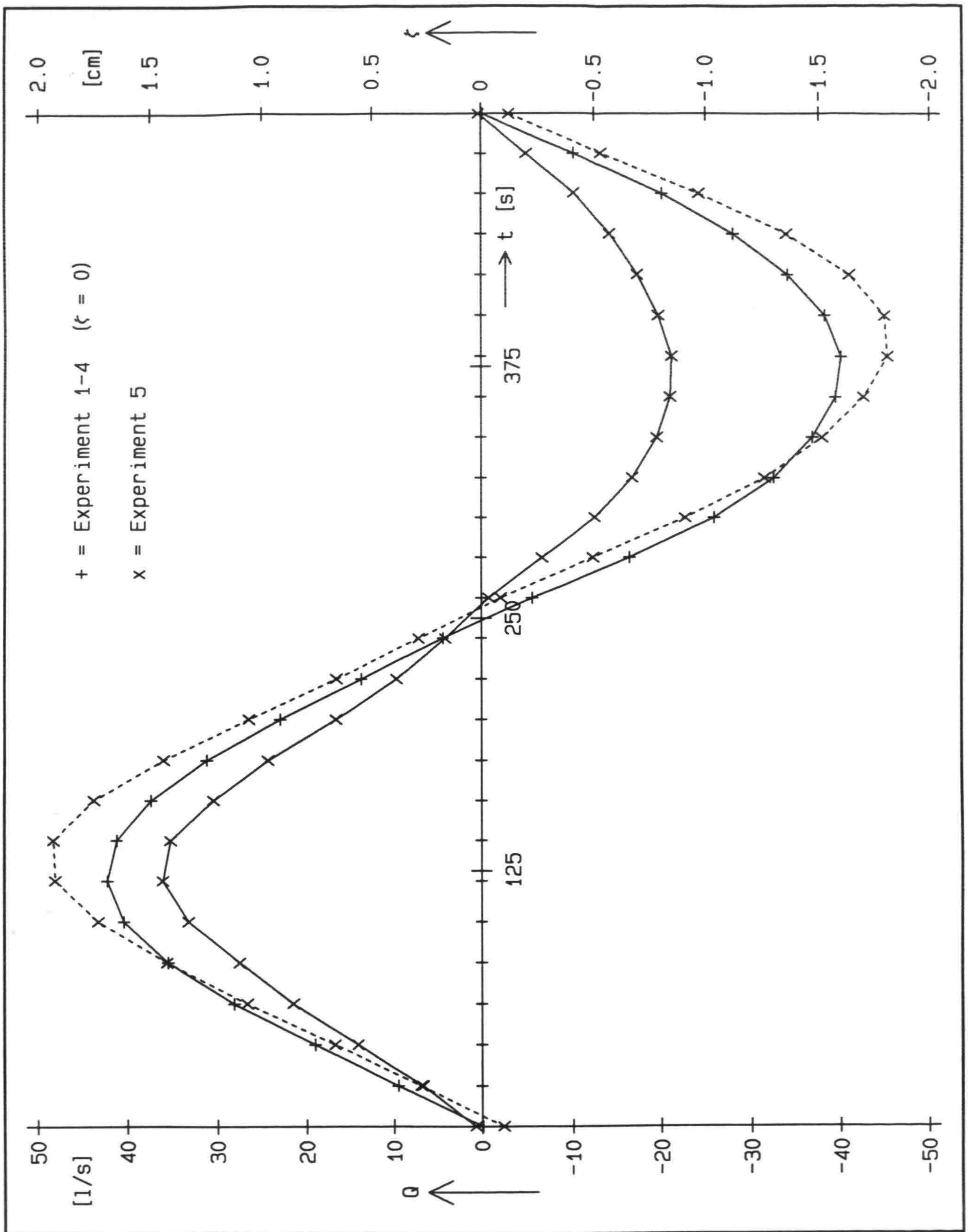

Time-histories of discharge and water level elevation in the river.	——— = Q ------ = ζ
Delft University of Technology	Fig. 2.4

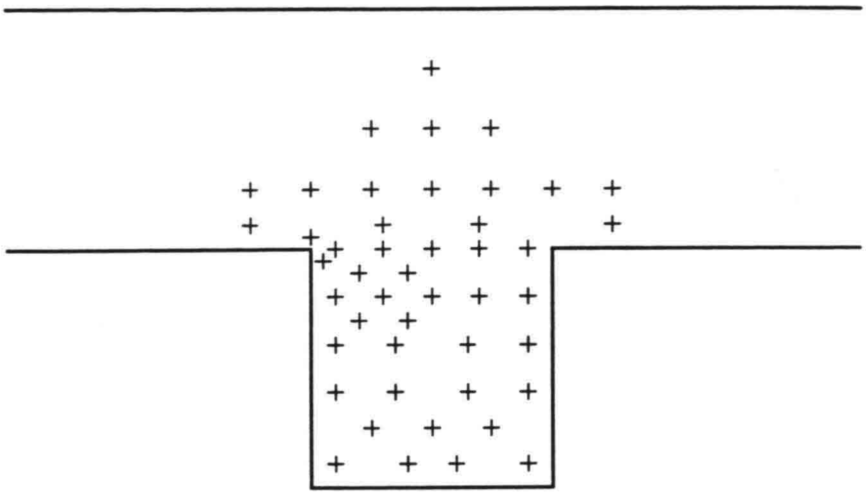

a) velocity measurements

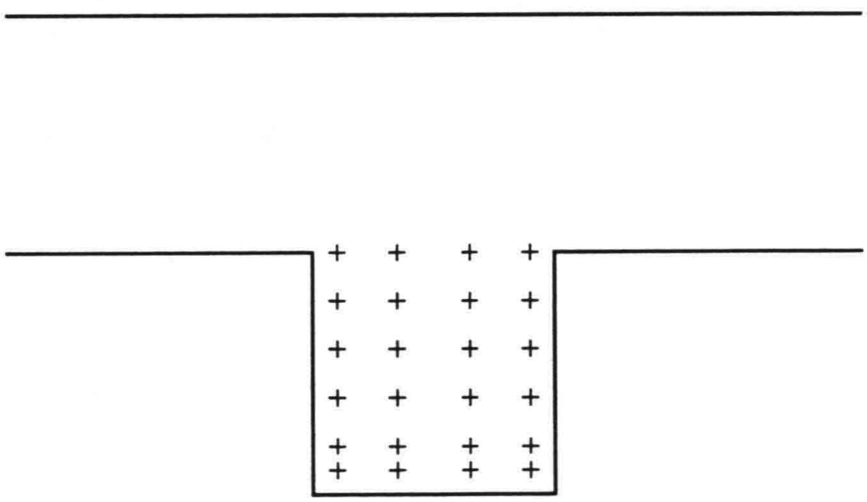

b) temperature measurements

Measurement locations Model harbor (1)	
Delft University of Technology	Fig. 2.5

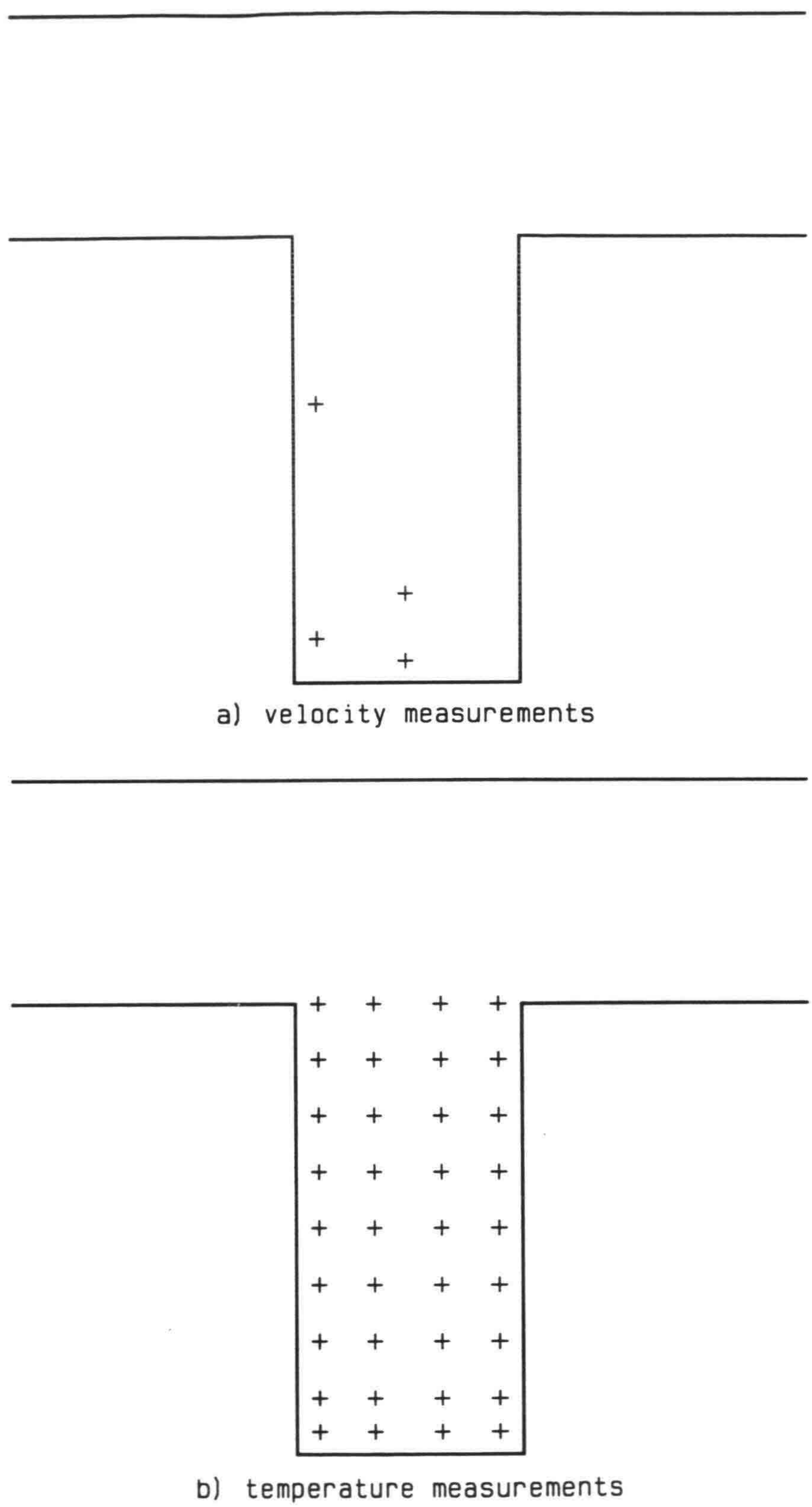

Measurement locations

Model harbor (2)

Delft University of Technology

Fig. 2.6

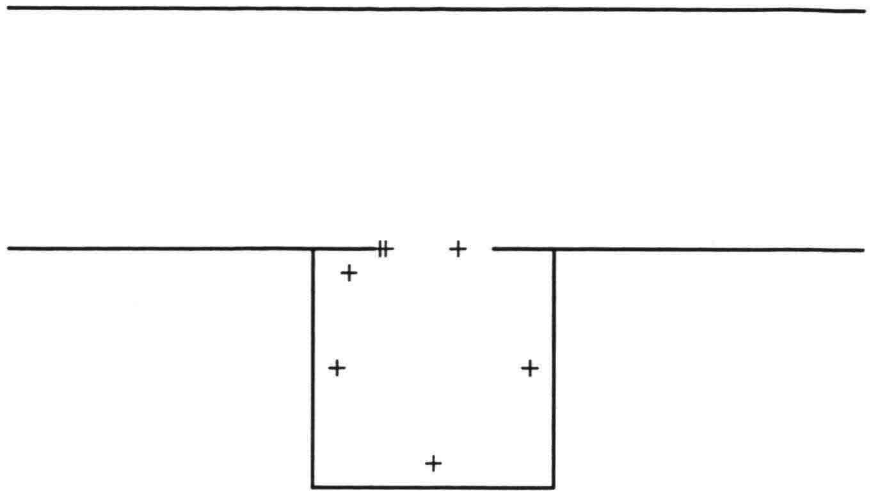

a) velocity measurements

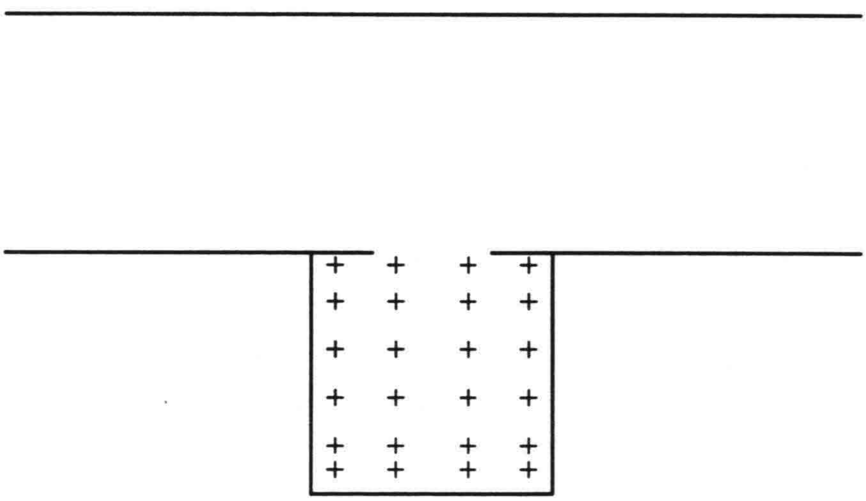

b) temperature measurements

Measurement locations Model harbor (3)	
Delft University of Technology	Fig. 2.7

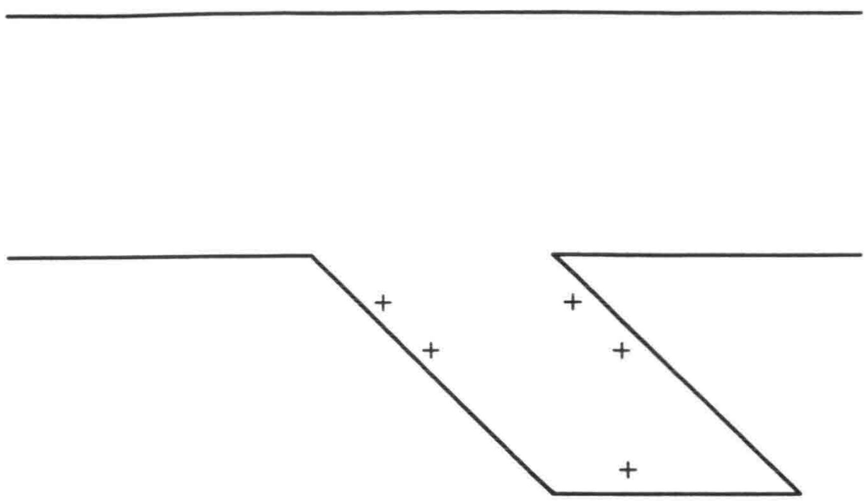

a) velocity measurements

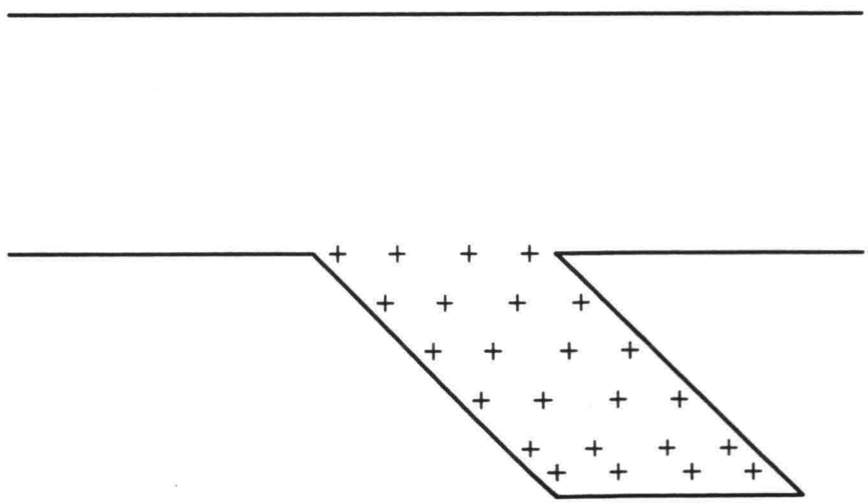

b) temperature measurements

Measurement locations
Model harbor (4)

Delft University of Technology

Fig. 2.8

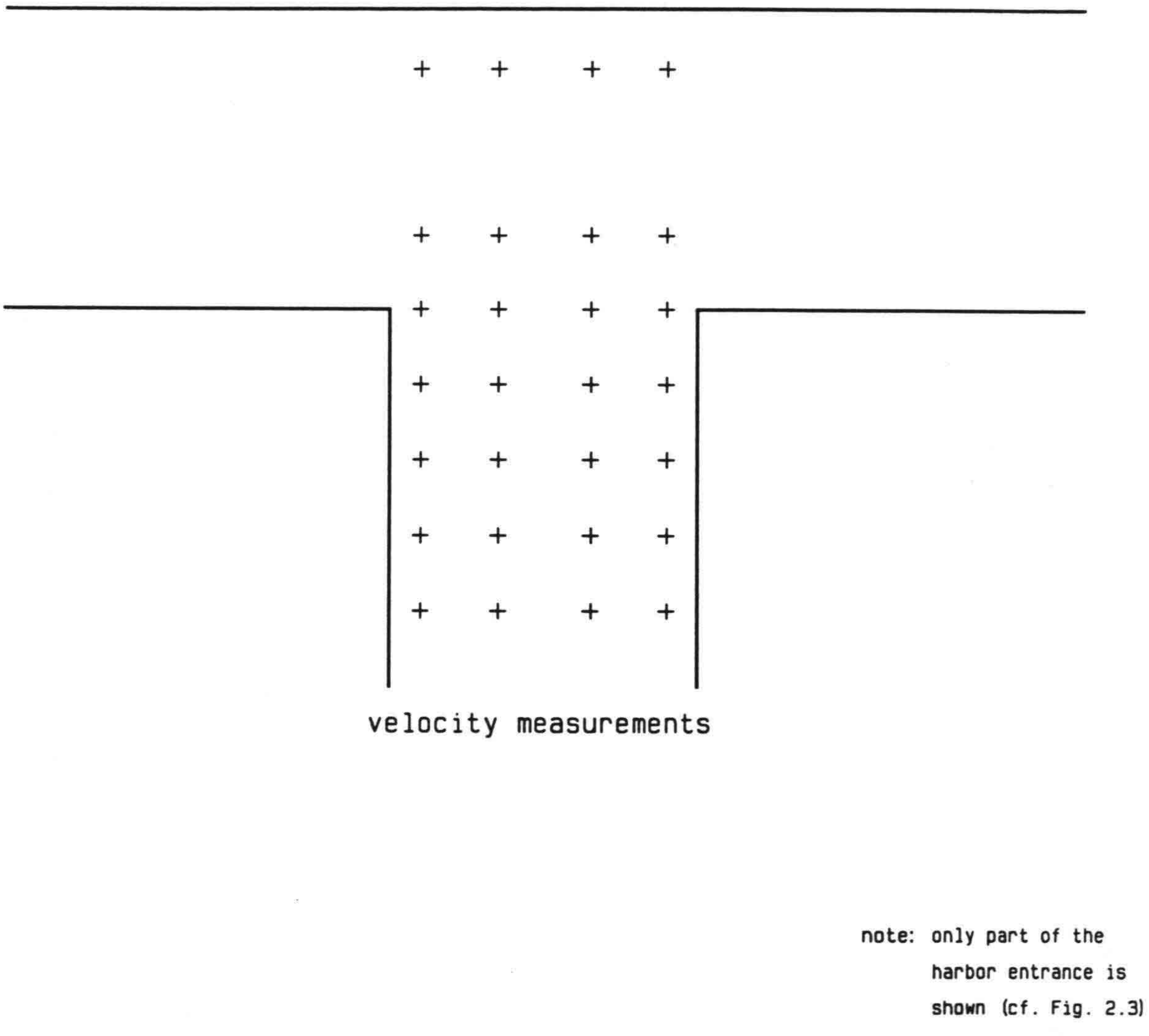

Measurement locations
Model harbor (5)

Delft University of Technology | Fig. 2.9

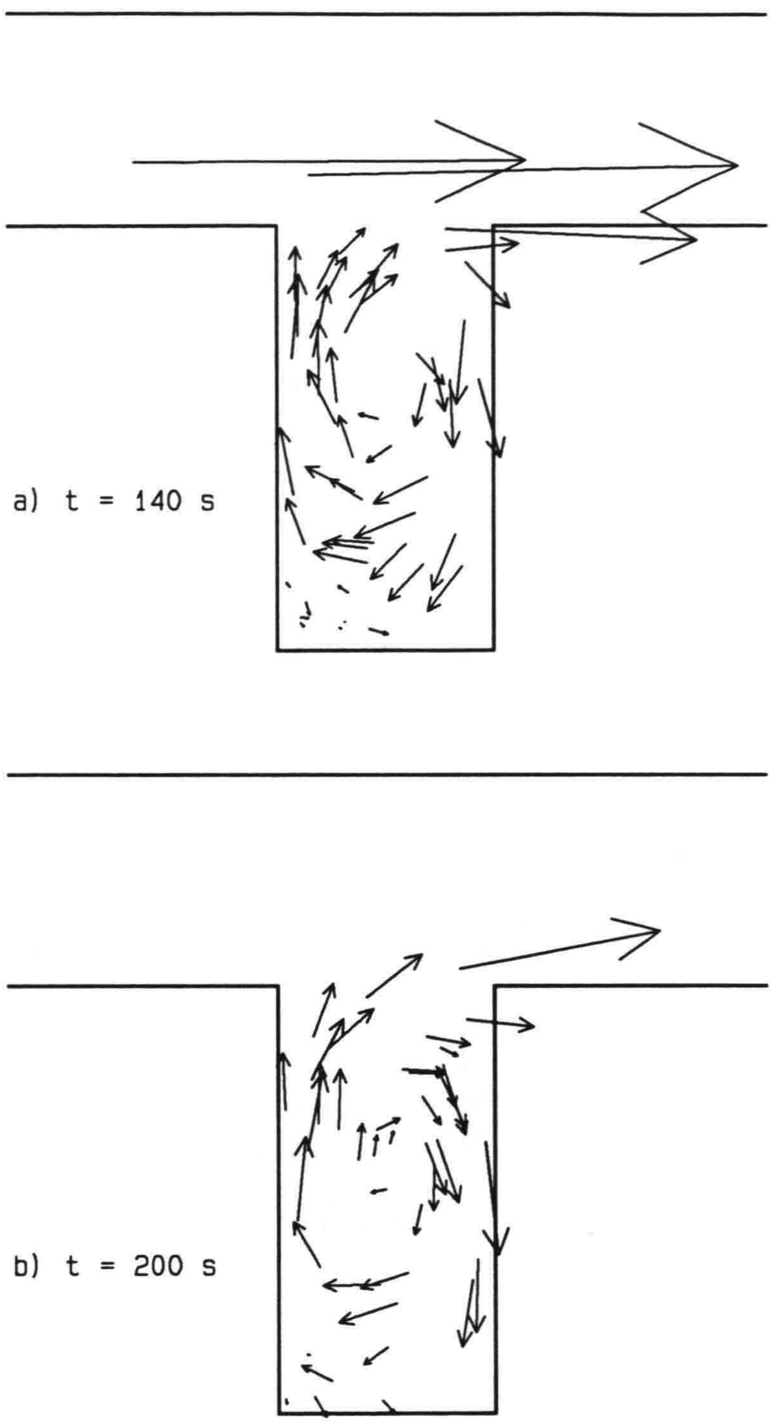

Observed depth averaged flow patterns Model harbor (2), T = 500 s	⟼ = 0.07 m/s
Delft University of Technology	Fig. 3.1

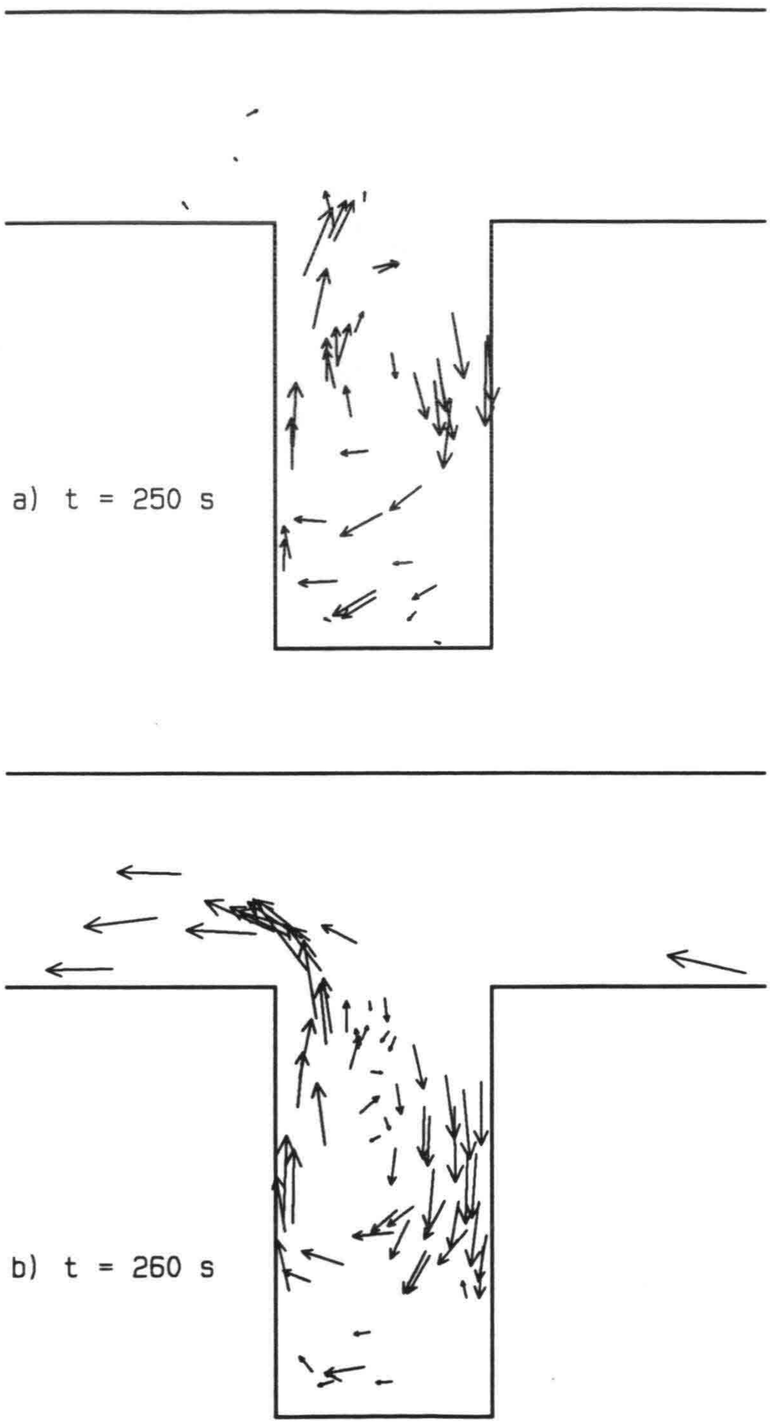

Observed depth averaged flow patterns Model harbor (2), T = 500 s	⟼ = 0.07 m/s
Delft University of Technology	Fig. 3.2

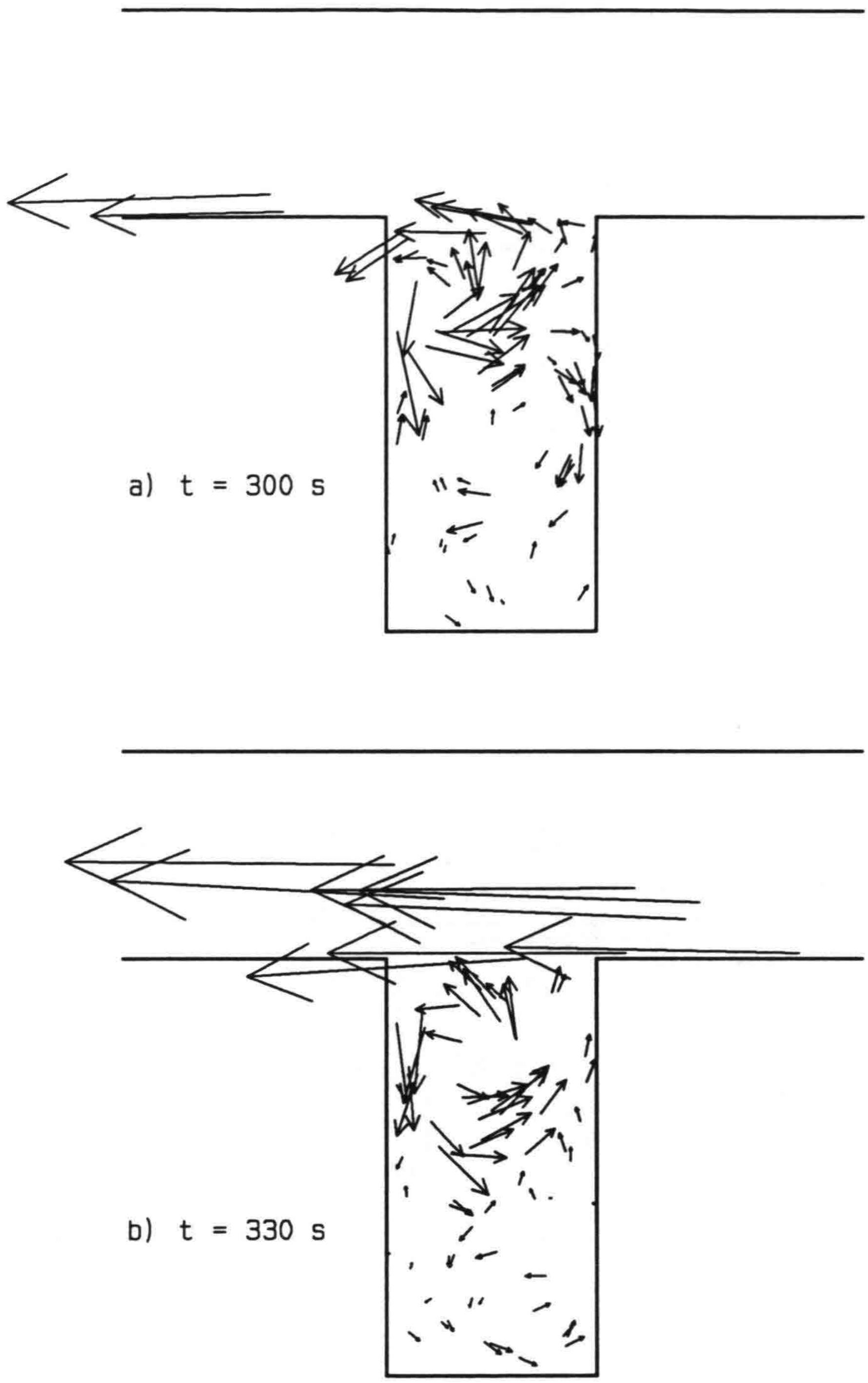

Observed depth averaged flow patterns Model harbor (2), T = 500 s	⟼ = 0.07 m/s
Delft University of Technology	Fig. 3.3

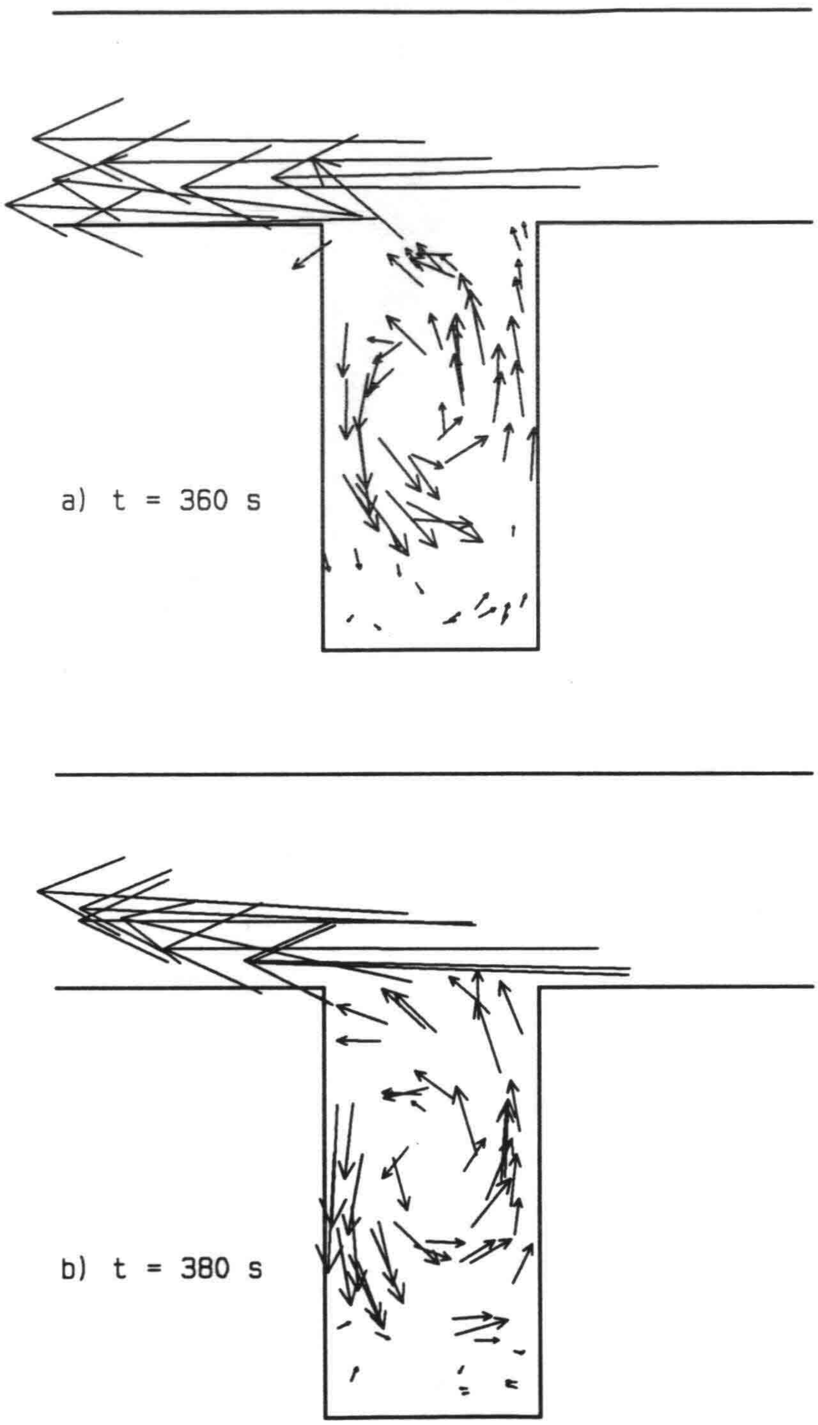

Observed depth averaged flow patterns
Model harbor (2), T = 500 s

⟼ = 0.07 m/s

Delft University of Technology

Fig. 3.4

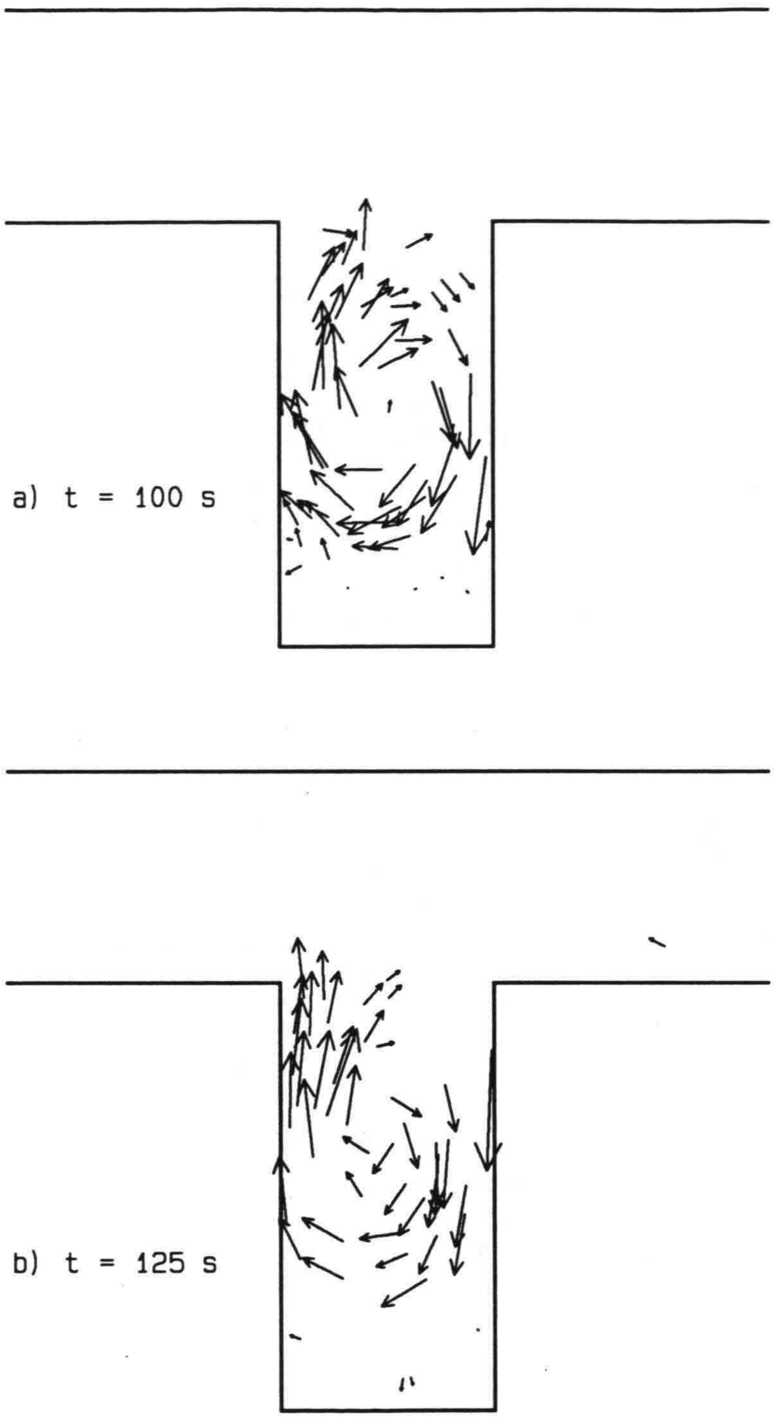

Observed depth averaged flow patterns
Model harbor (2), T = 250 s

⟼ = 0.07 m/s

Delft University of Technology

Fig. 3.5

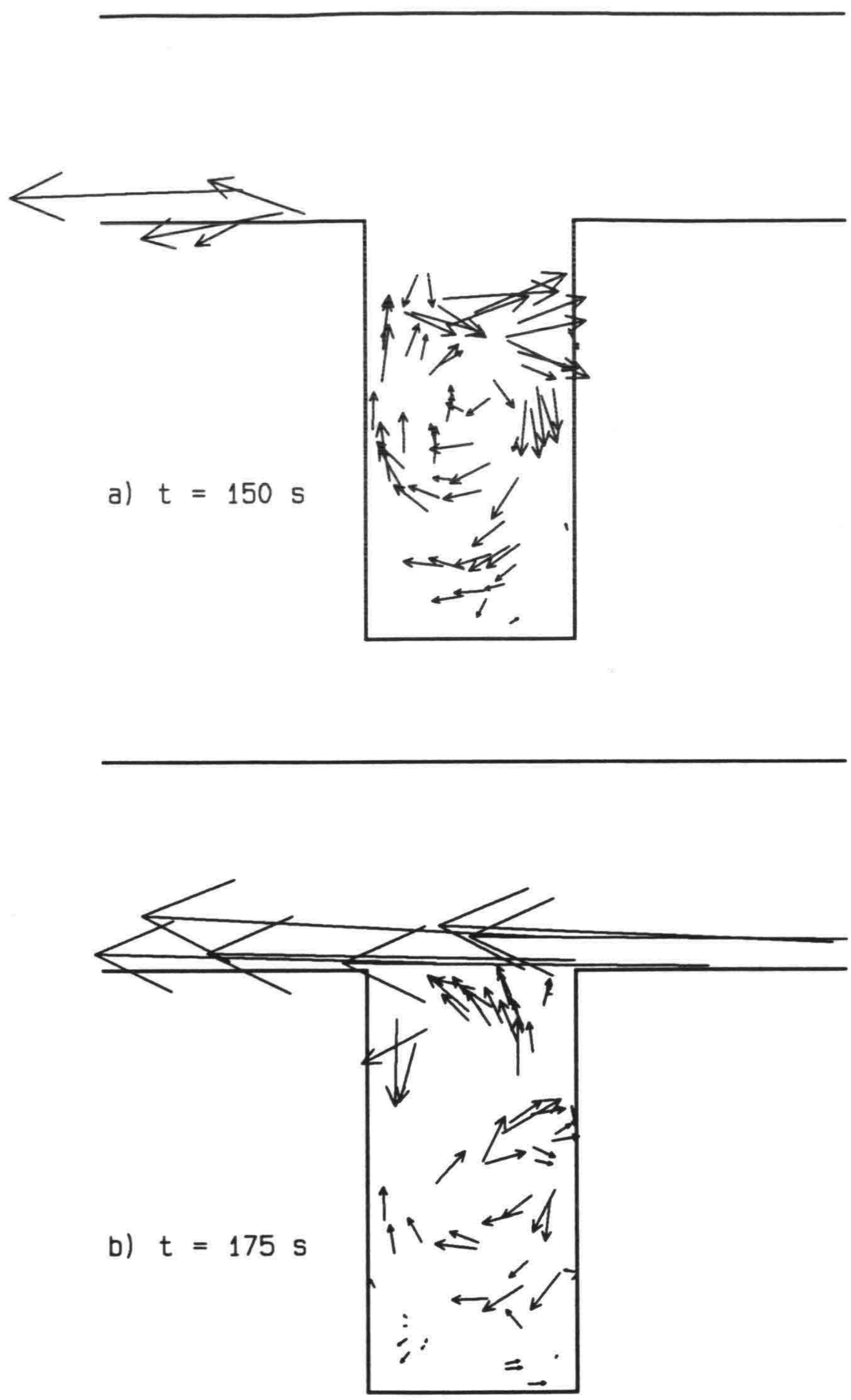

Observed depth averaged flow patterns Model harbor (2), T = 250 s	⟼ = 0.07 m/s
Delft University of Technology	Fig. 3.6

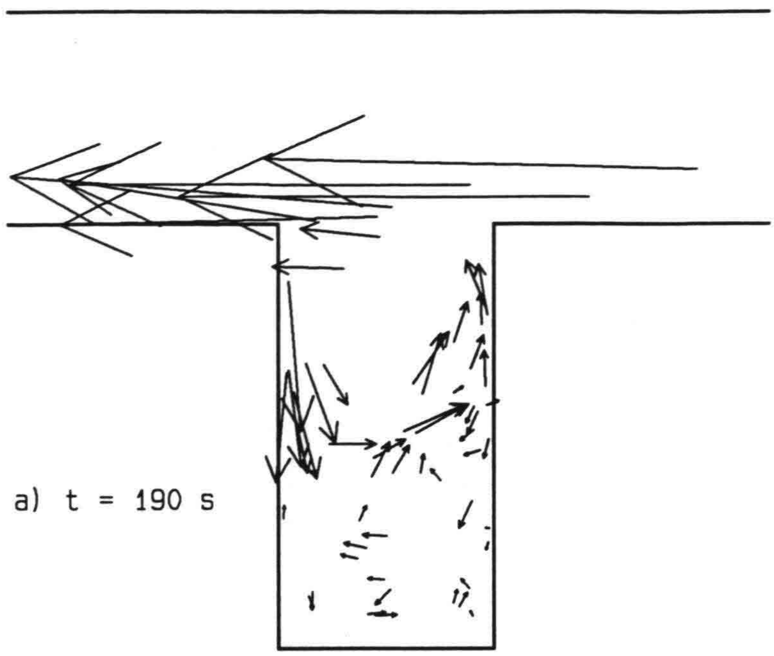

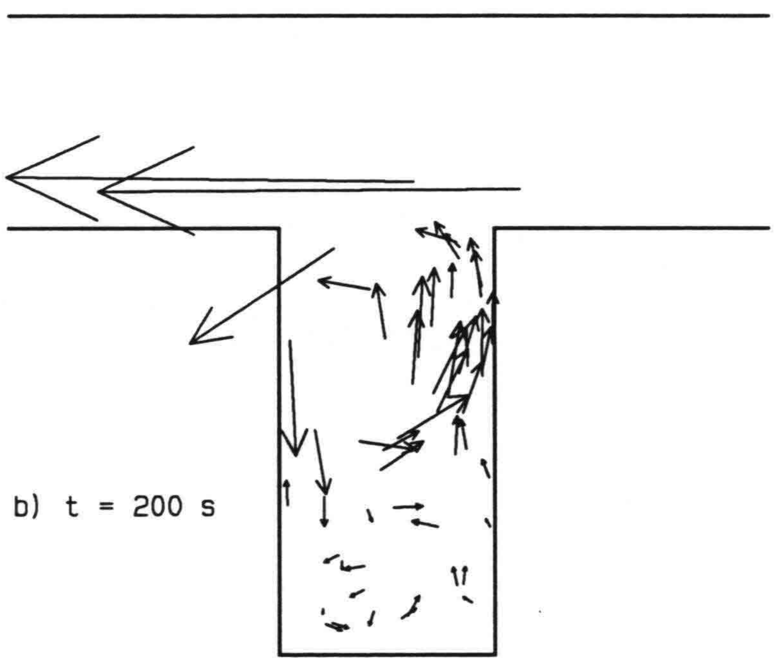

Observed depth averaged flow patterns
Model harbor (2), T = 250 s

⟼ = 0.07 m/s

Delft University of Technology

Fig. 3.7

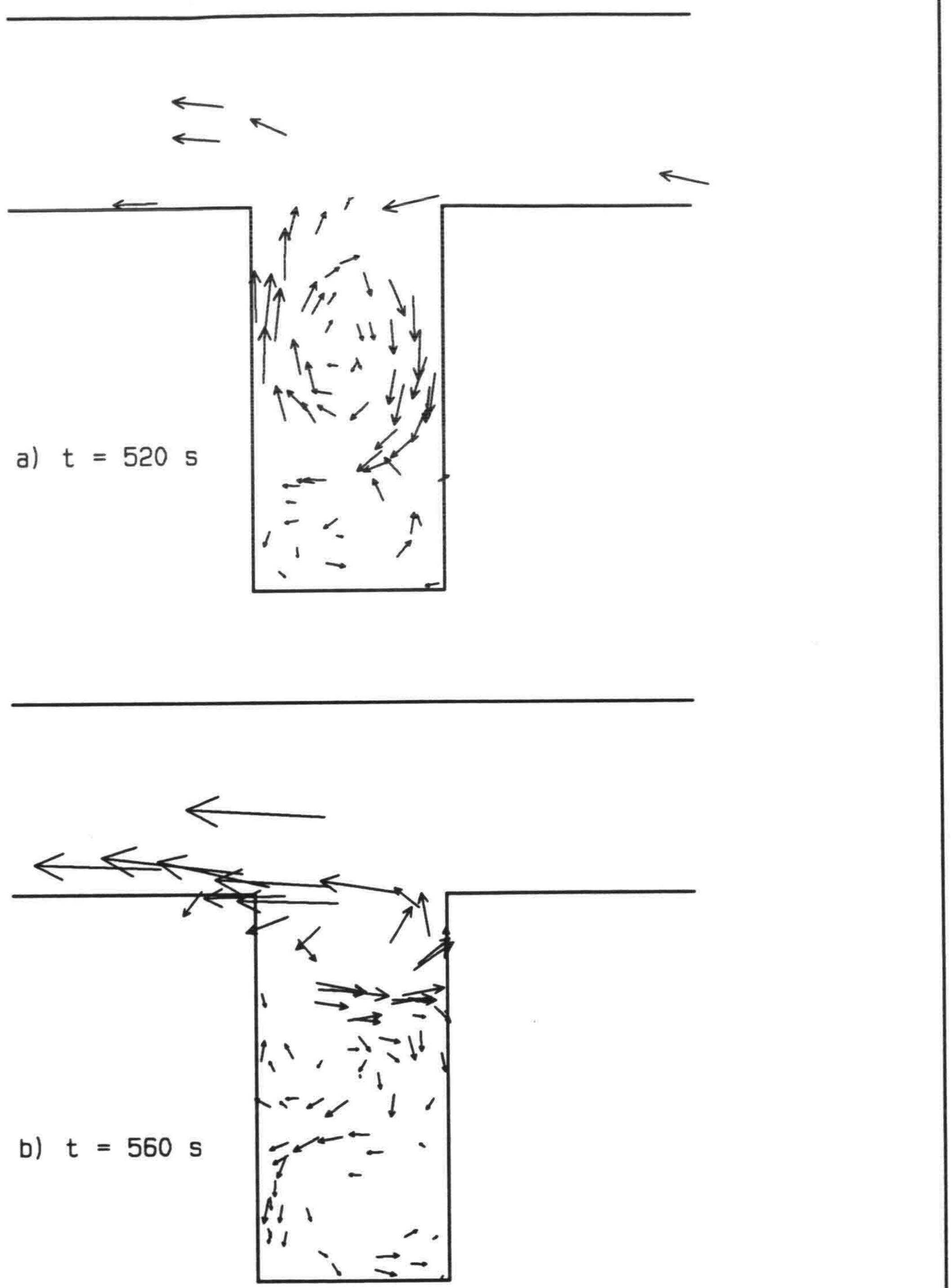

Observed depth averaged flow patterns
Model harbor (2), T = 1000 s

Delft University of Technology

Fig. 3.8

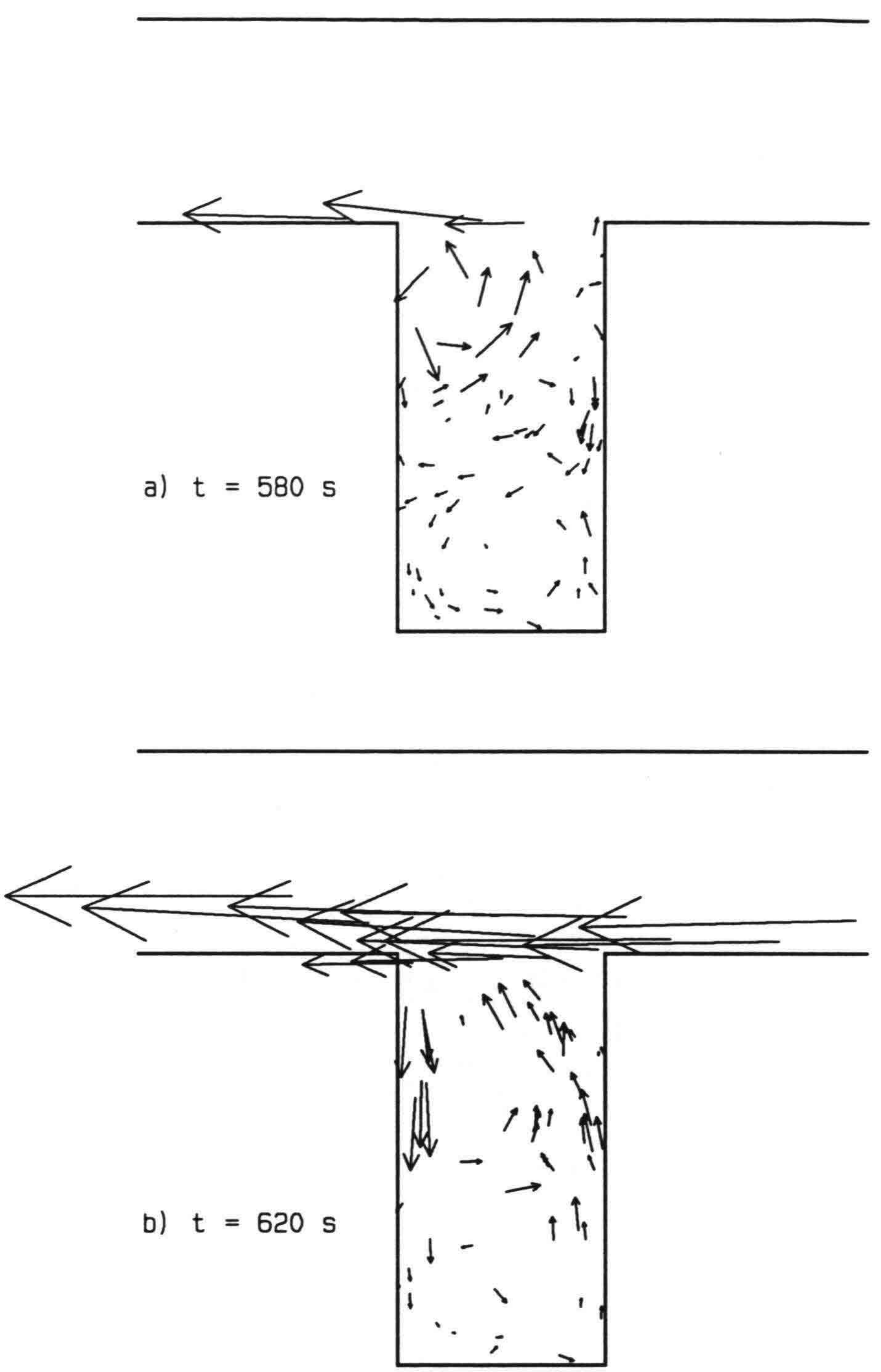

Observed depth averaged flow patterns Model harbor (2), T = 1000 s	⟼ = 0.07 m/s
Delft University of Technology	Fig. 3.9

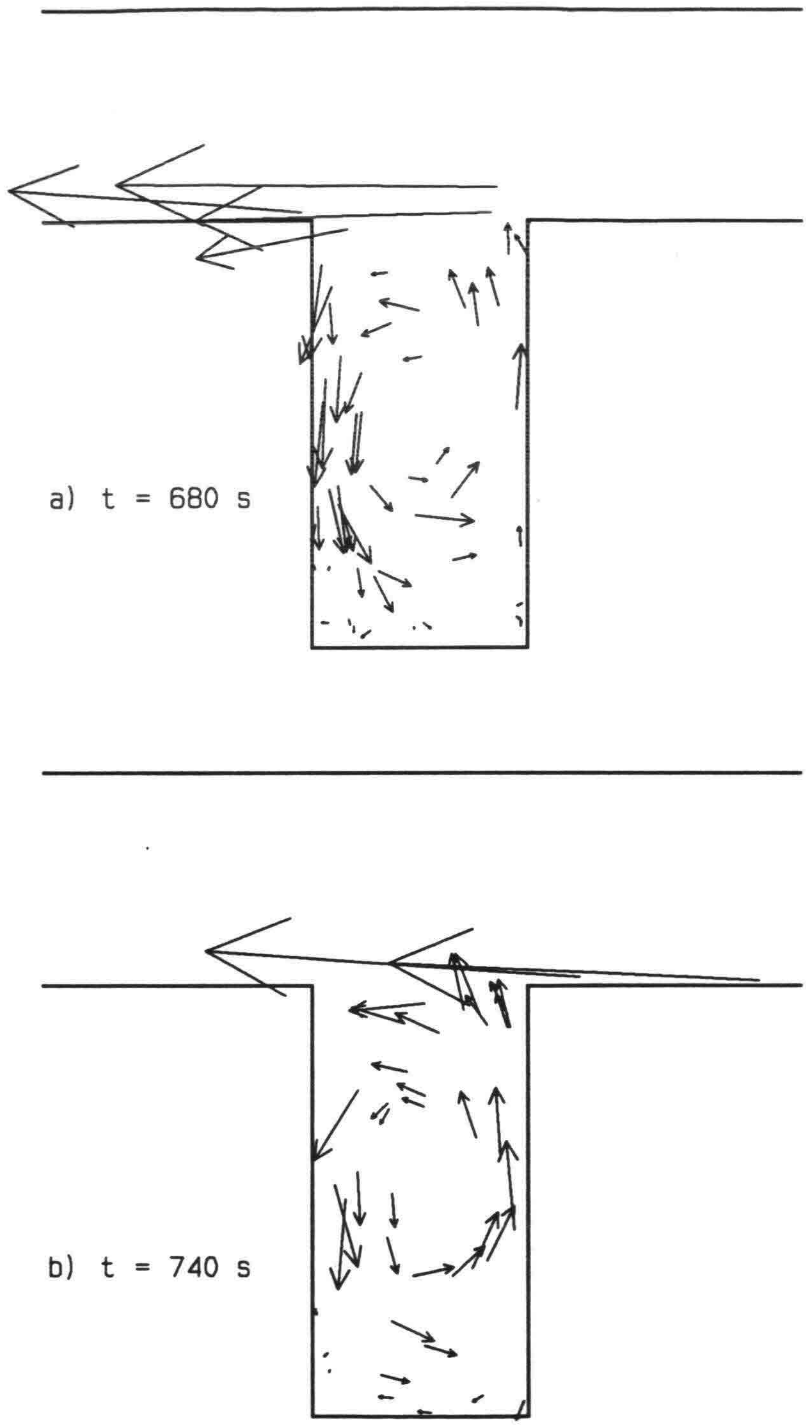

Observed depth averaged flow patterns
Model harbor (2), T = 1000 s

⟼ = 0.07 m/s

Delft University of Technology

Fig. 3.10

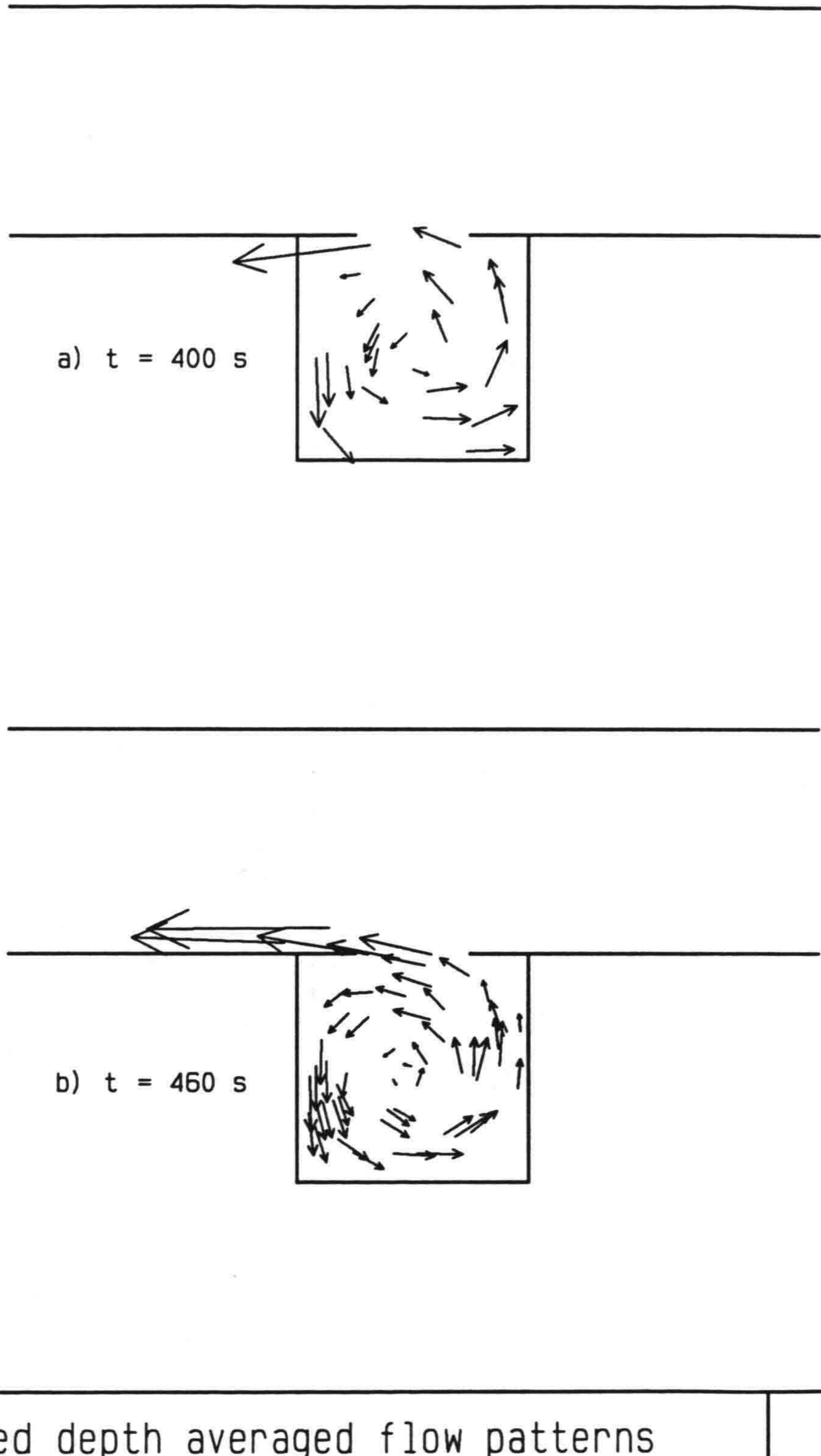

Observed depth averaged flow patterns
Model harbor (3)

⟼ = 0.07 m/s

Delft University of Technology

Fig. 3.11

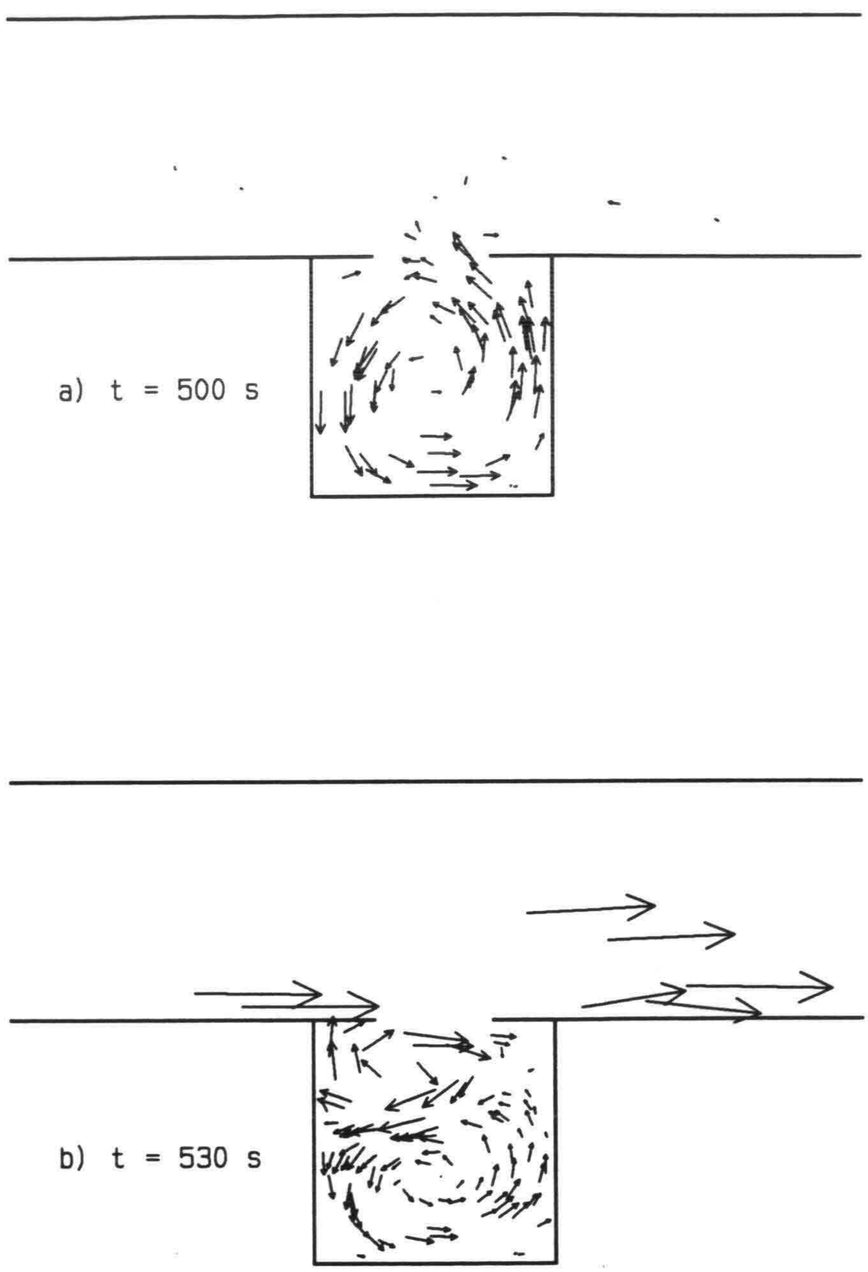

Observed depth averaged flow patterns Model harbor (3)	⟼ = 0.07 m/s
Delft University of Technology	Fig. 3.12

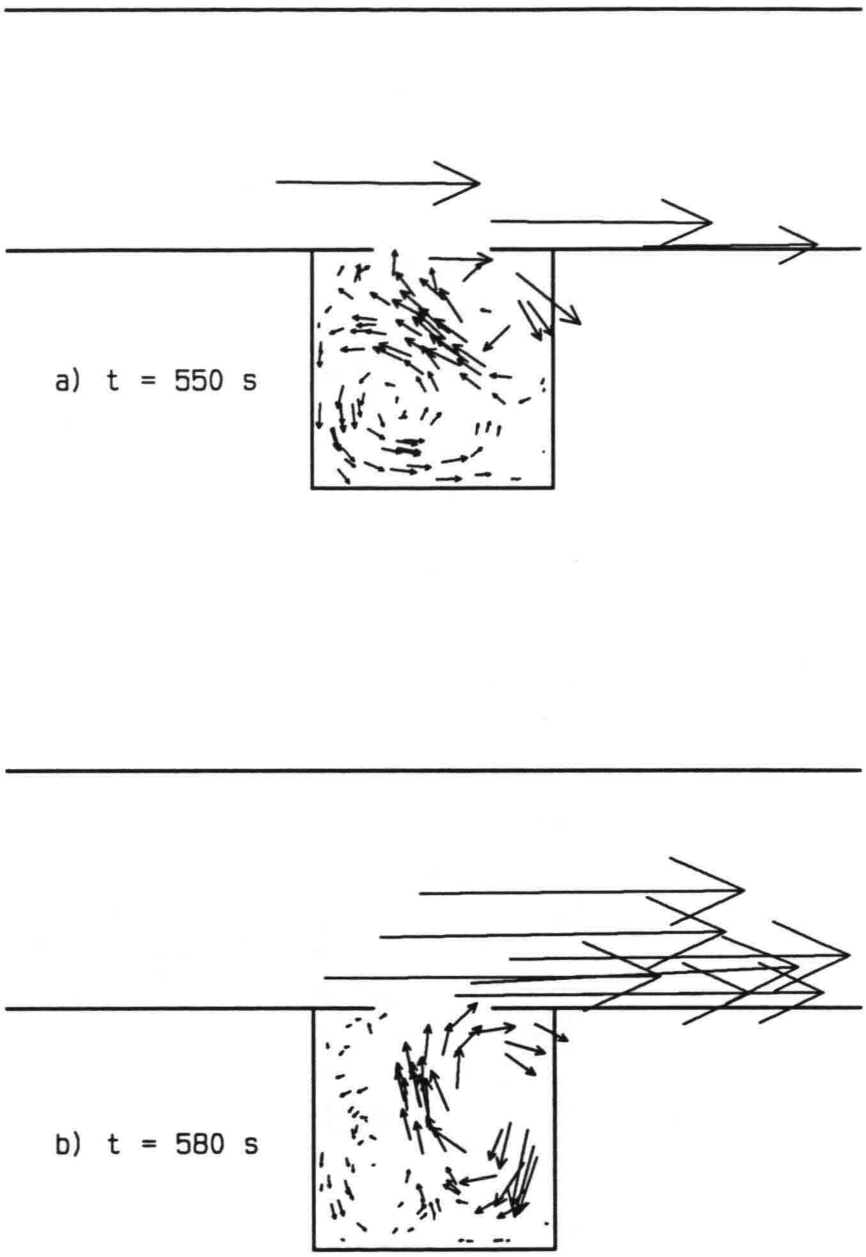

Observed depth averaged flow patterns Model harbor (3)	⟼ = 0.07 m/s
Delft University of Technology	Fig. 3.13

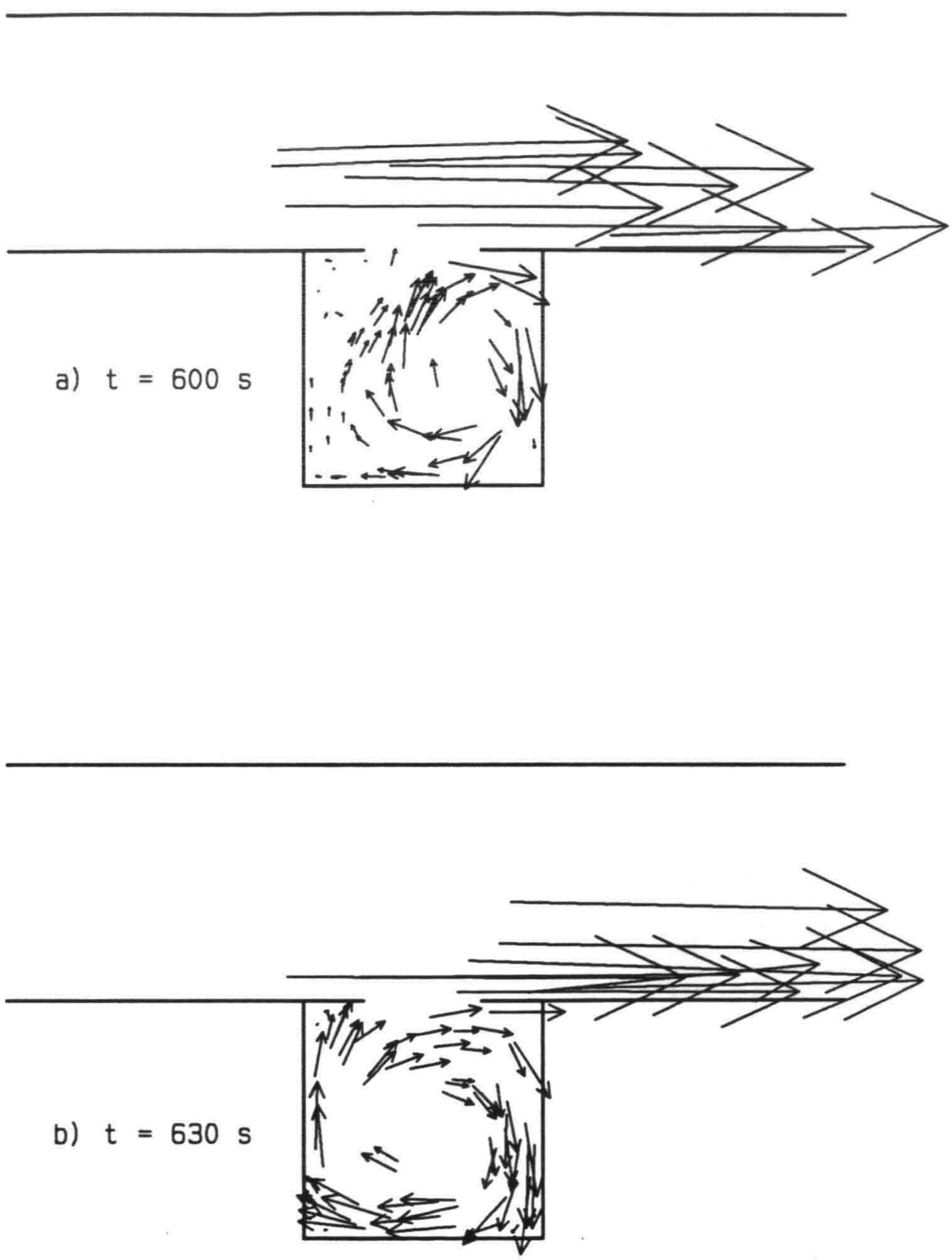

Observed depth averaged flow patterns Model harbor (3)	⟼ = 0.07 m/s
Delft University of Technology	Fig. 3.14

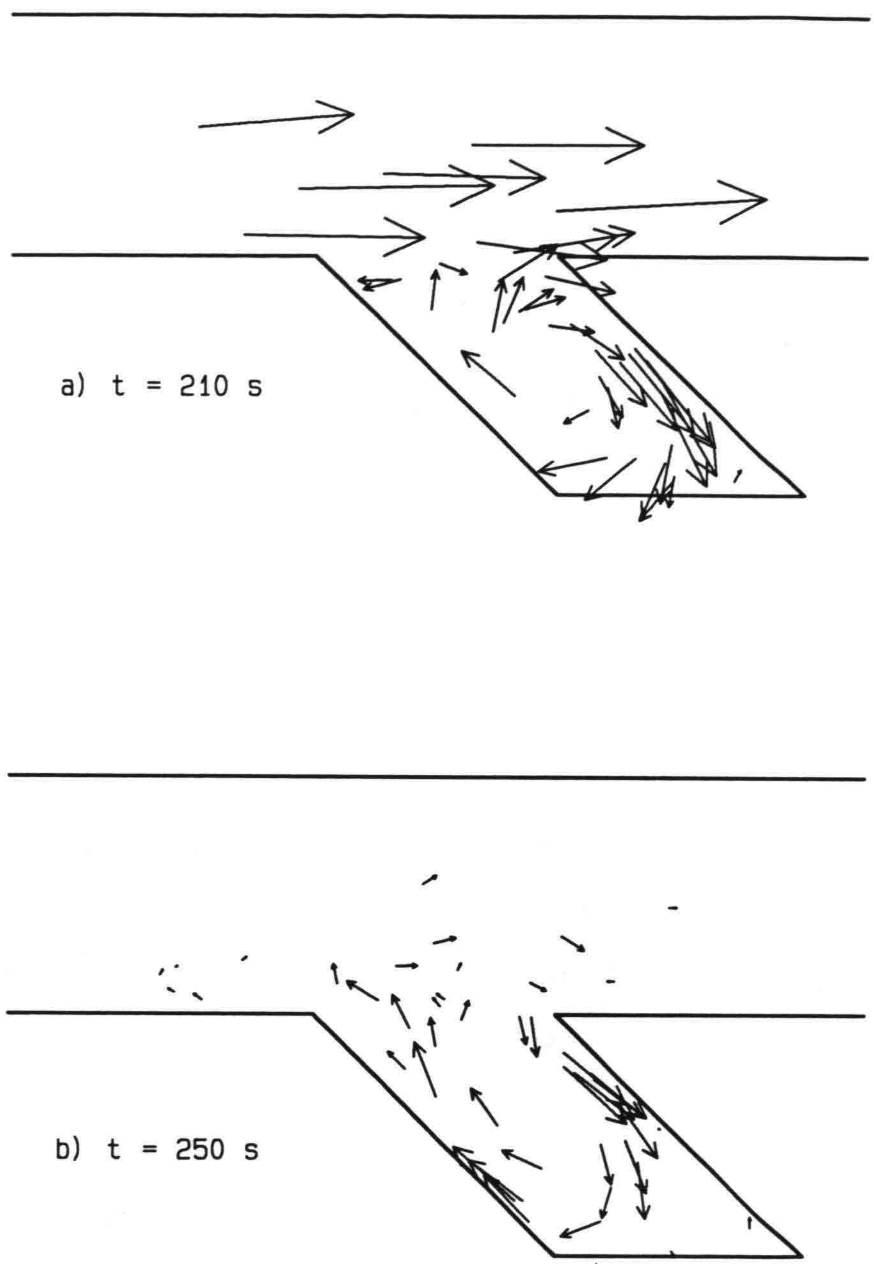

Observed depth averaged flow patterns Model harbor (4)	⟼ = 0.07 m/s
Delft University of Technology	Fig. 3.15

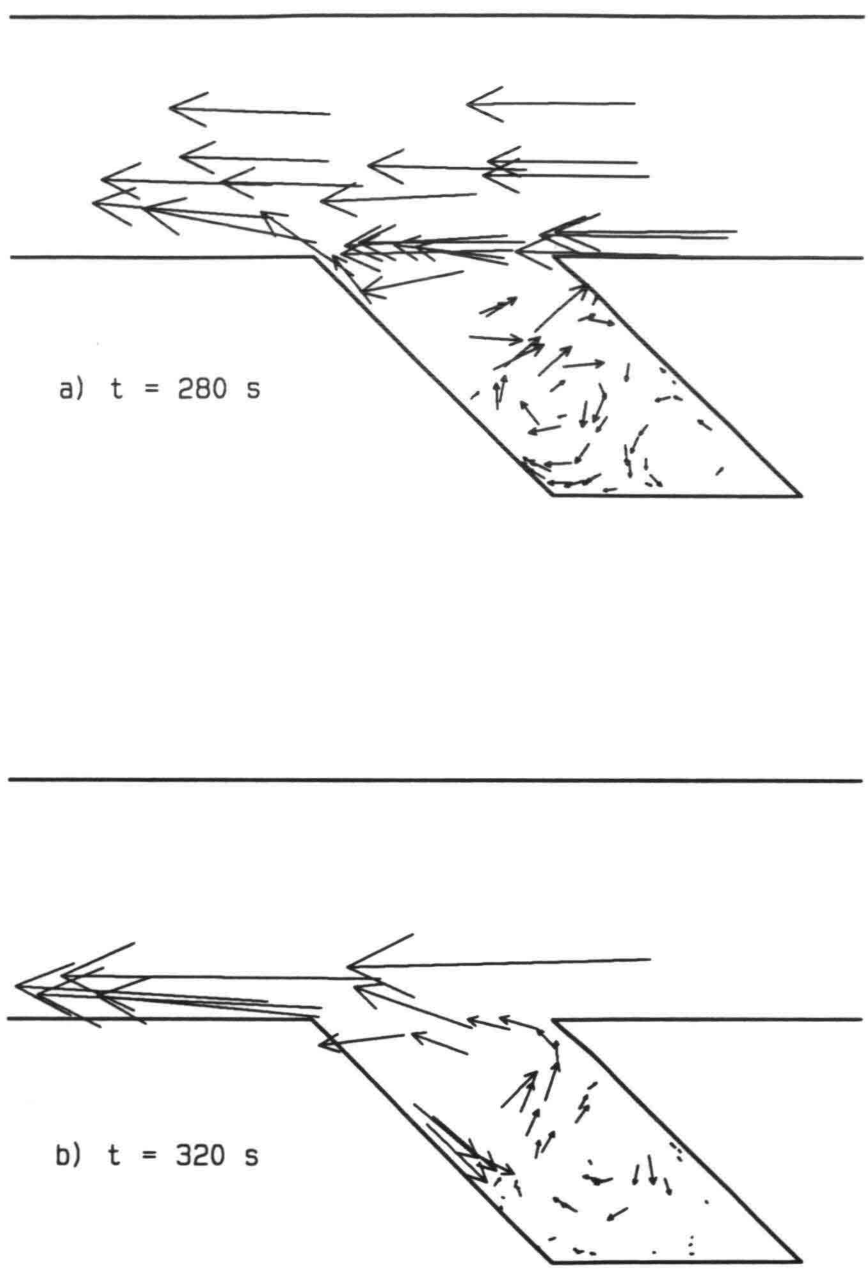

Observed depth averaged flow patterns
Model harbor (4)

⟼ = 0.07 m/s

Delft University of Technology

Fig. 3.16

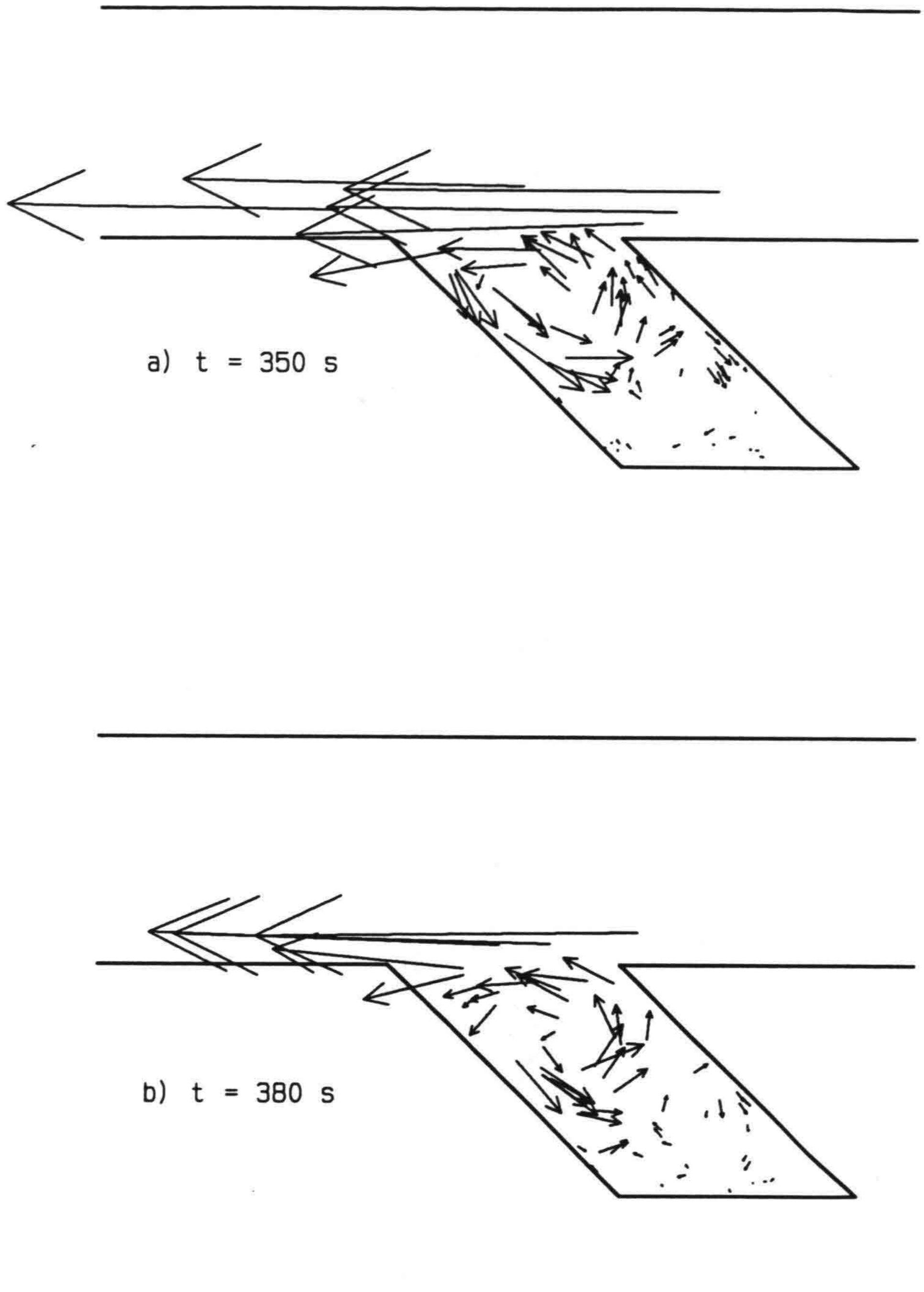

Observed depth averaged flow patterns Model harbor (4)	⟼ = 0.07 m/s
Delft University of Technology	Fig. 3.17

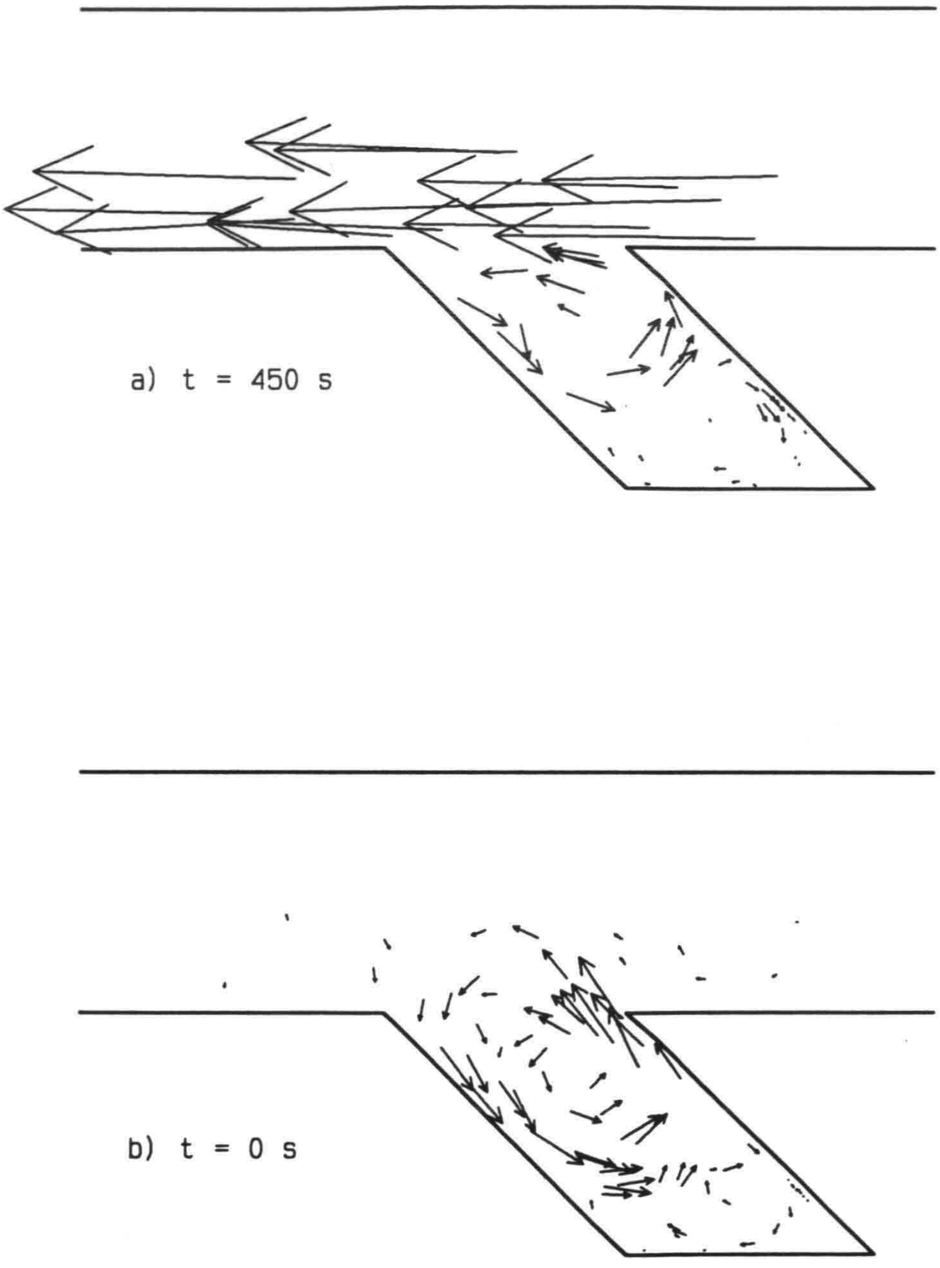

Observed depth averaged flow patterns Model harbor (4)	⟼ = 0.07 m/s
Delft University of Technology	Fig. 3.18

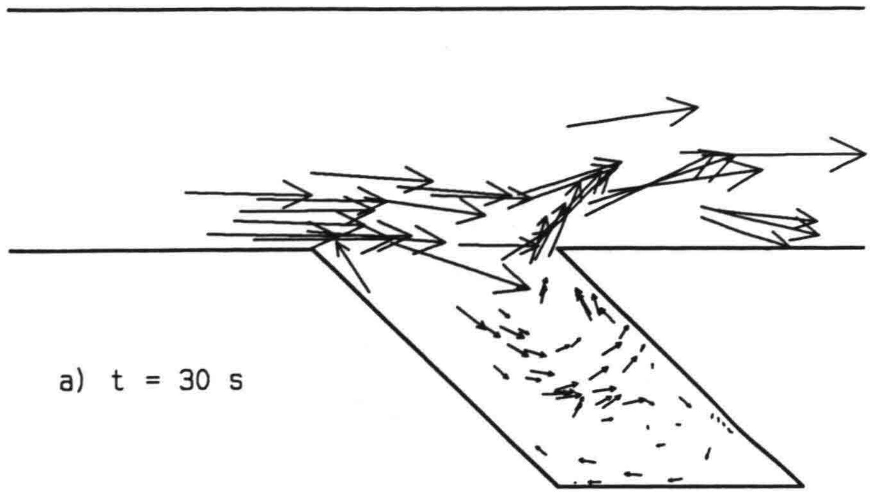

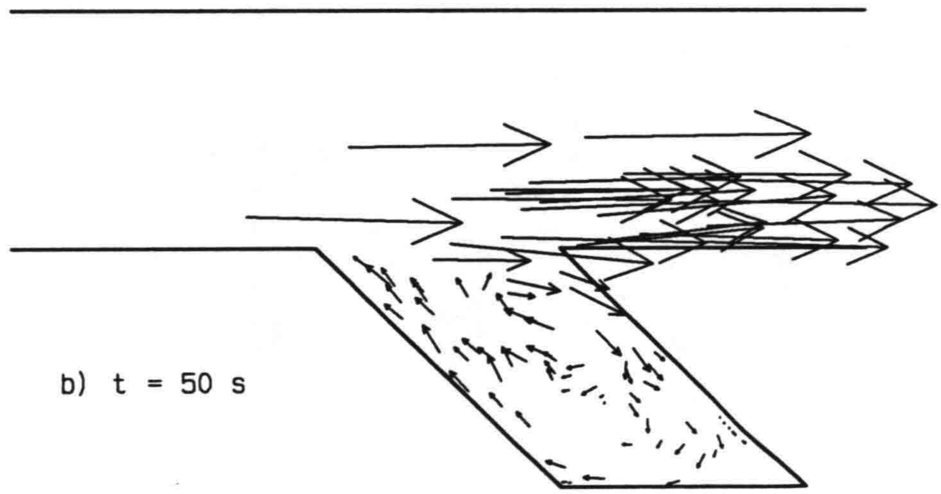

Observed depth averaged flow patterns Model harbor (4)	⟼ = 0.07 m/s
Delft University of Technology	Fig. 3.19

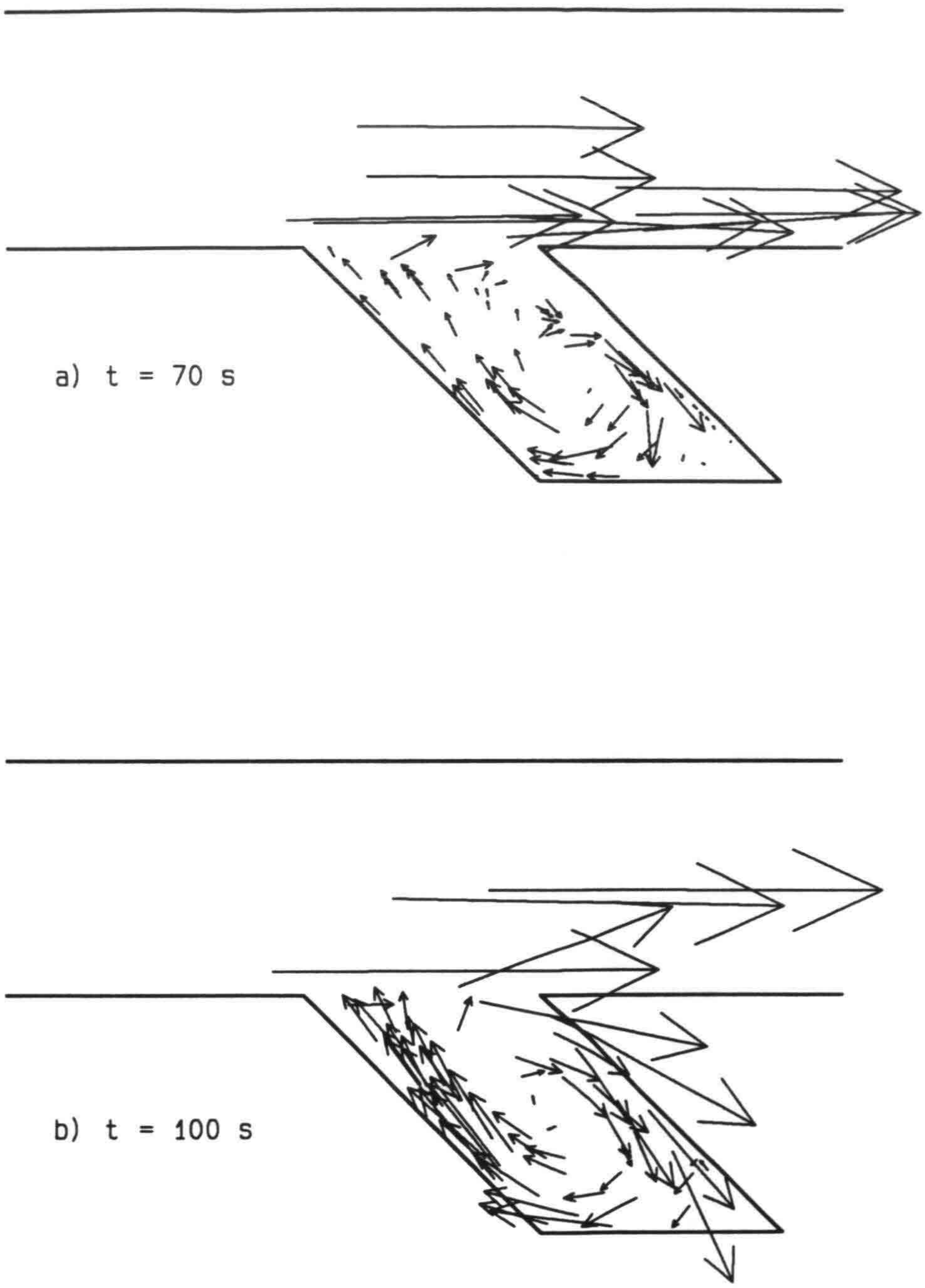

Observed depth averaged flow patterns Model harbor (4)	⟼ = 0.07 m/s
Delft University of Technology	Fig. 3.20

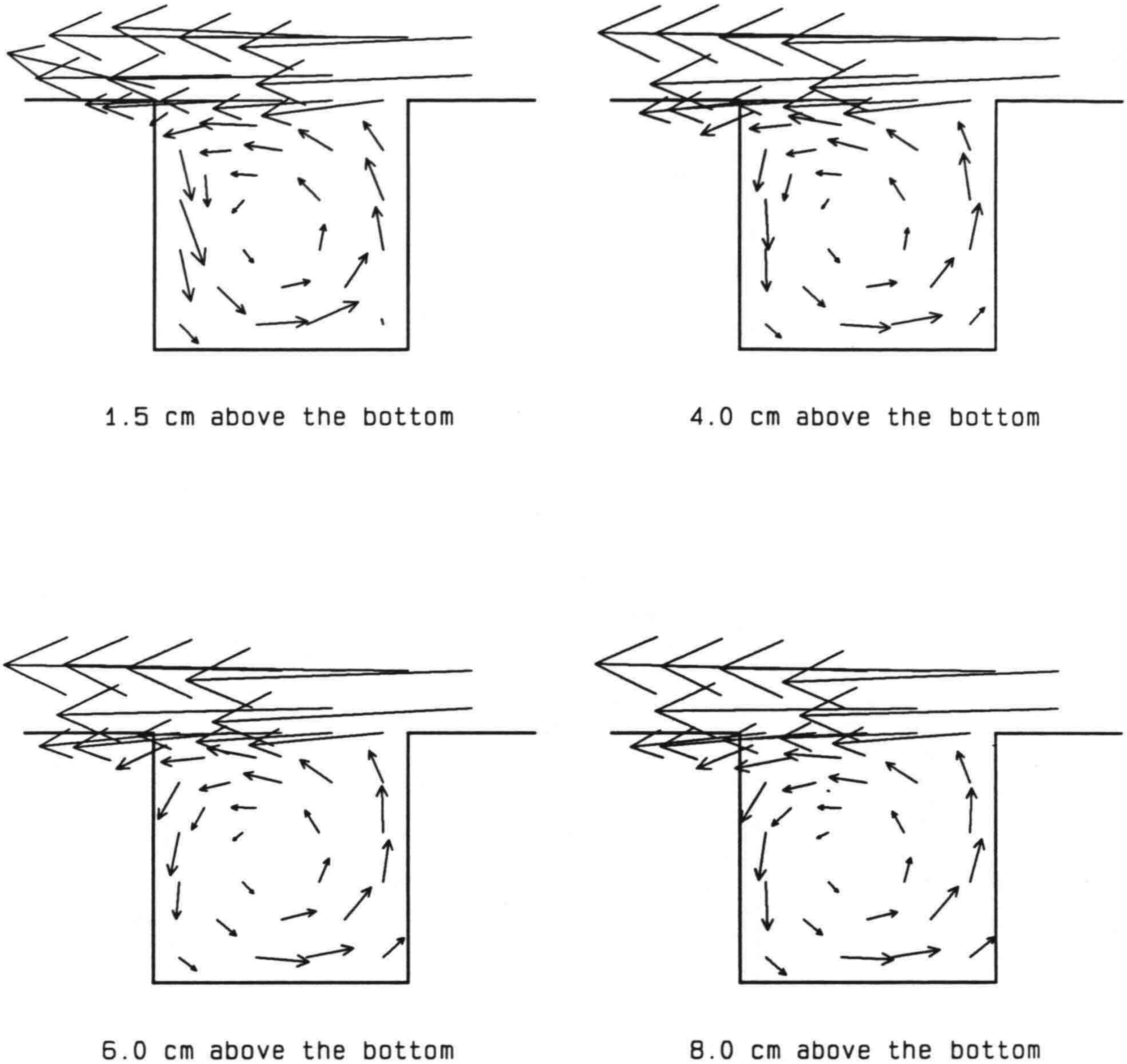

Flow patterns at four levels Experiment 1B	TIME = 375 s ⟼ = 0.10 m/s
Delft University of Technology	Fig. 4.1

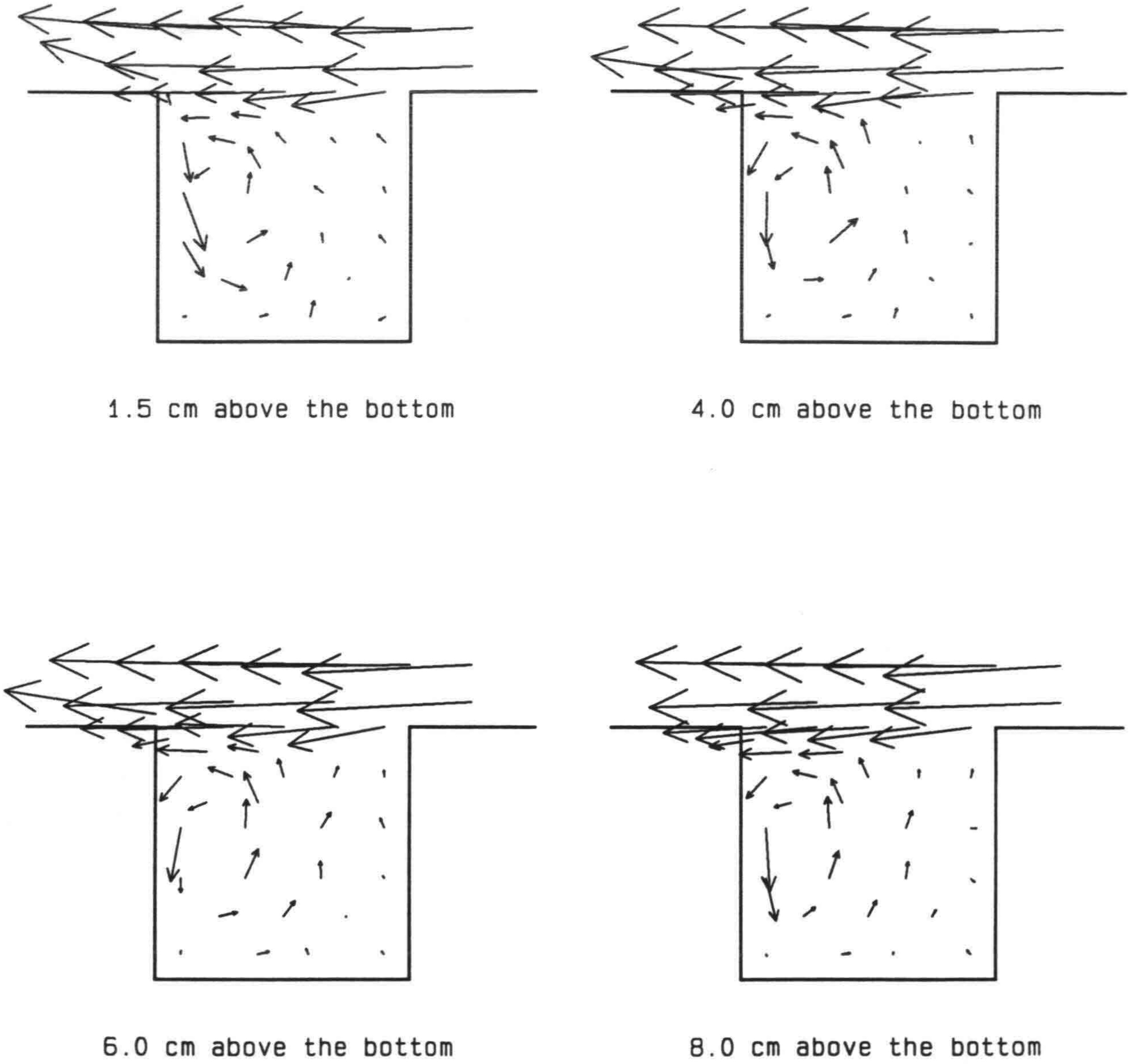

Flow patterns at four levels Experiment 1B	TIME = 300 s ⟼ = 0.10 m/s
Delft University of Technology	Fig. 4.2

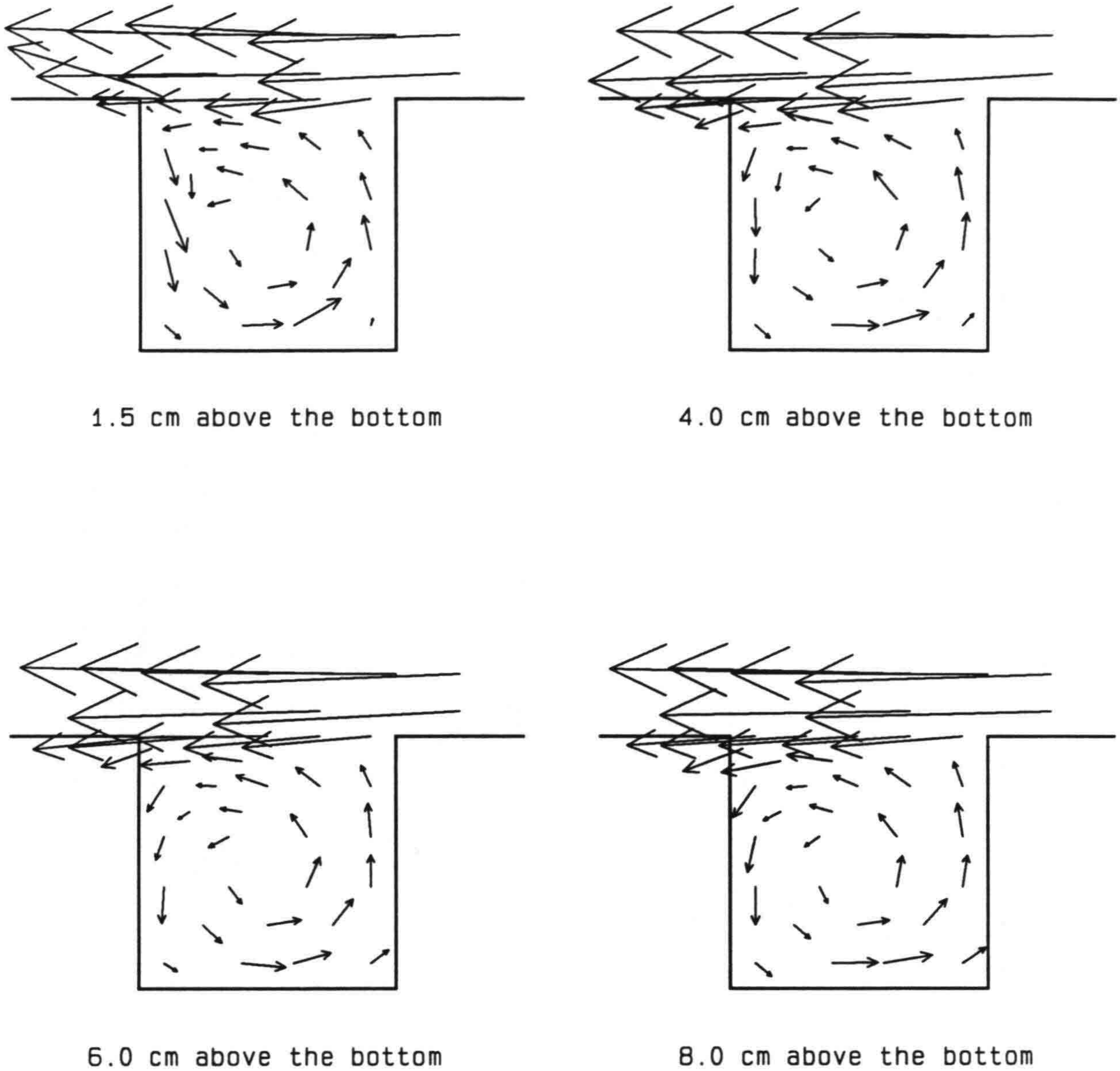

Flow patterns at four levels
Experiment 1B

TIME = 340 s

$\longmapsto$ = 0.10 m/s

Delft University of Technology

Fig. 4.3

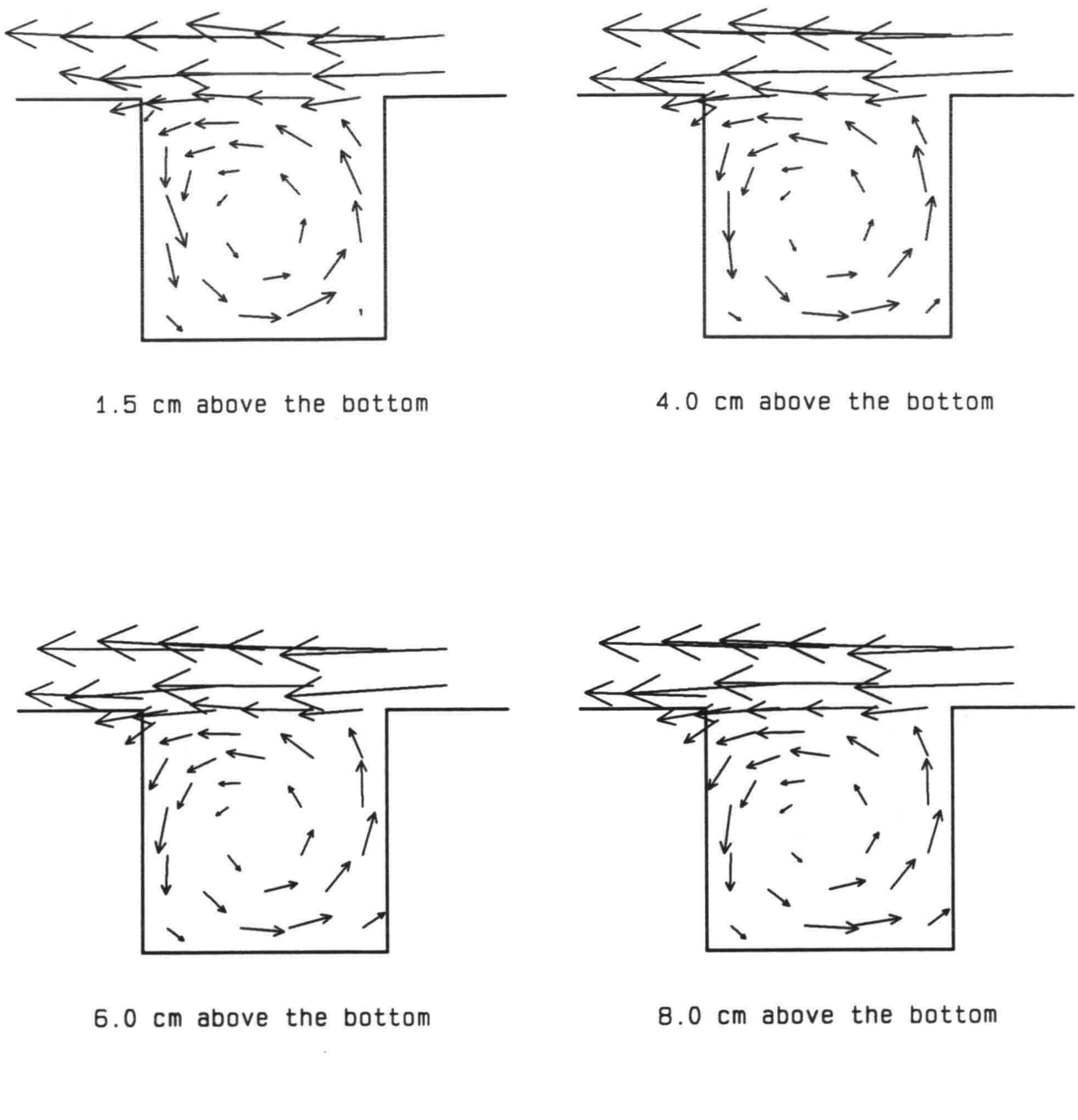

Flow patterns at four levels Experiment 1B	TIME = 450 s ⟼ = 0.10 m/s
Delft University of Technology	Fig. 4.4

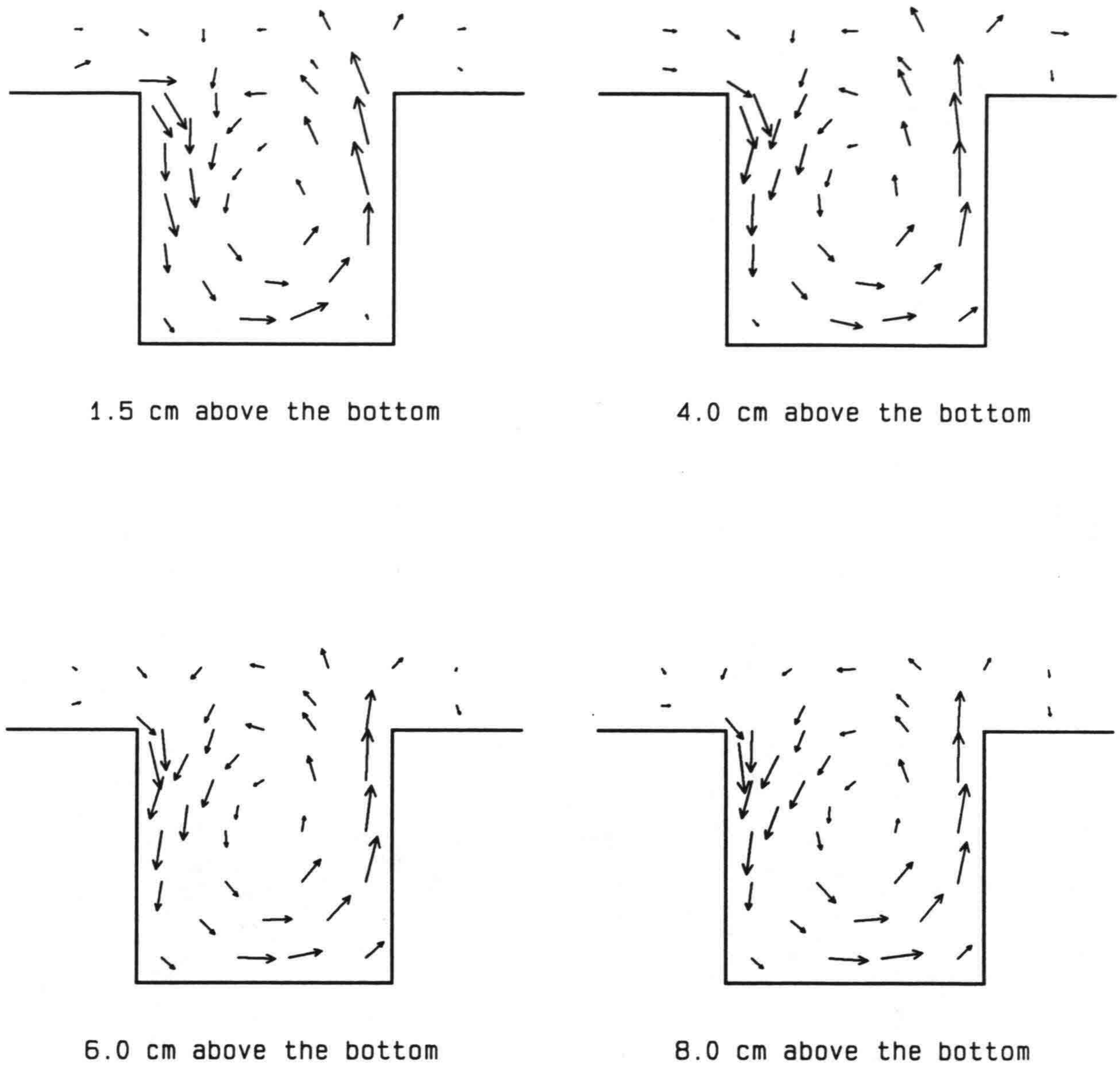

Flow patterns at four levels
Experiment 1B

TIME = 500 s

⟼ = 0.10 m/s

Delft University of Technology

Fig. 4.5

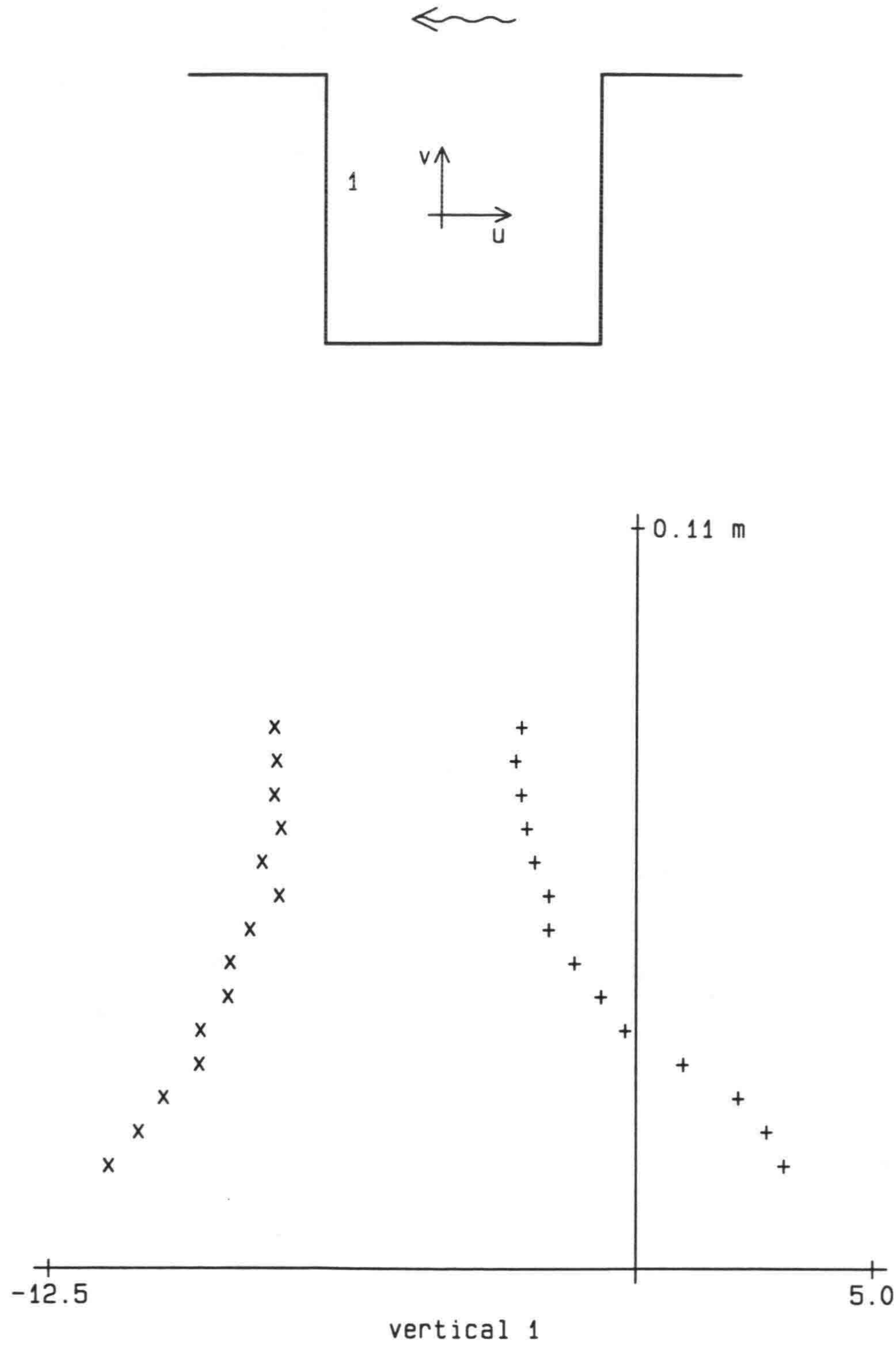

Velocity distribution in the water column (Model harbor 1).

TIME = 375 s
+ = u [cm/s]
x = v

Delft University of Technology

Fig. 4.6

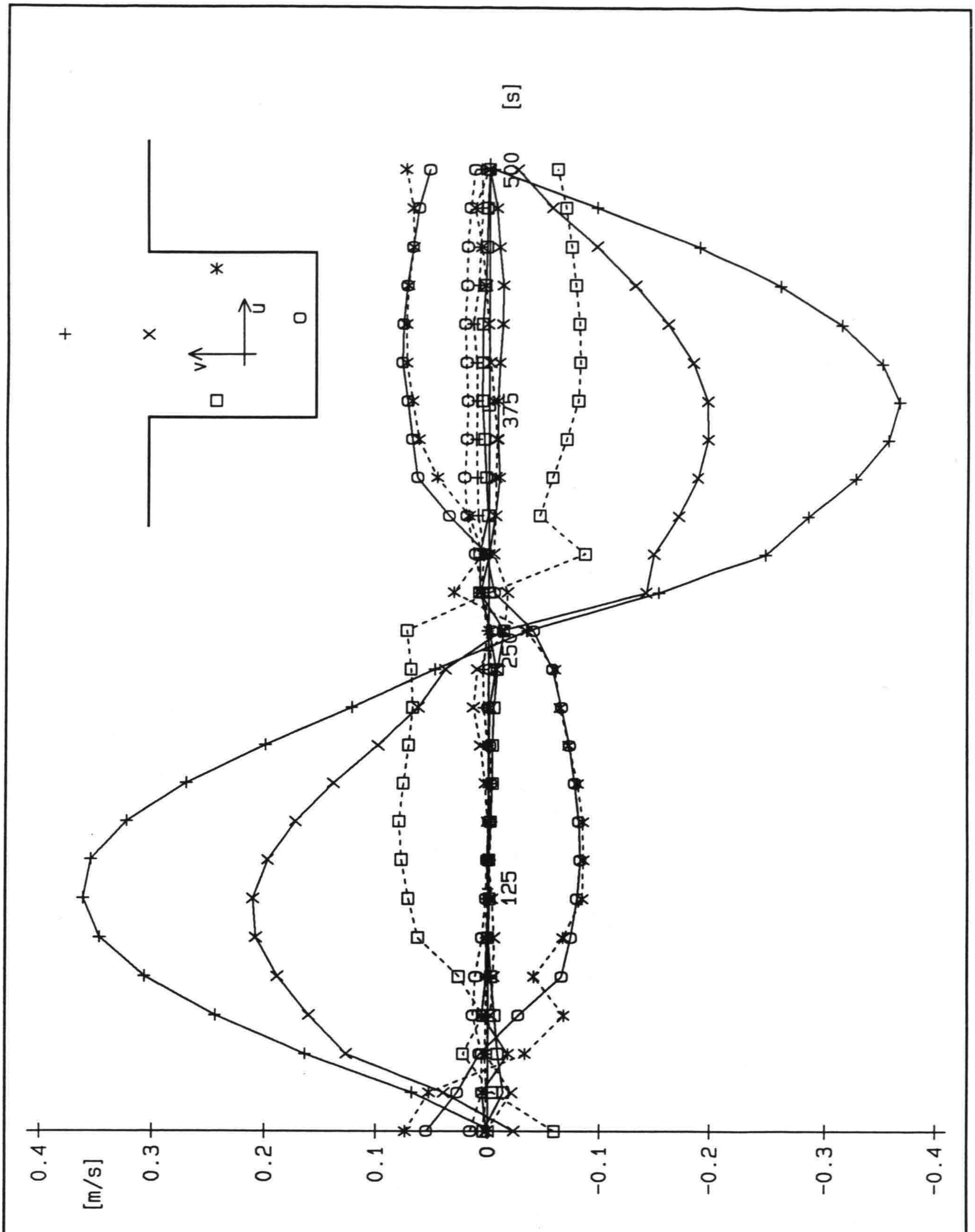

Time histories of depth averaged velocity components (Experiment 1B).	—— = u ------ = v
Delft University of Technology	Fig. 4.7

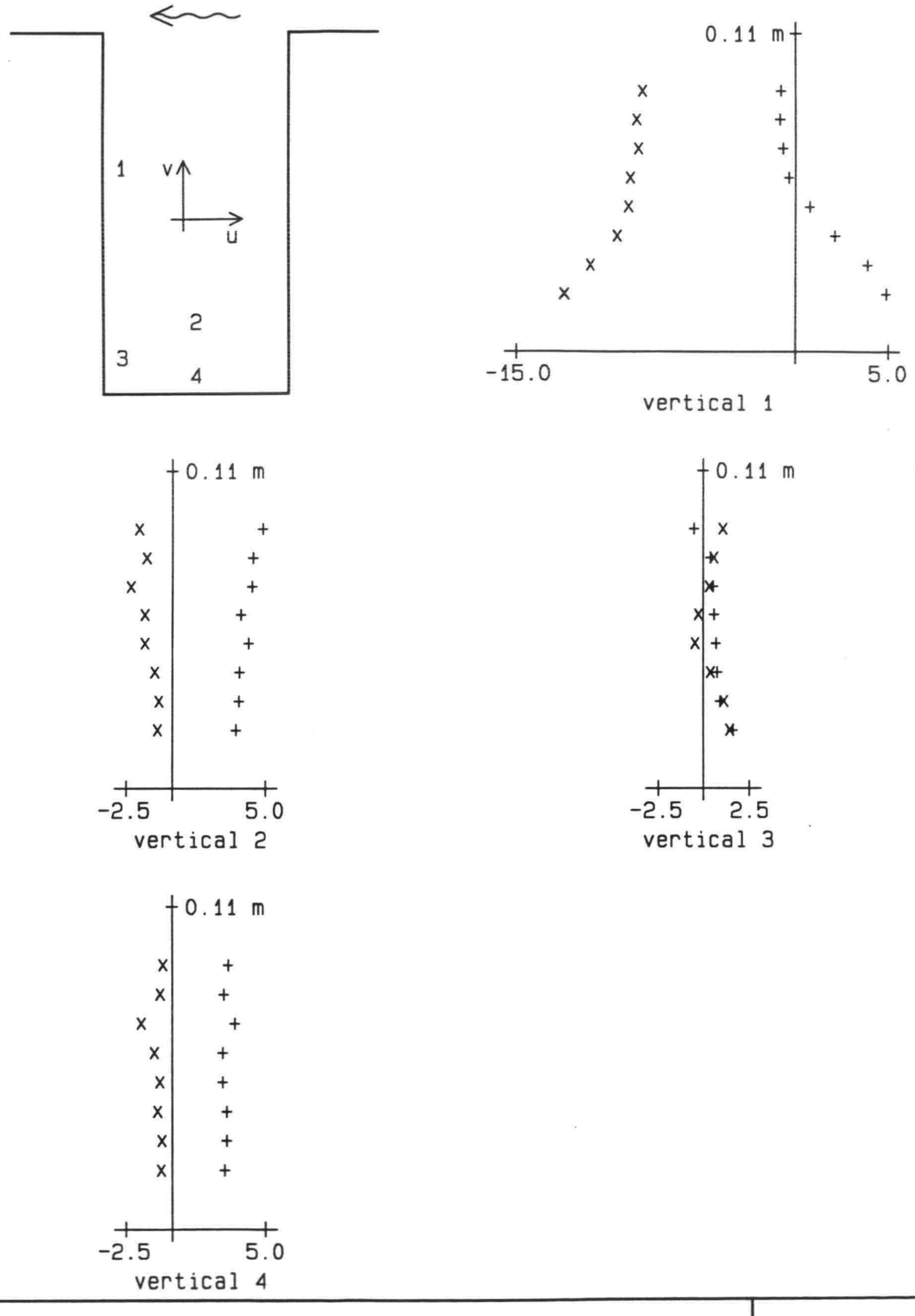

Velocity distributions in the water column (Model harbor 2).	TIME = 375 s + = u [cm/s] x = v
Delft University of Technology	Fig. 4.8

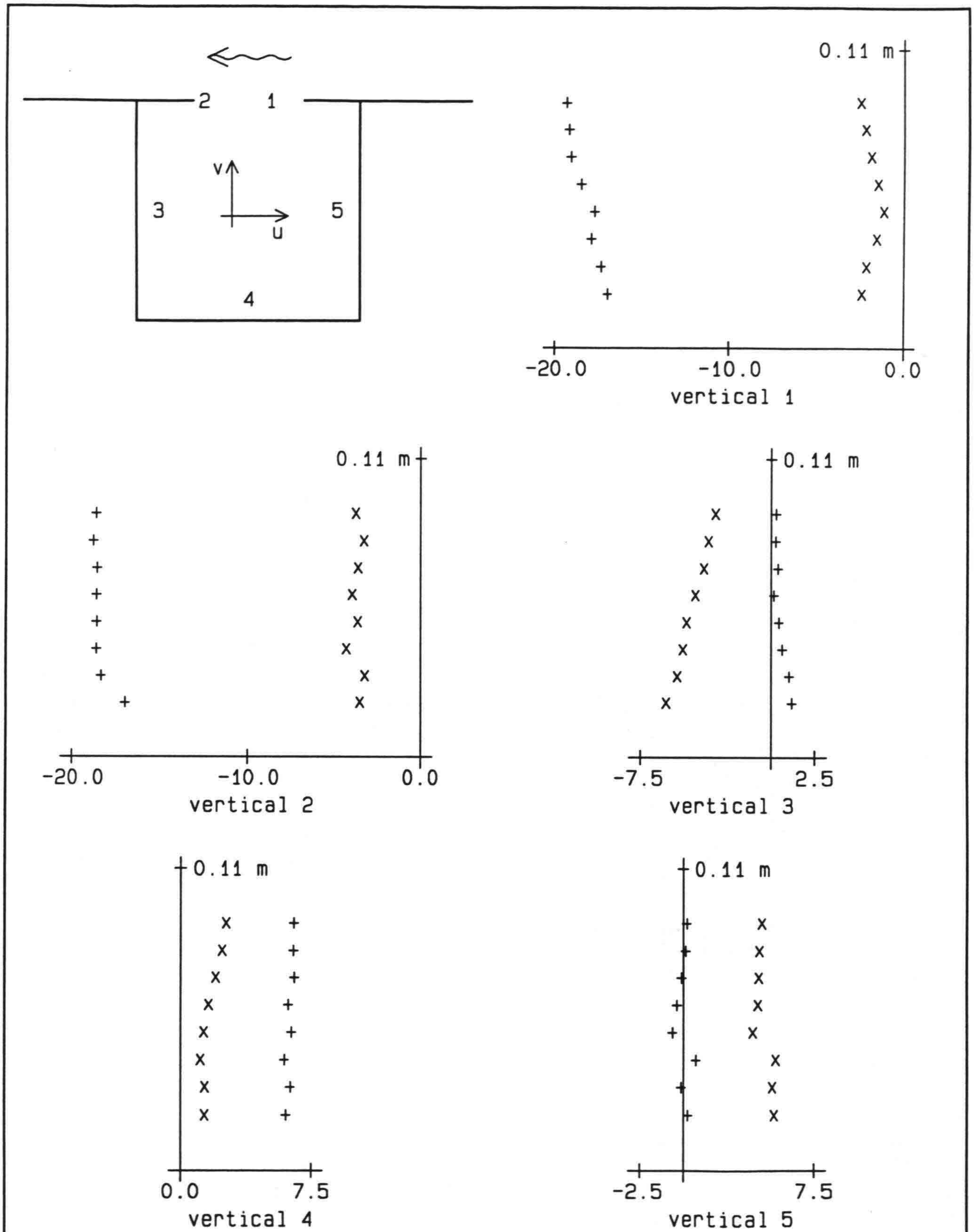

Velocity distributions in the water column (Model harbor 3).

TIME = 375 s
+ = u [cm/s]
x = v

Delft University of Technology

Fig. 4.9

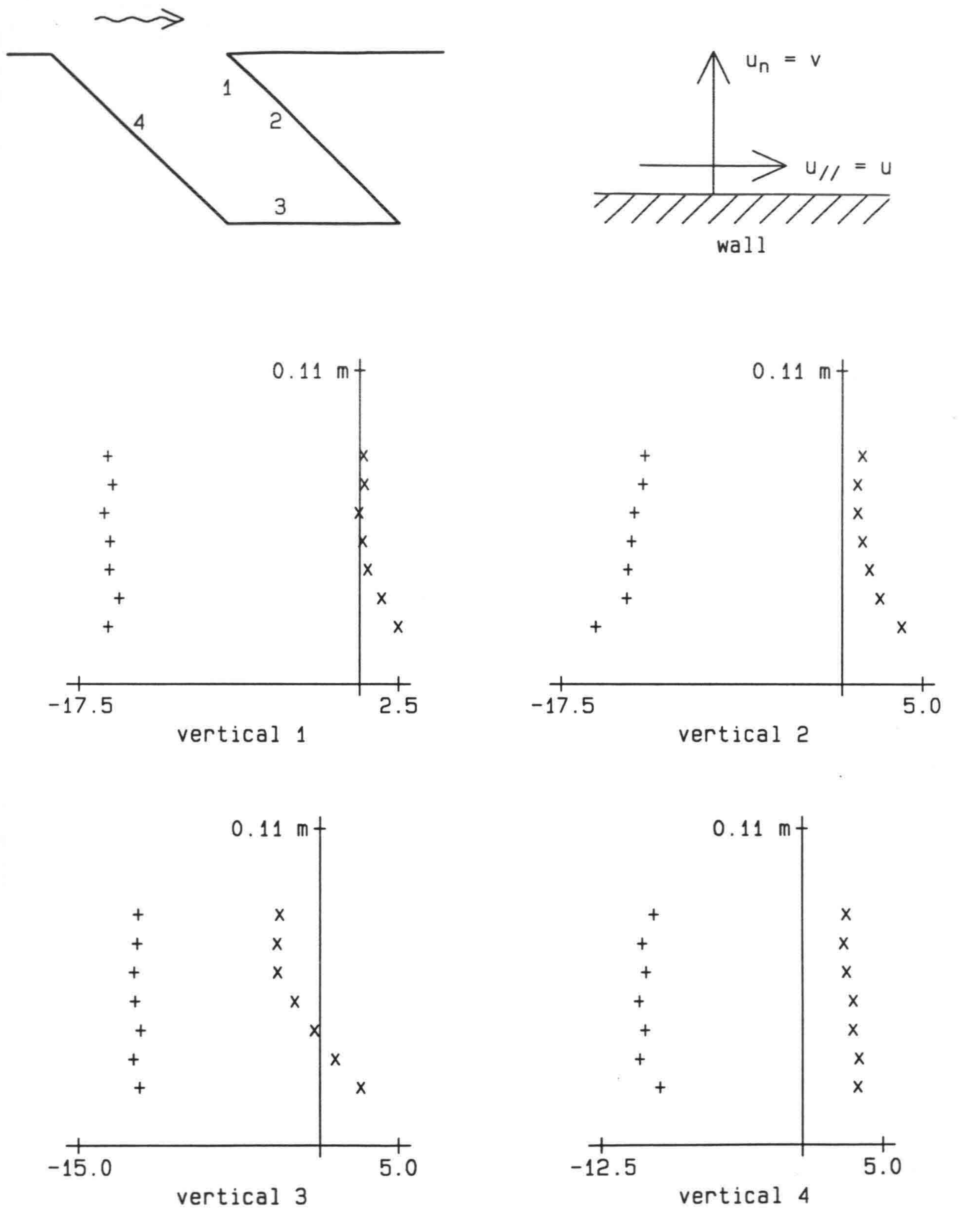

Velocity distributions in the water column (Model harbor 4).	TIME = 125 s + = u x = v [cm/s]
Delft University of Technology	Fig. 4.10

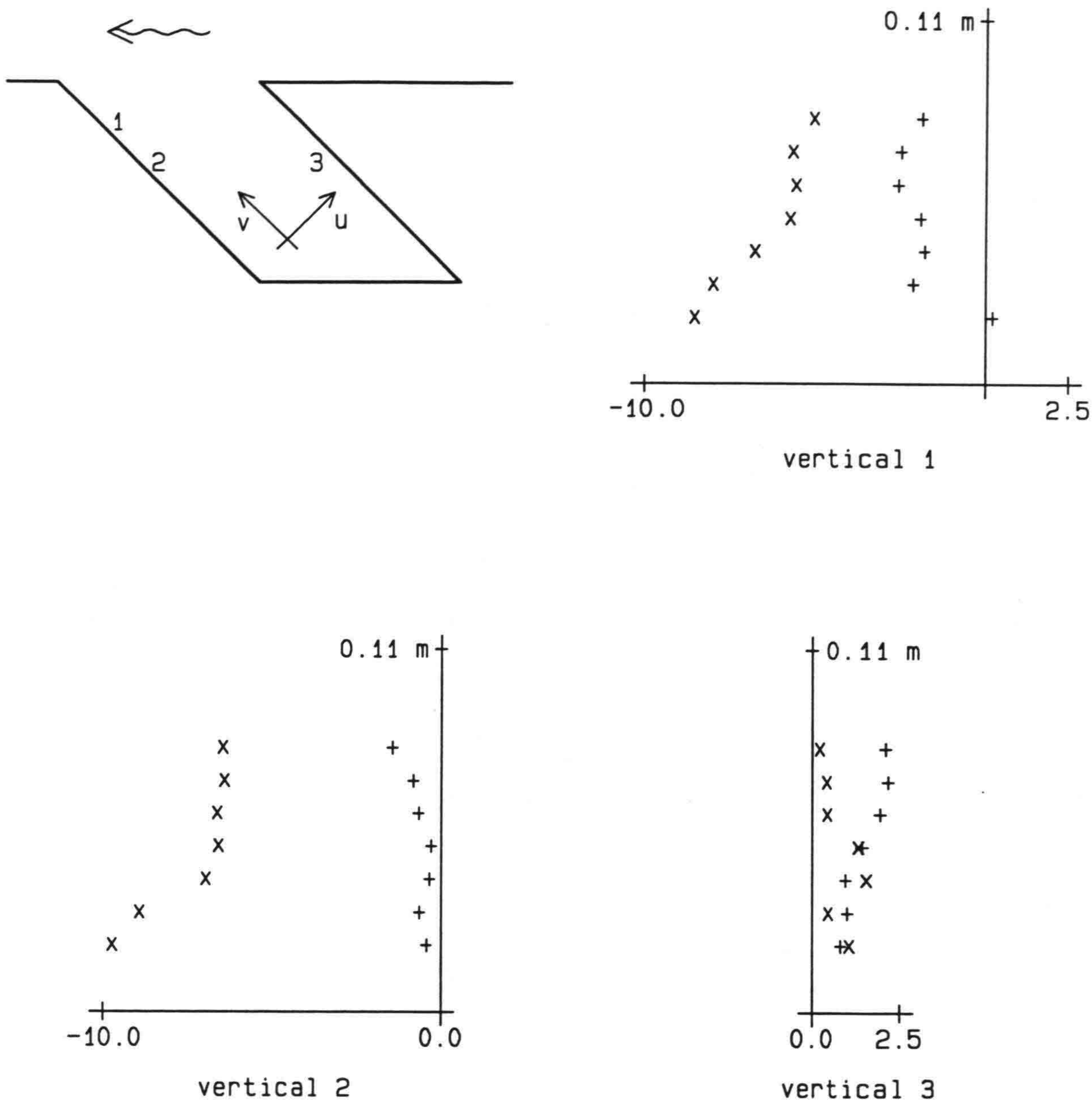

Velocity distributions in the water column (Model harbor 4).	TIME = 375 s + = u x = v [cm/s]
Delft University of Technology	Fig. 4.11

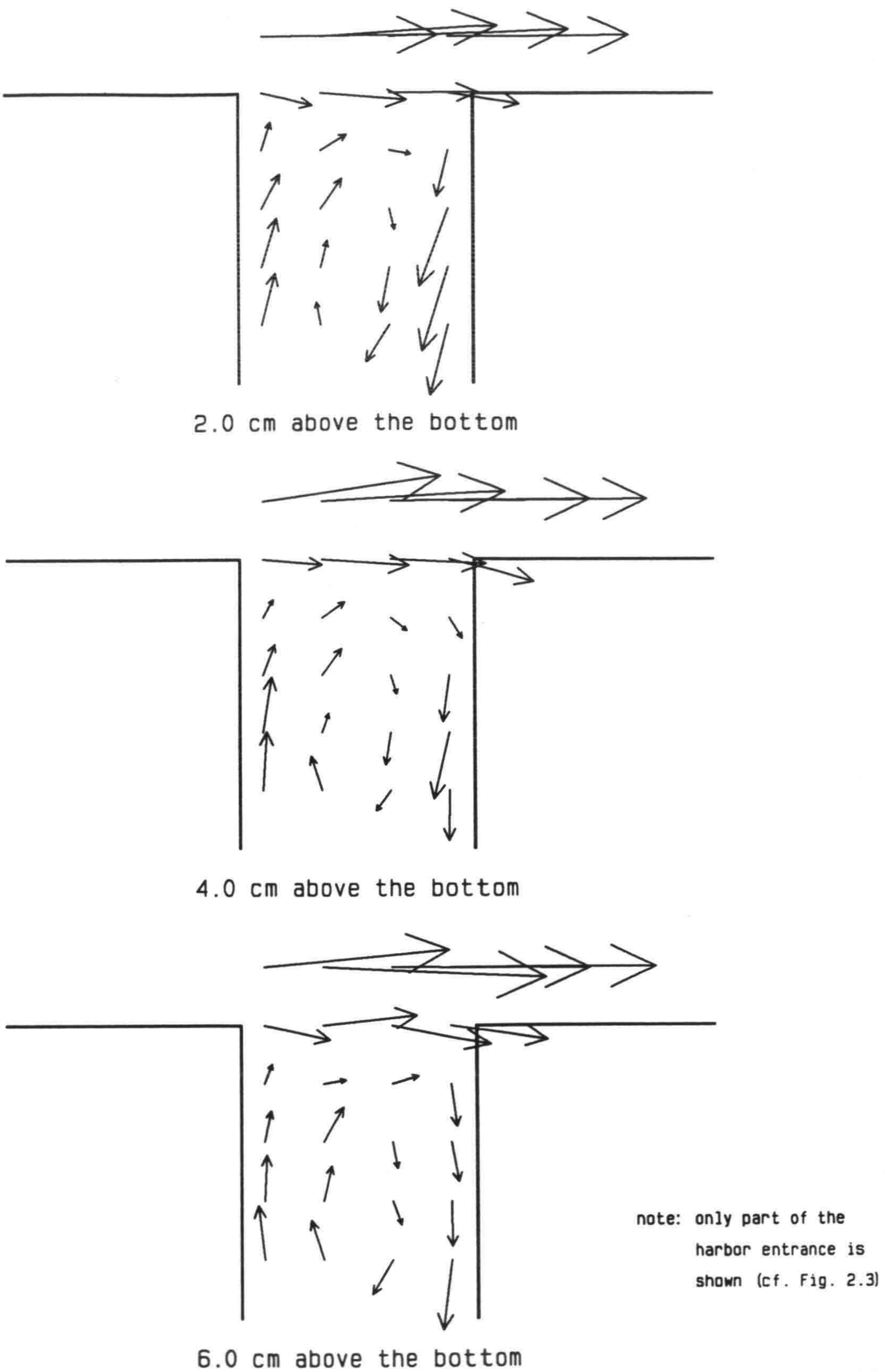

Flow patterns at three levels
Experiment 5

TIME = 125 s

⟼ = 0.10 m/s

Delft University of Technology

Fig. 4.12

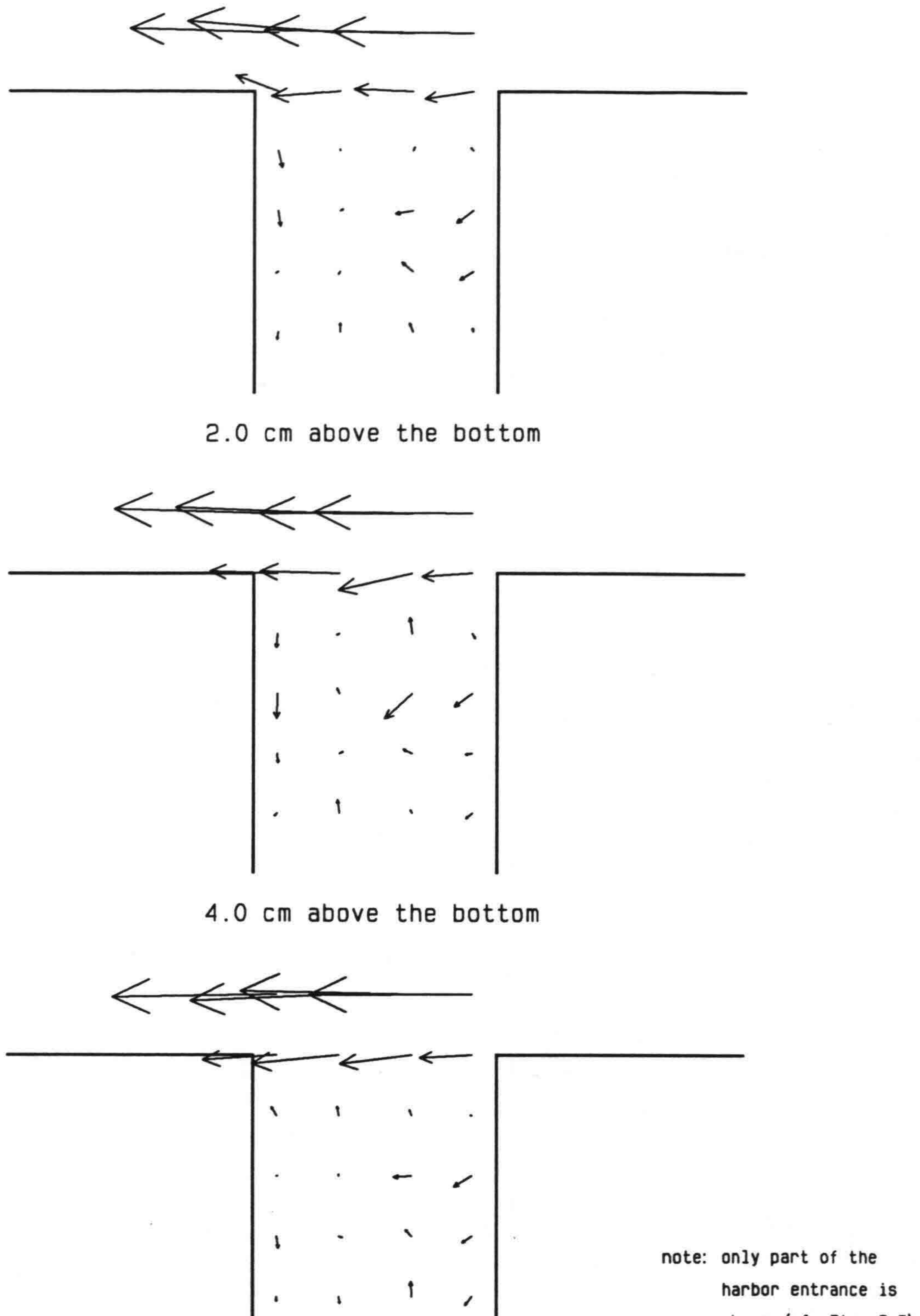

Flow patterns at three levels Experiment 5	TIME = 375 s ⟼ = 0.10 m/s
Delft University of Technology	Fig. 4.13

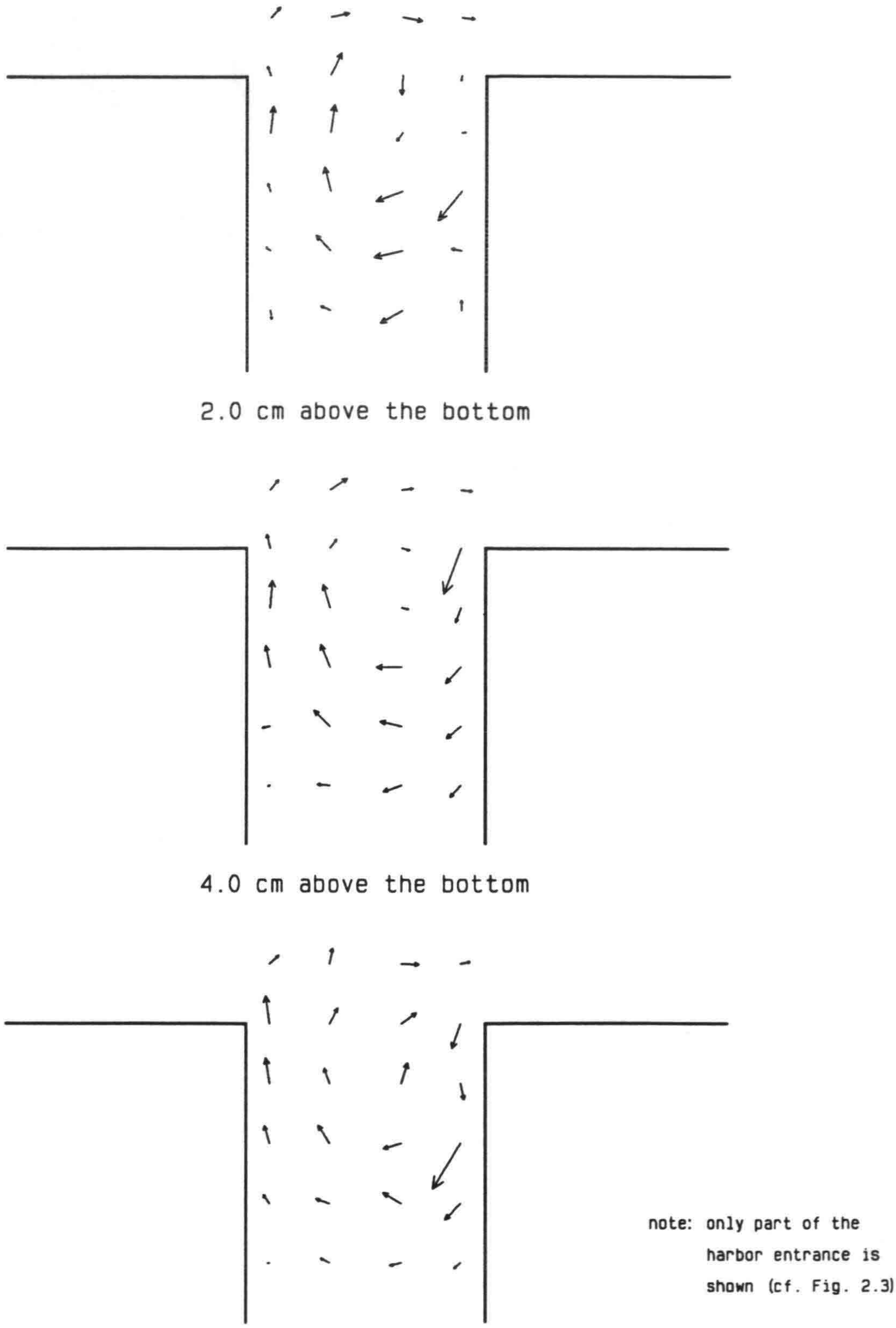

Flow patterns at three levels Experiment 5	TIME = 250 s ⟼ = 0.10 m/s
Delft University of Technology	Fig. 4.14

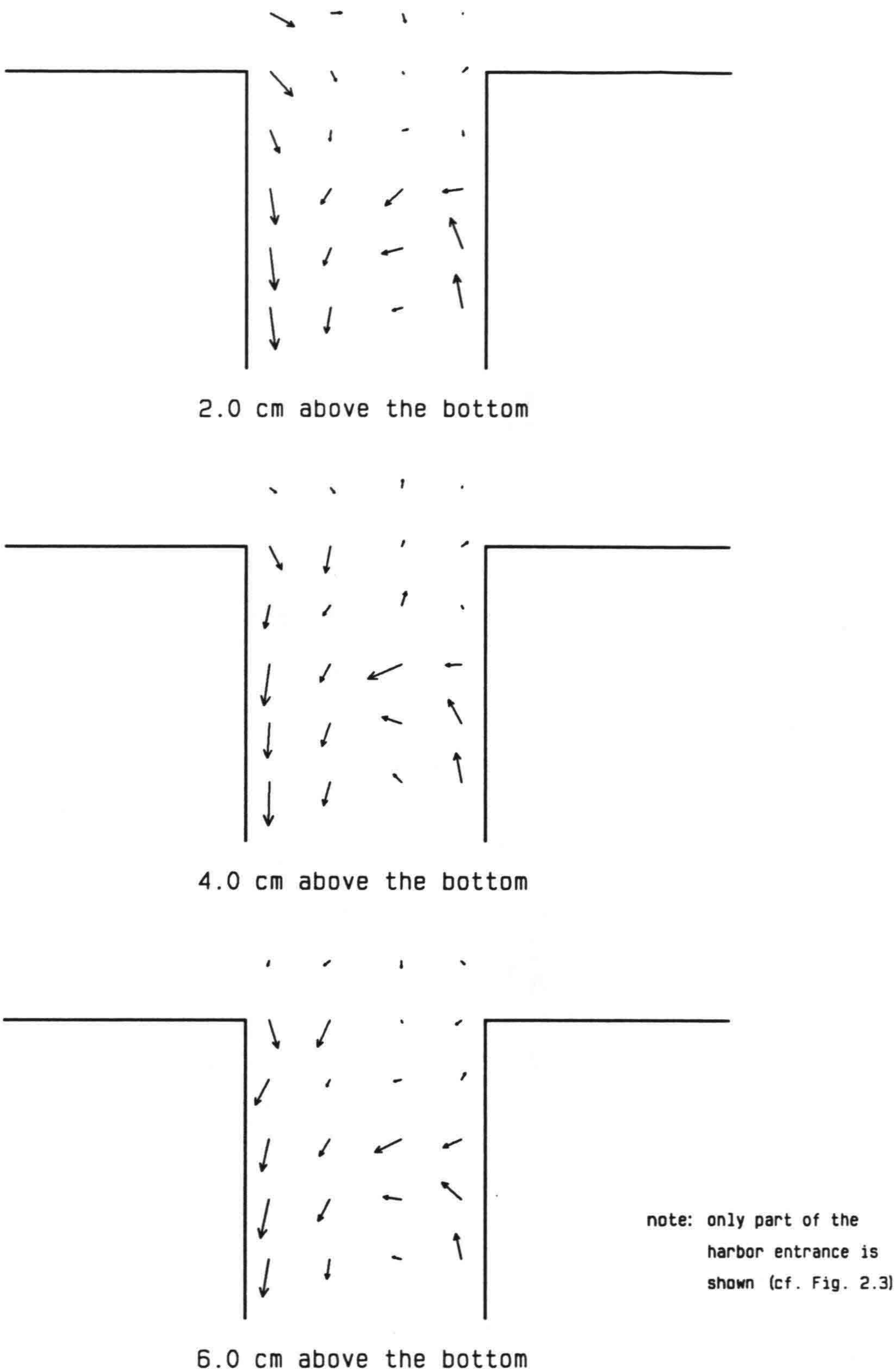

Flow patterns at three levels Experiment 5	TIME = 500 s ⟼ = 0.10 m/s
Delft University of Technology	Fig. 4.15

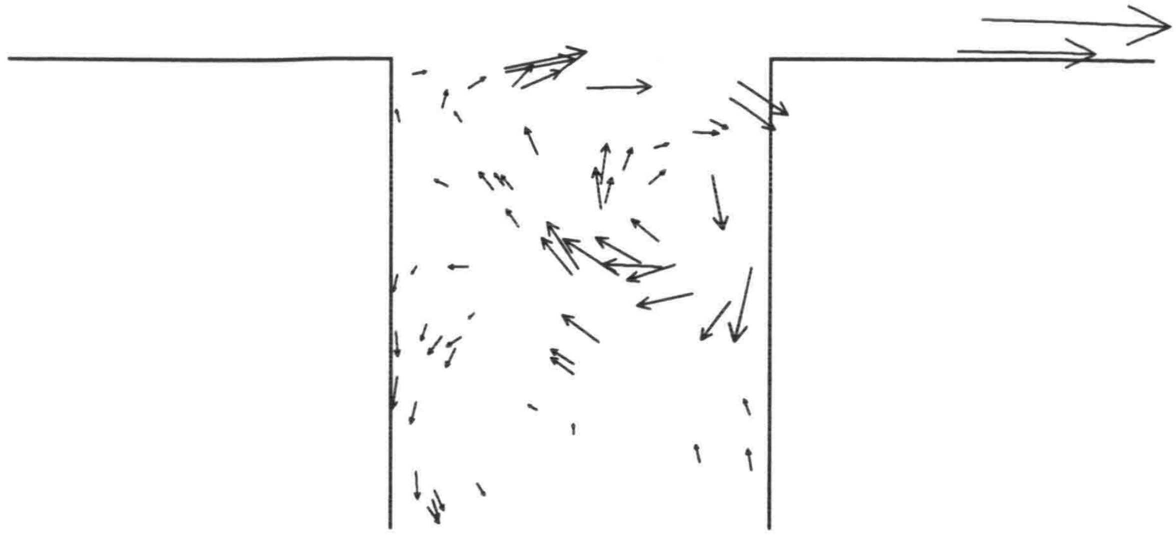

Experiment 2B

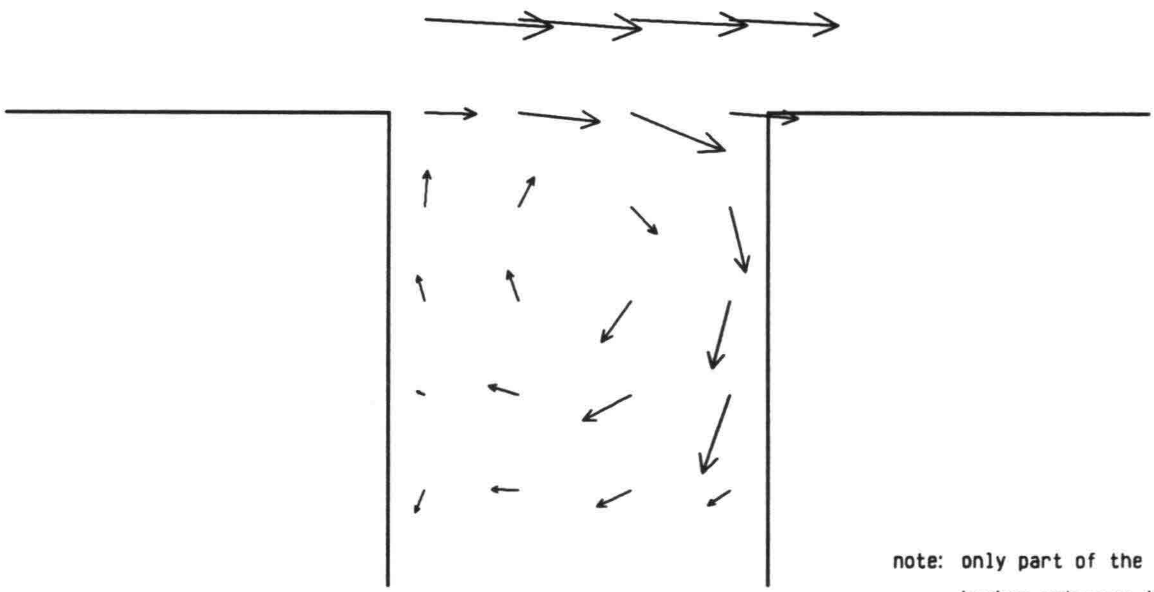

note: only part of the harbor entrance is shown (cf. Fig. 2.3)

Experiment 5

Observed depth averaged flow patterns	TIME = 50 s ⟼ = 0.10 m/s
Delft University of Technology	Fig. 4.16

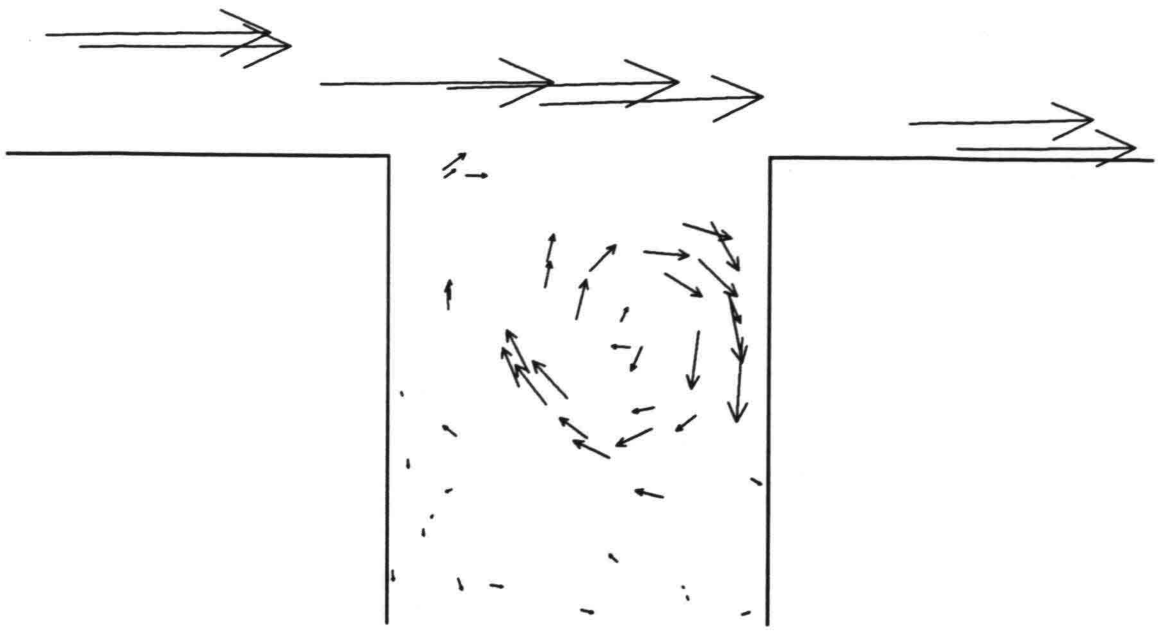

Experiment 2B

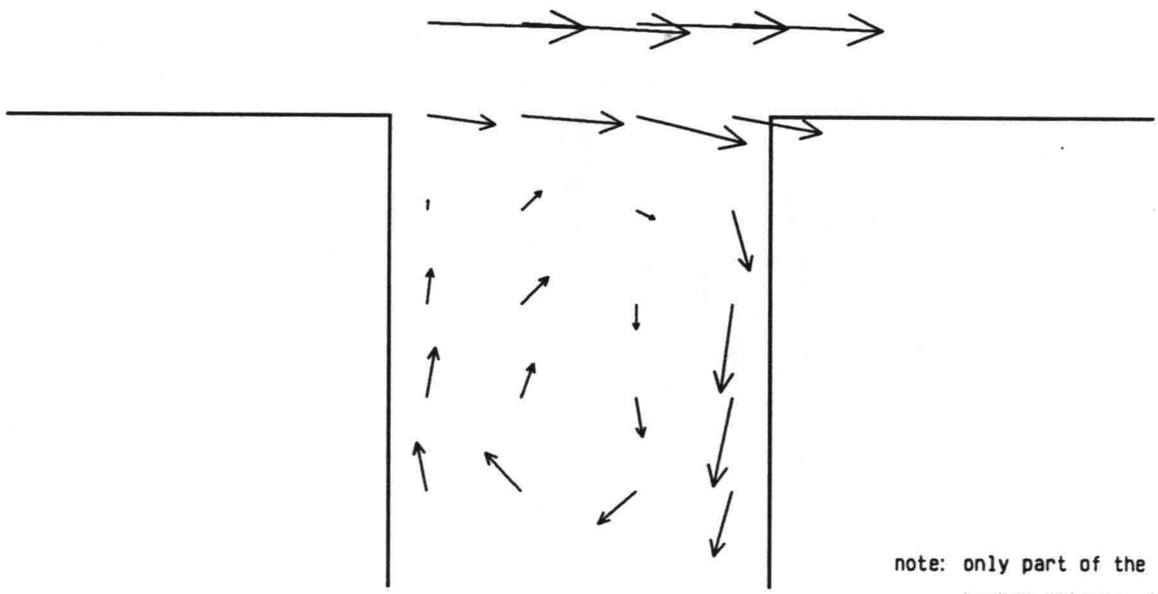

note: only part of the
harbor entrance is
shown (cf. Fig. 2.3)

Experiment 5

Observed depth averaged flow patterns	TIME = 70 s ⟼ = 0.10 m/s
Delft University of Technology	Fig. 4.17

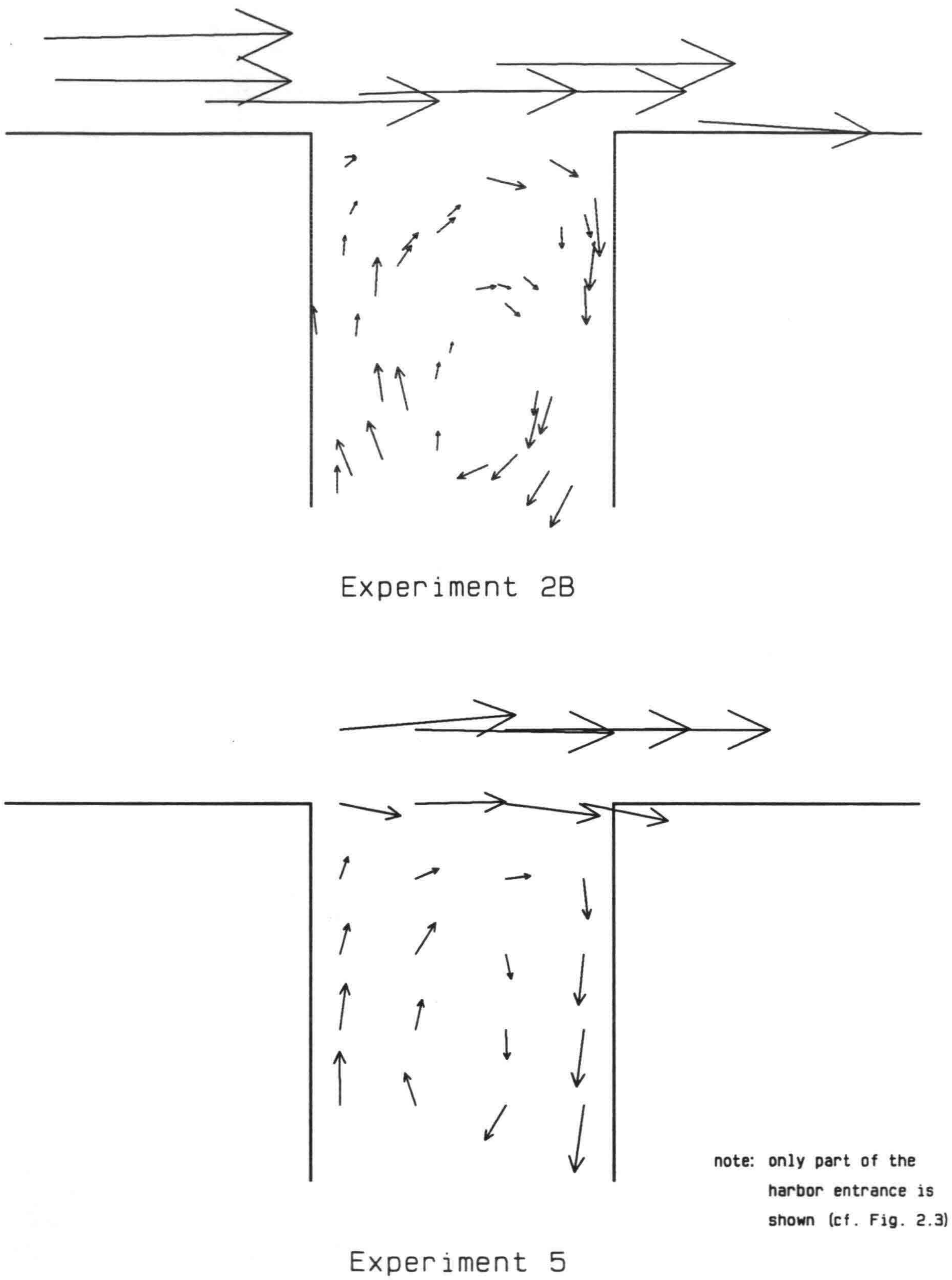

Observed depth averaged flow patterns	TIME = 120 s ⟼ = 0.10 m/s
Delft University of Technology	Fig. 4.18

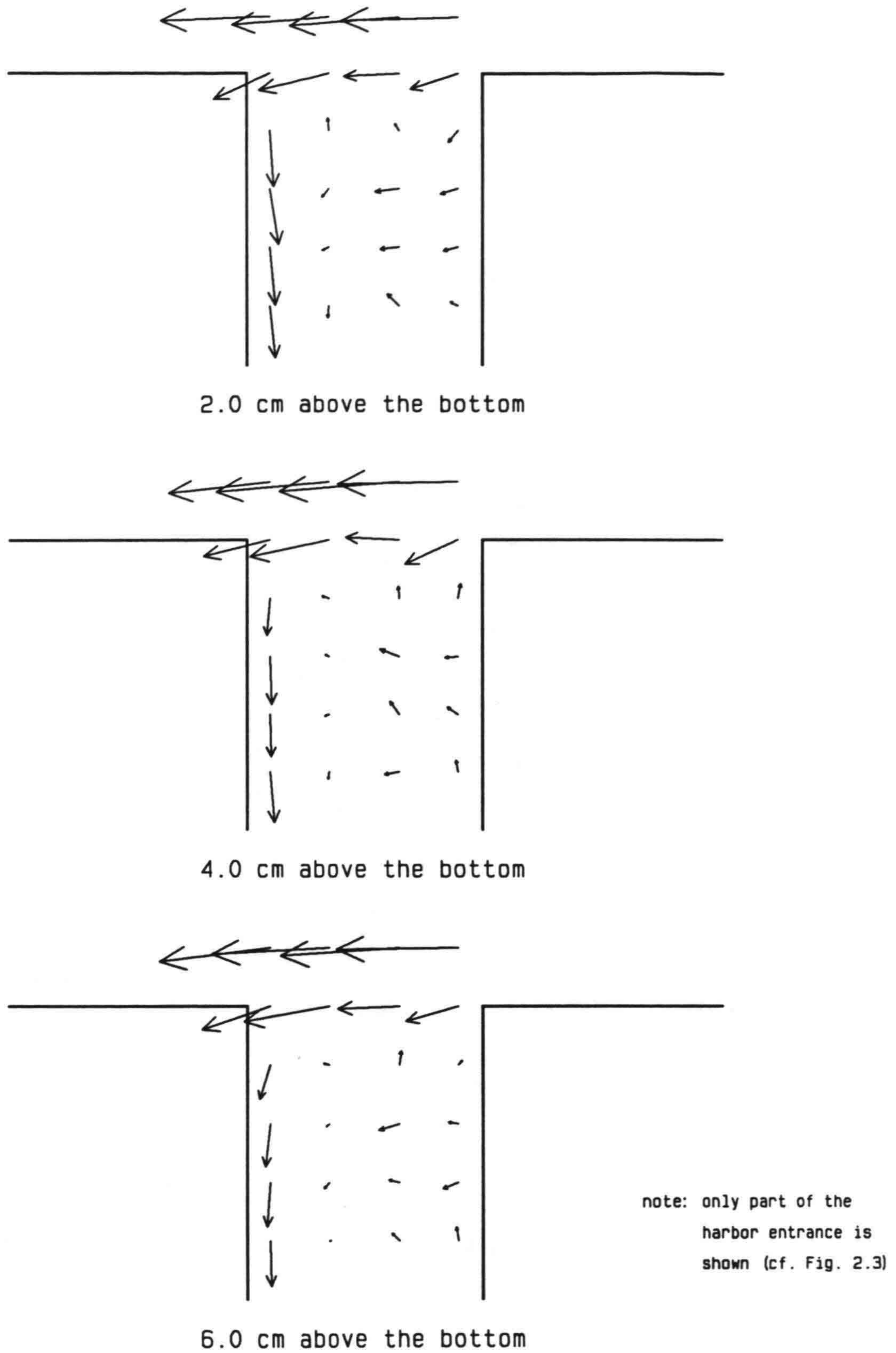

Flow patterns at three levels Experiment 5	TIME = 425 s ⟼ = 0.10 m/s
Delft University of Technology	Fig. 4.19

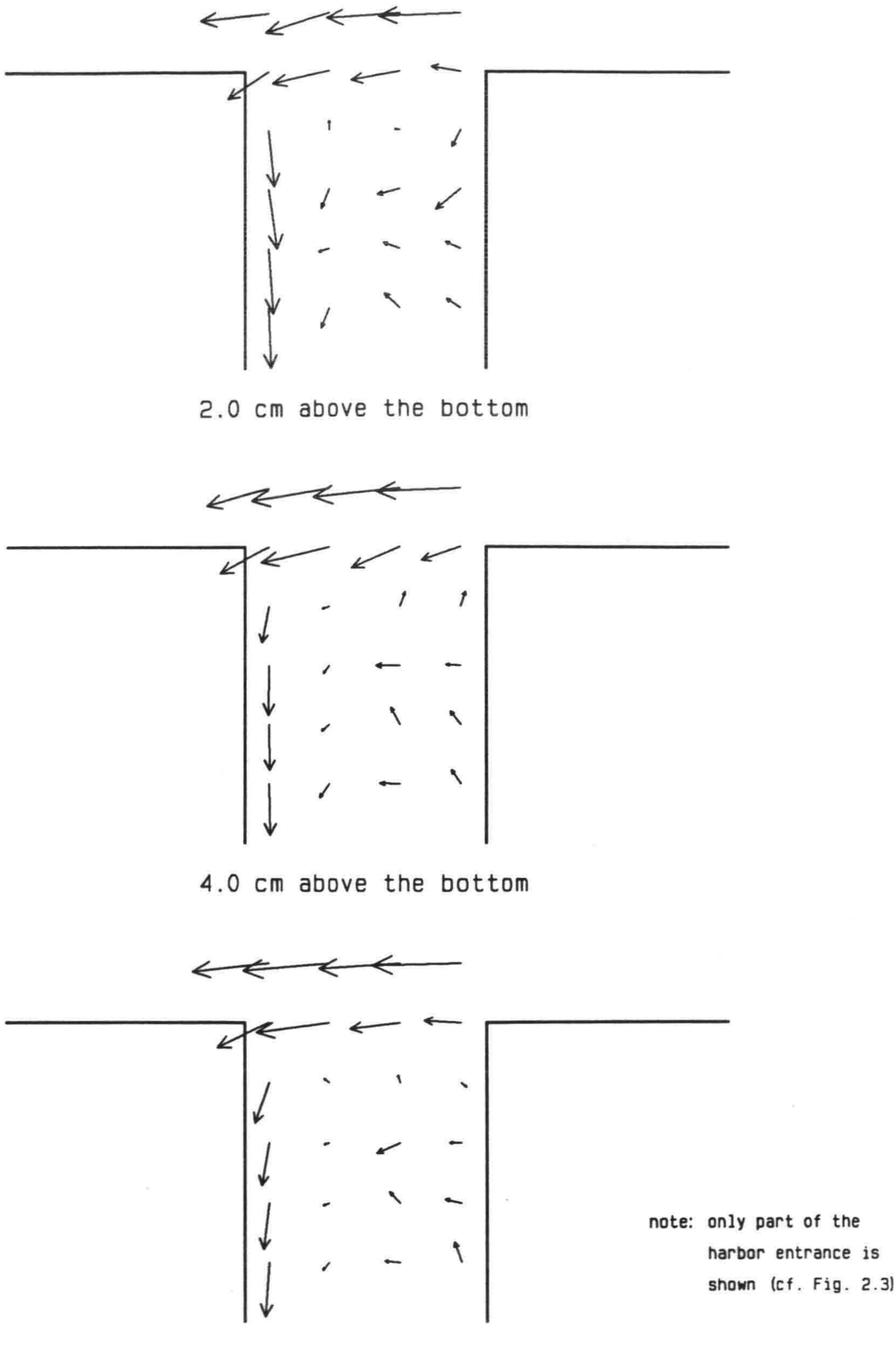

Flow patterns at three levels Experiment 5	TIME = 450 s ⟼ = 0.10 m/s
Delft University of Technology	Fig. 4.20

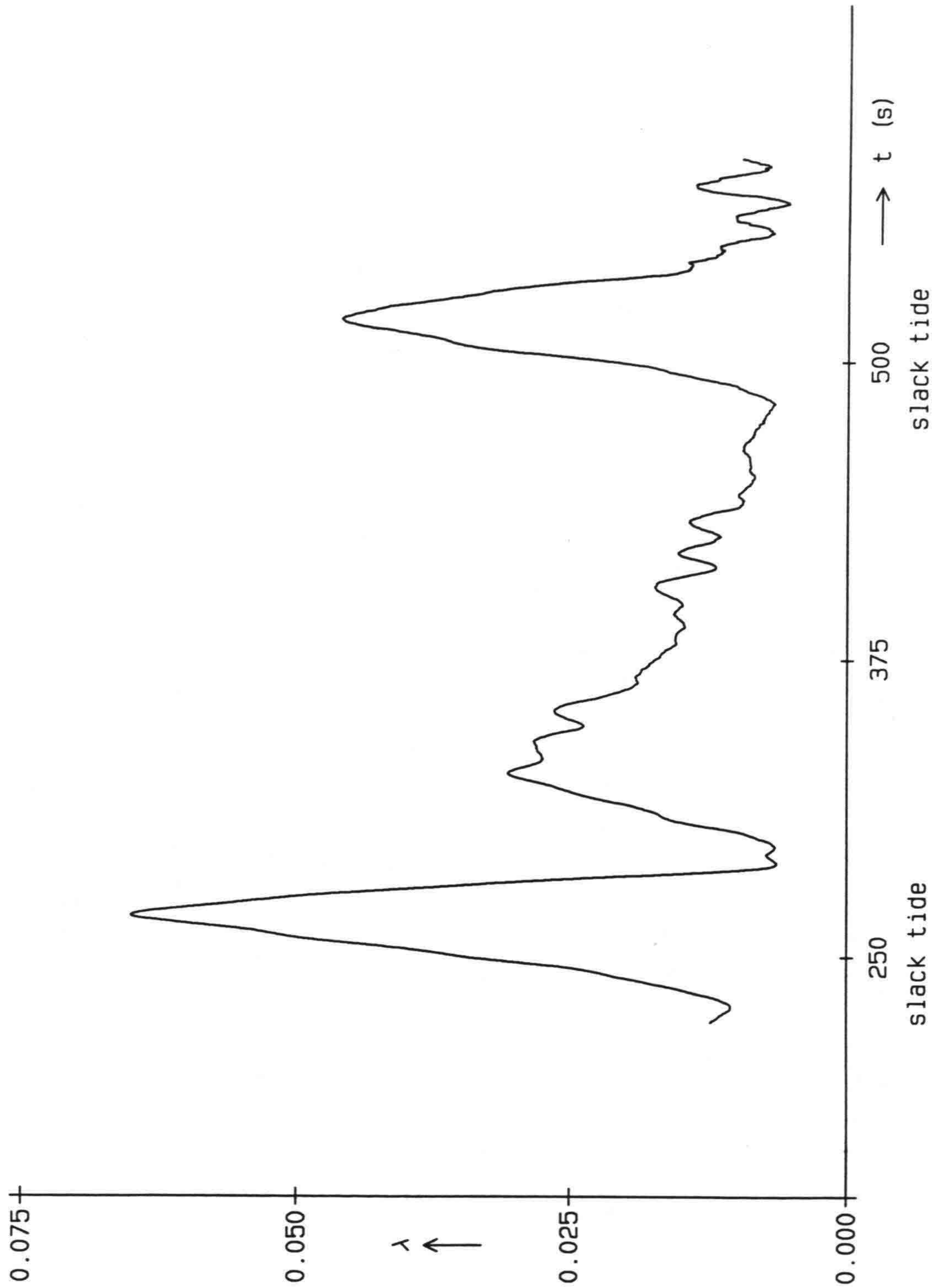

Normalized heat transport through the entrance (Experiment 1B).

Delft University of Technology

Fig. 5.1

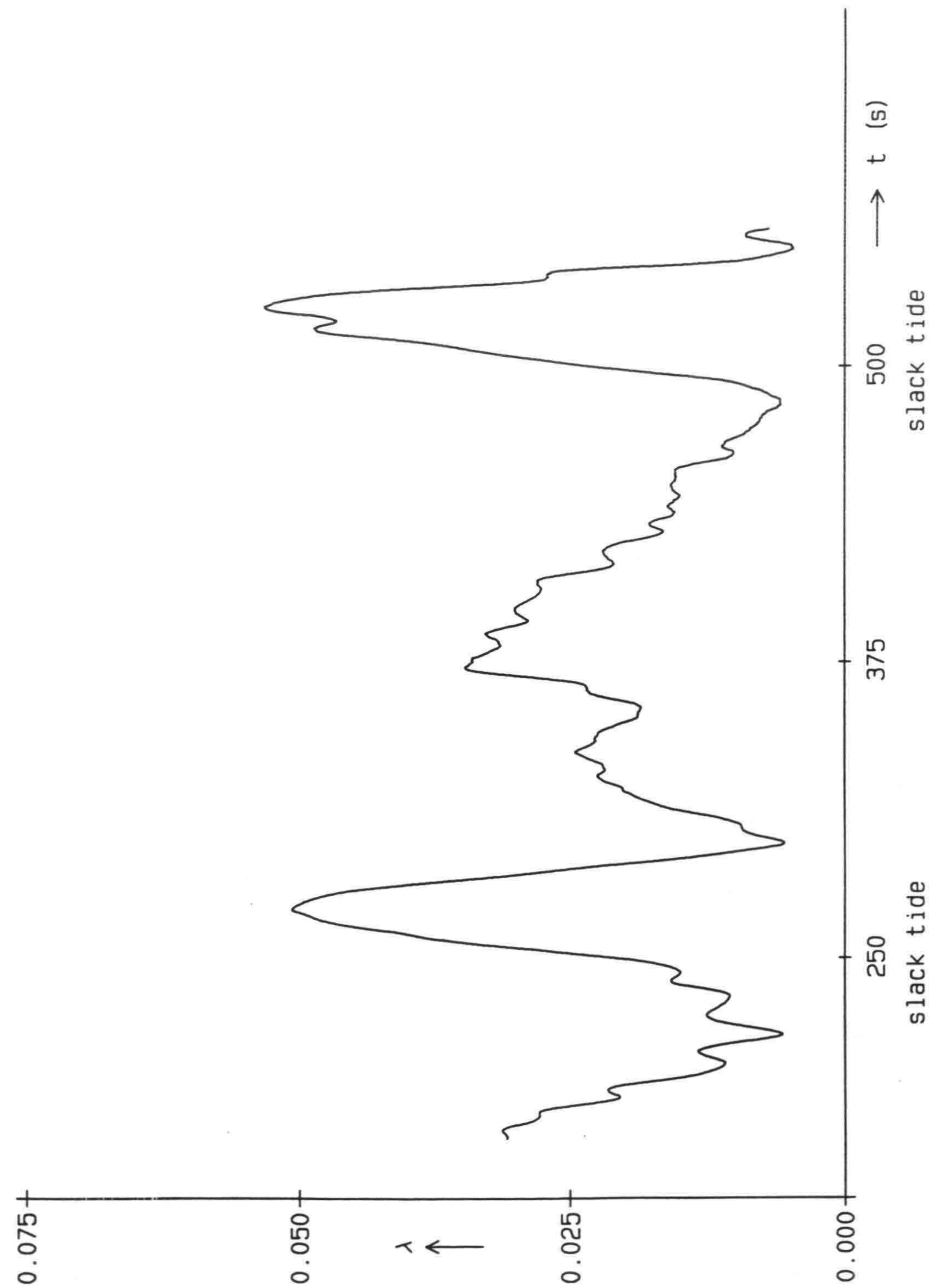

Normalized heat transport through the entrance (Experiment 2B).

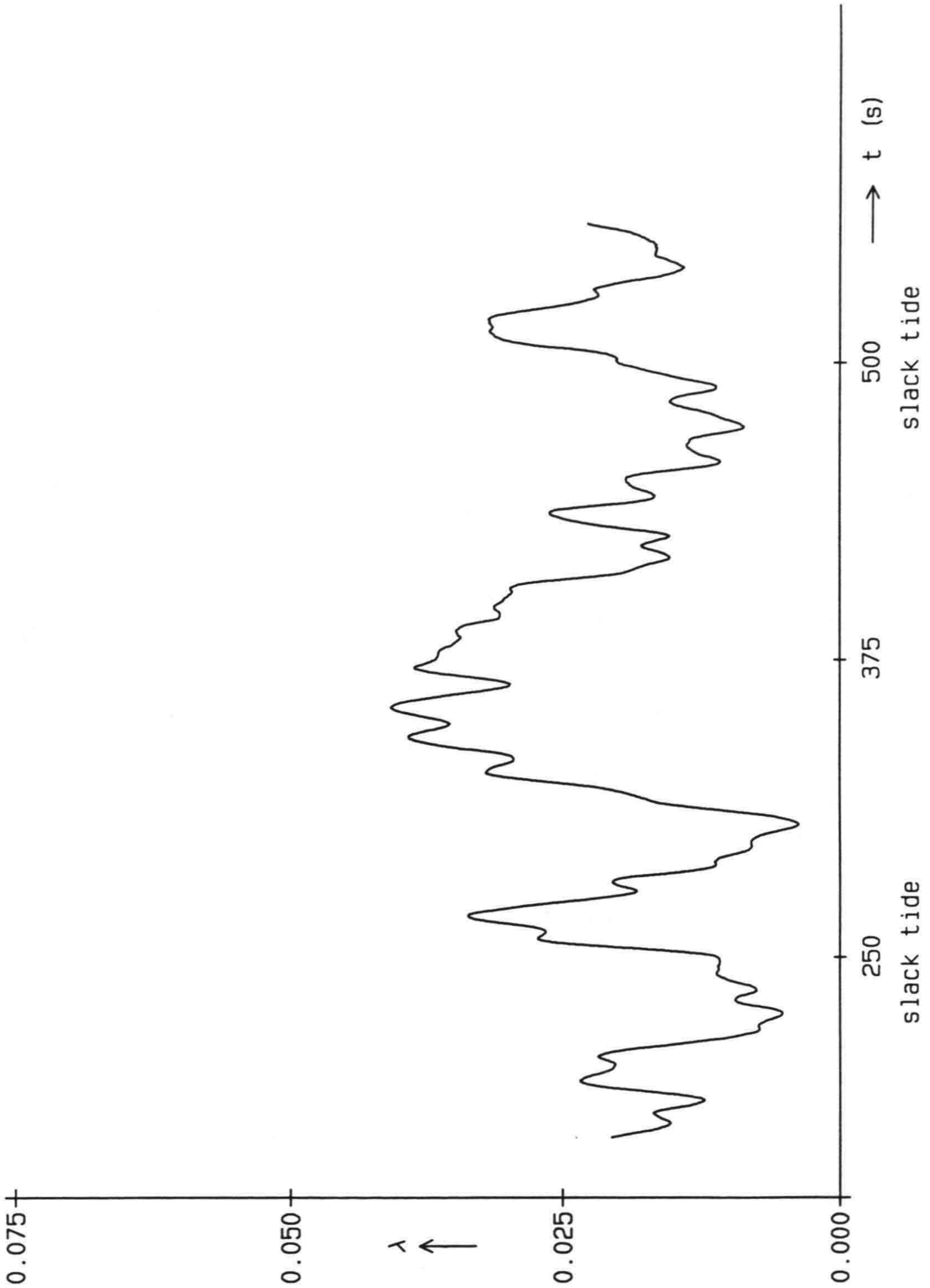

Normalized heat transport through the entrance (Experiment 3).

Delft University of Technology

Fig. 5.3

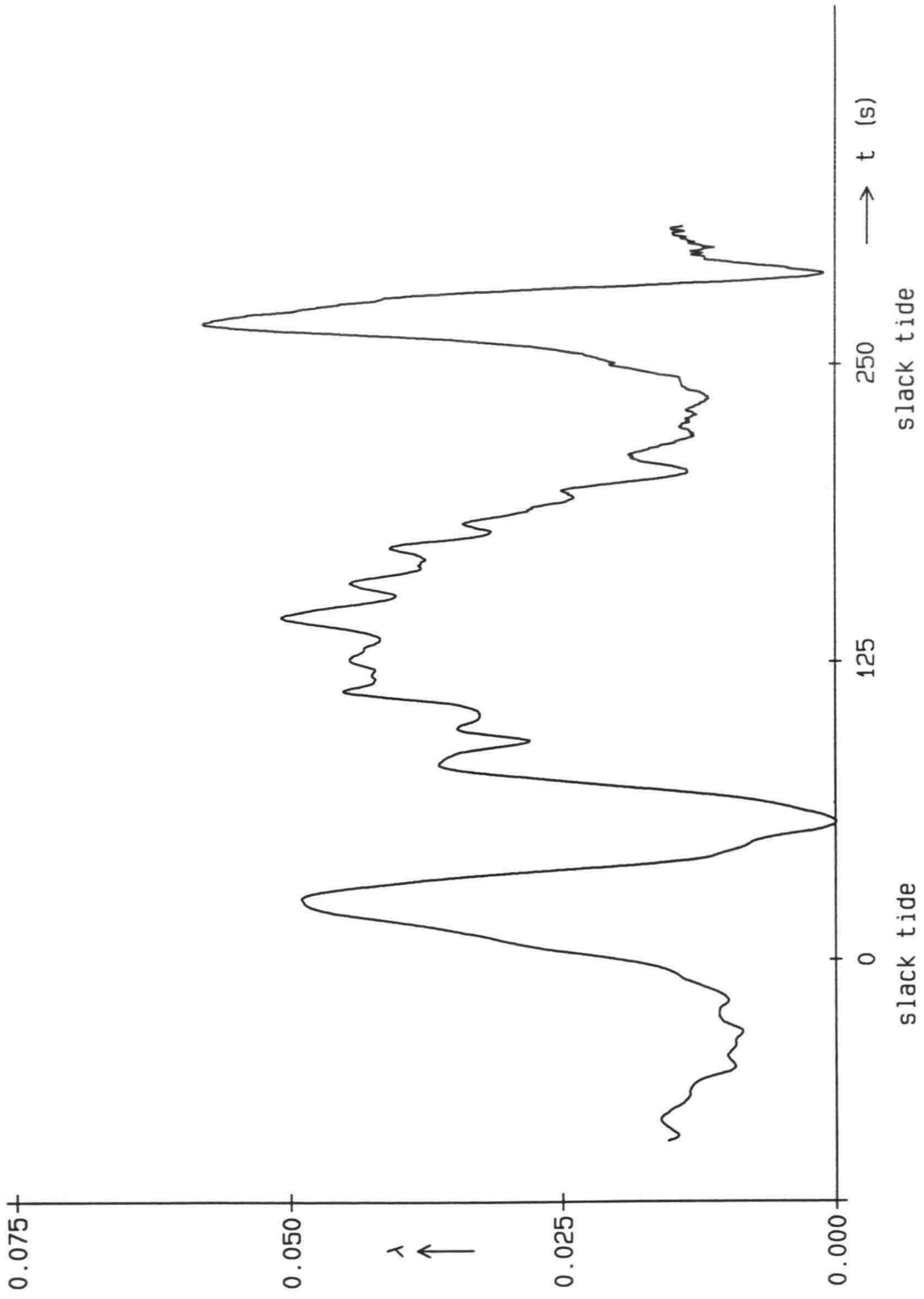

Normalized heat transport through the entrance (Experiment 4).

Delft University of Technology

Fig. 5.4

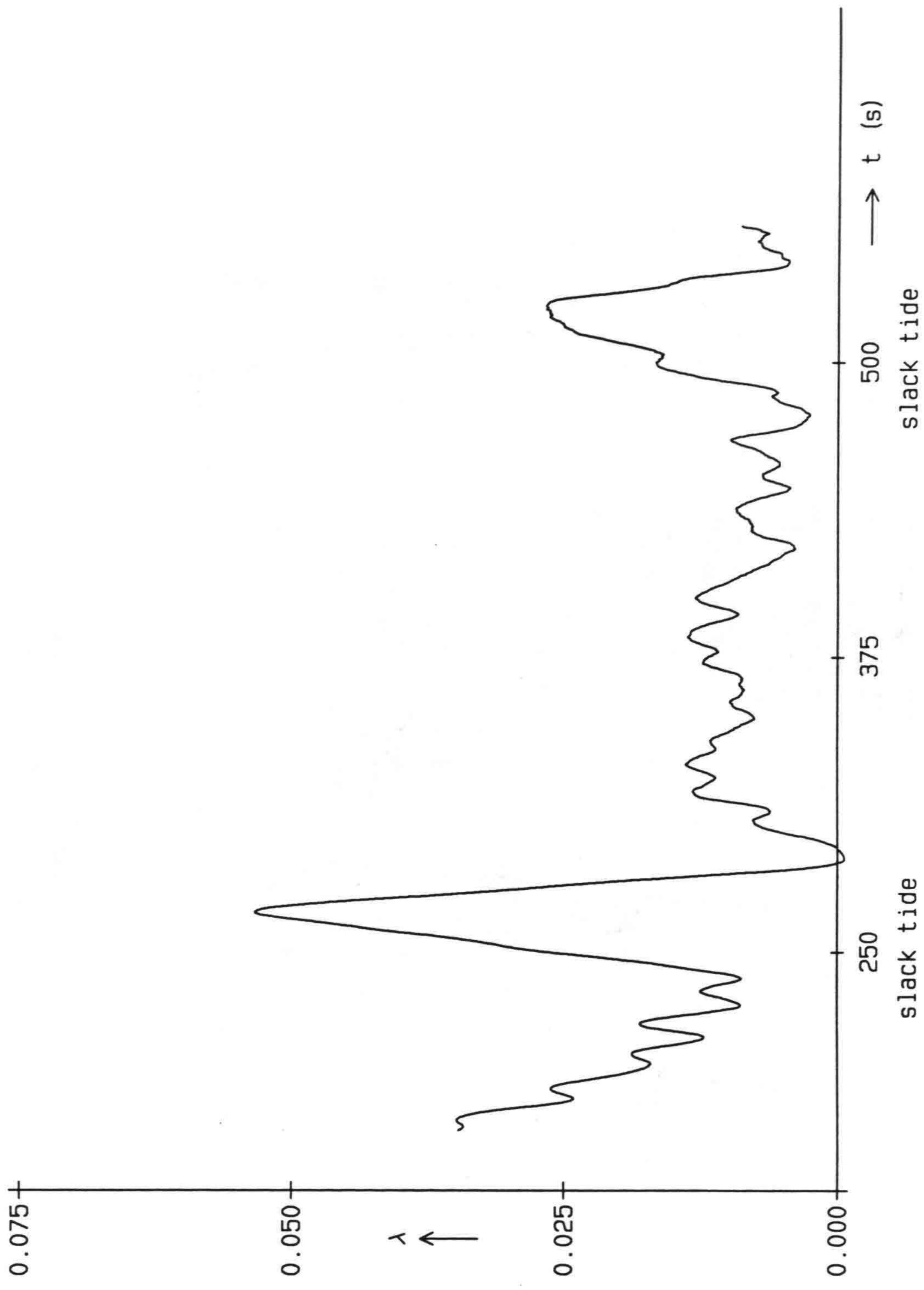

Normalized heat transport through the entrance (Experiment 4).

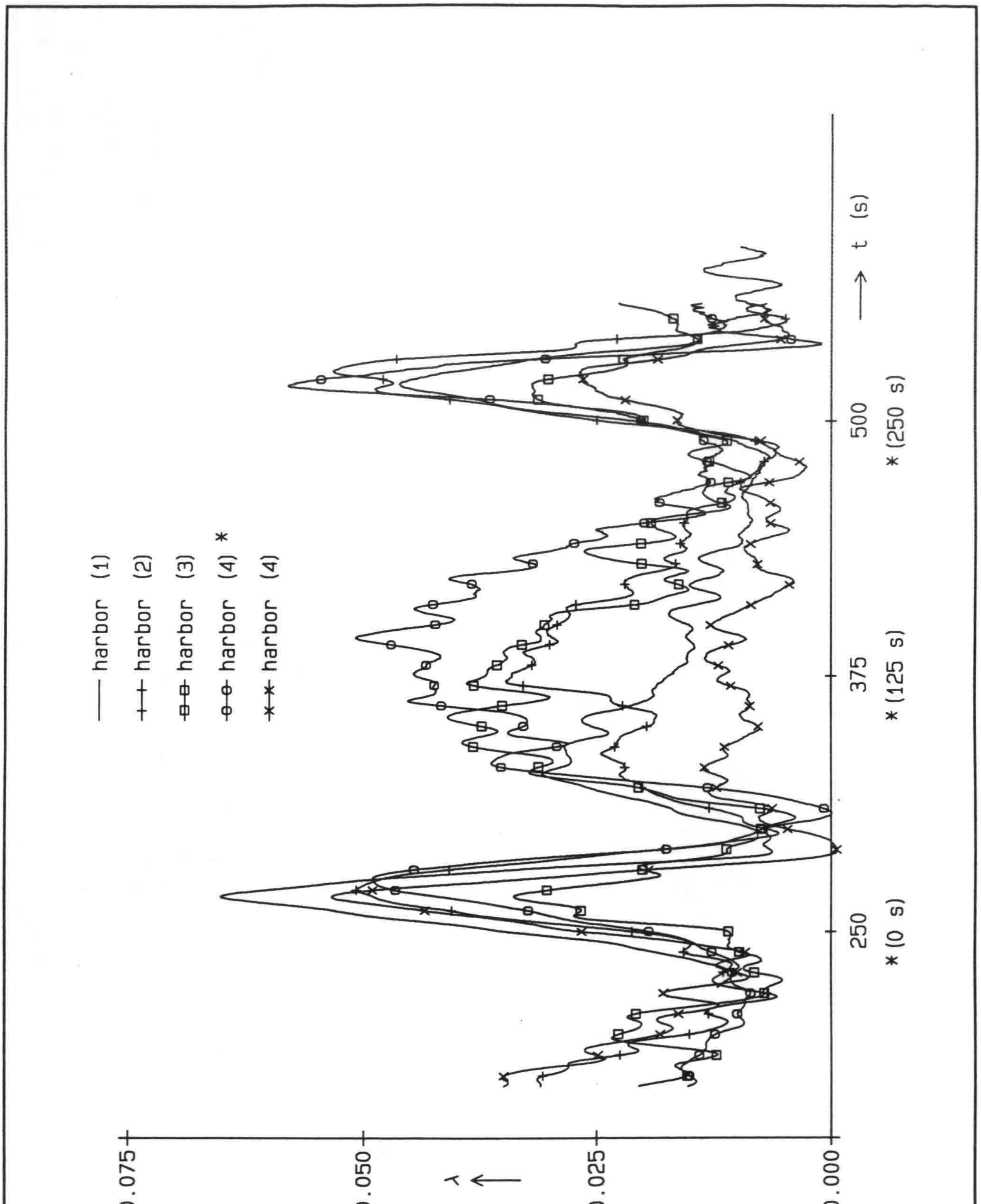

Normalized heat transport through the entrance.

Delft University of Technology

Fig. 5.6

Photos

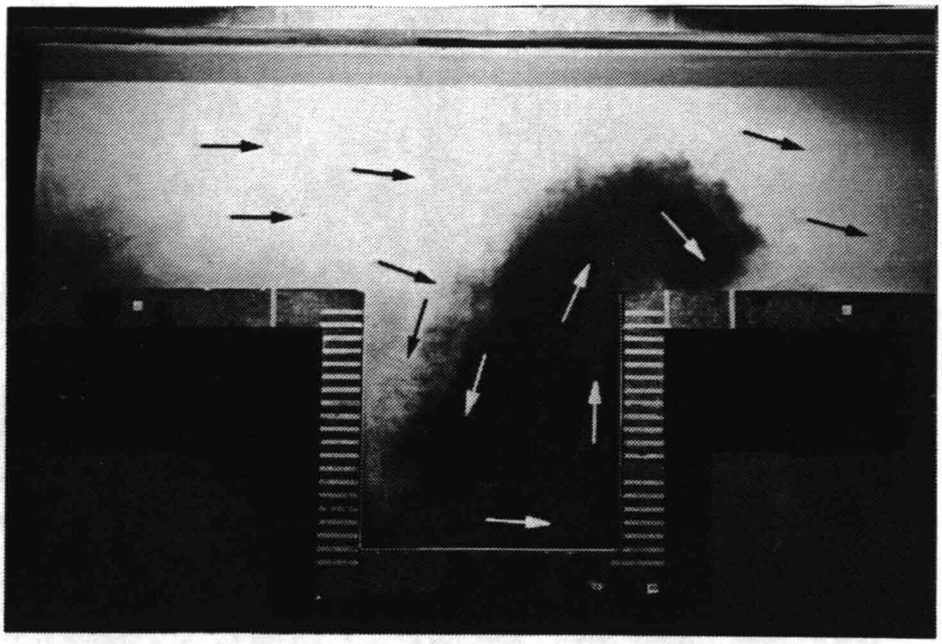

Photo 1 Exchange of dyed water from the harbor and limpid river-water just after slack tide (Experiment 1B).

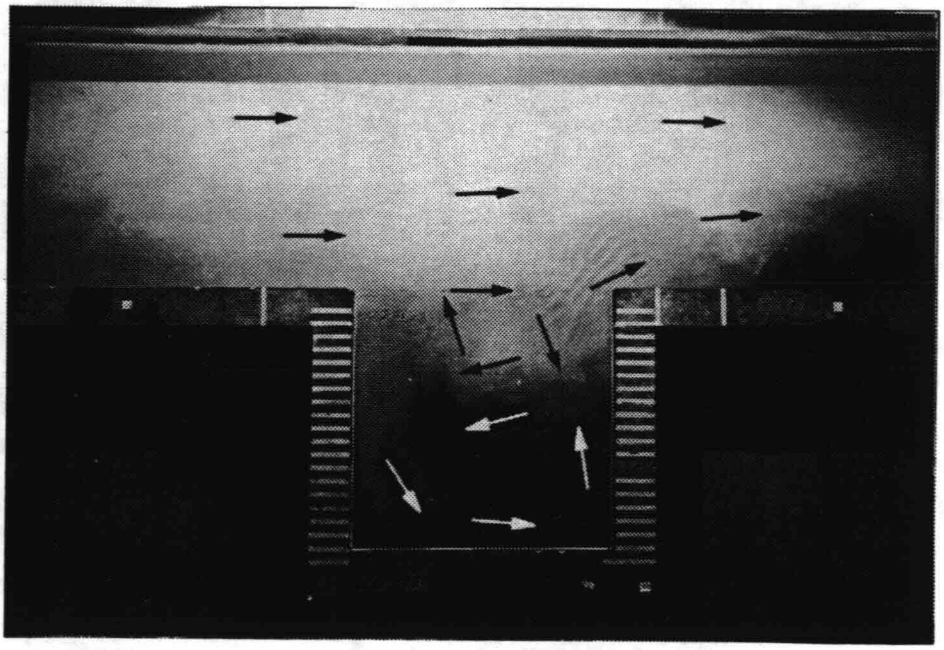

Photo 2 Exchange of dyed water from the harbor and limpid river-water at 50 s after slack tide (Experiment 1B).

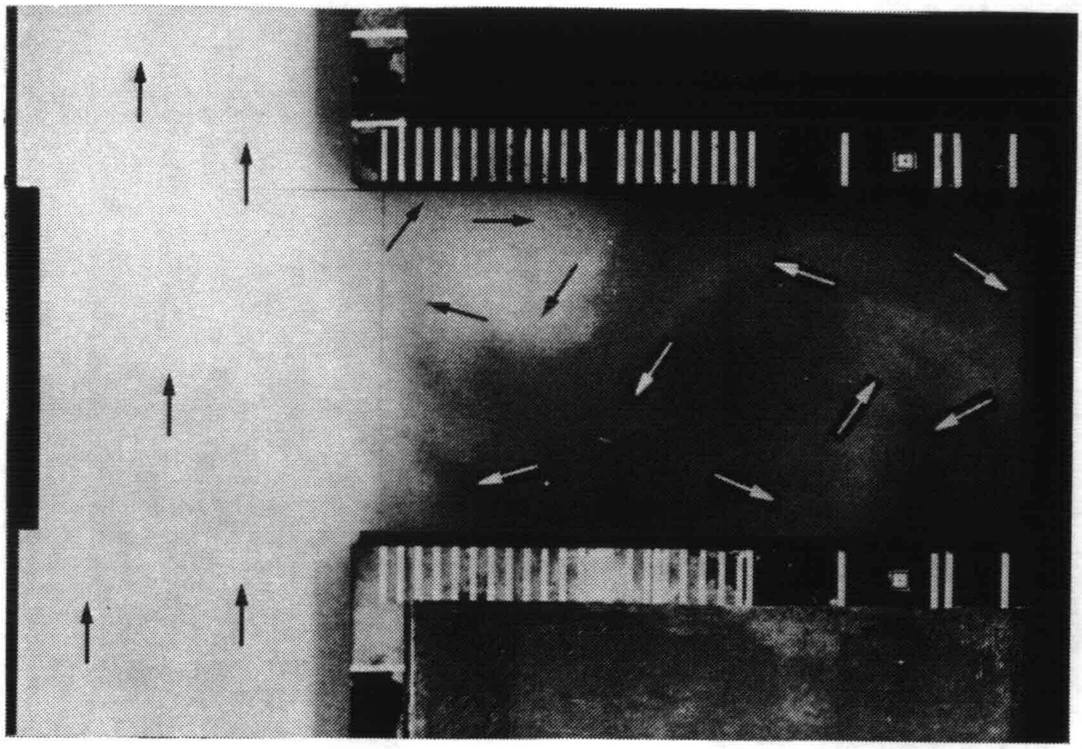

Photo 3 Exchange of dyed water from the harbor and limpid river-water at 50 s after slack tide (Experiment 2B).

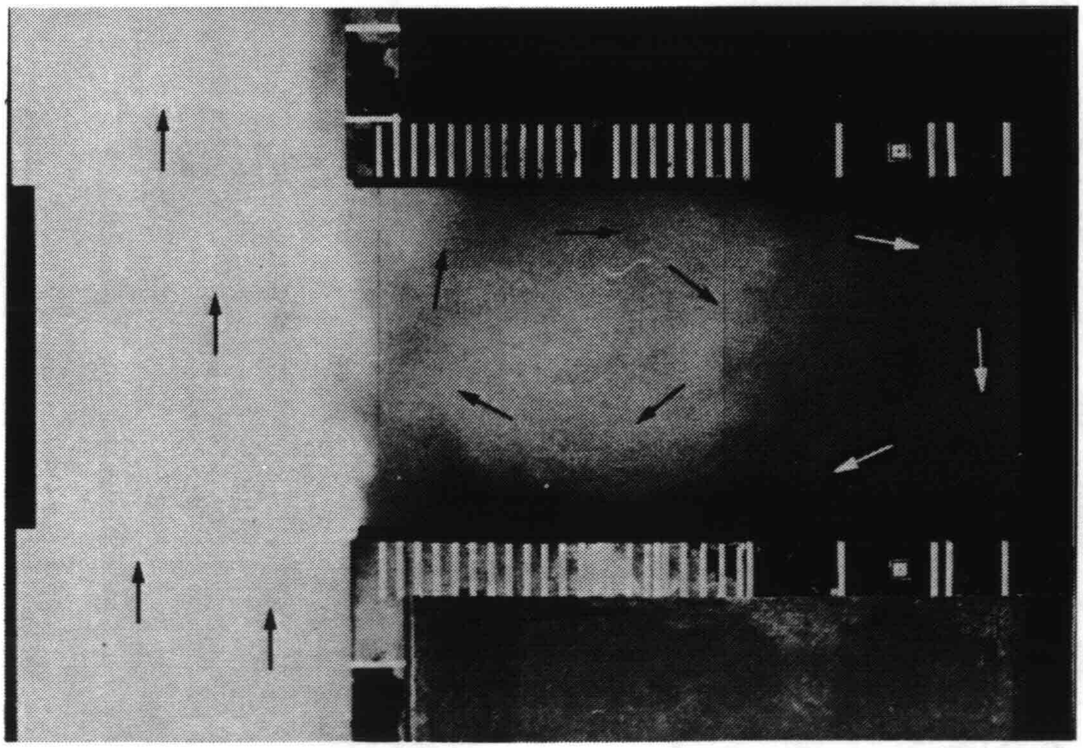

Photo 4 Exchange of dyed water from the harbor and limpid river-water at 90 s after slack tide (Experiment 2B).

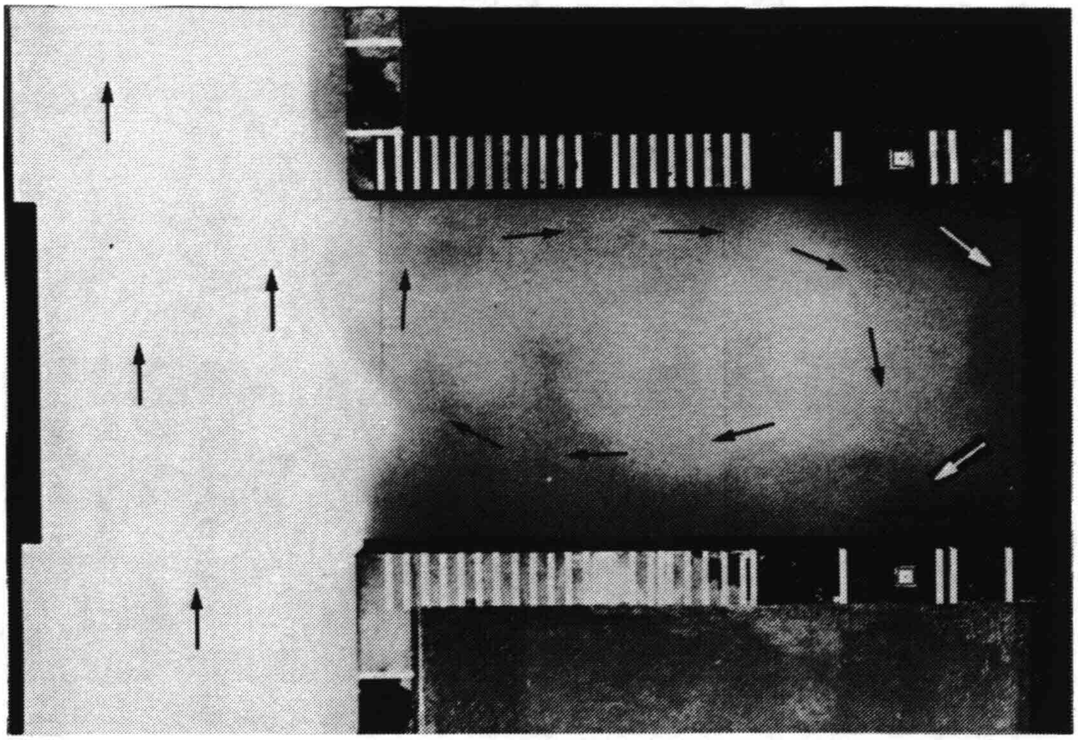

Photo 5 Exchange of dyed water from the harbor and limpid river-water just before maximum current in the river (Experiment 2B).

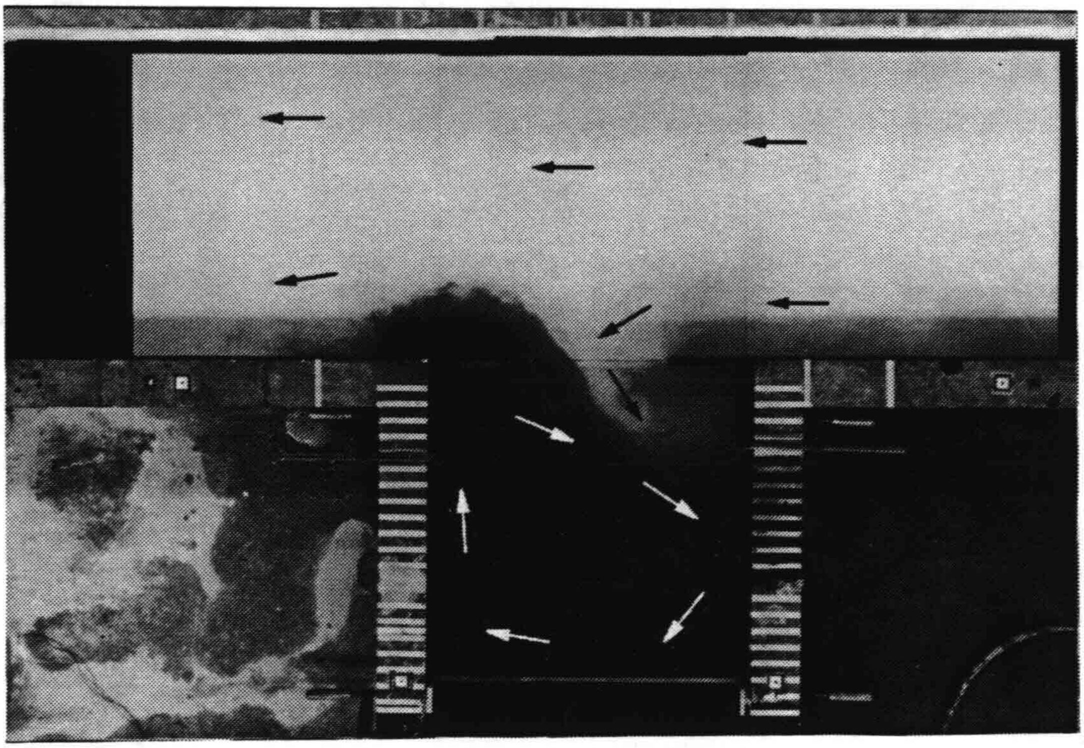

Photo 6 Exchange of dyed water from the harbor and limpid river-water just after slack tide (Experiment 3).

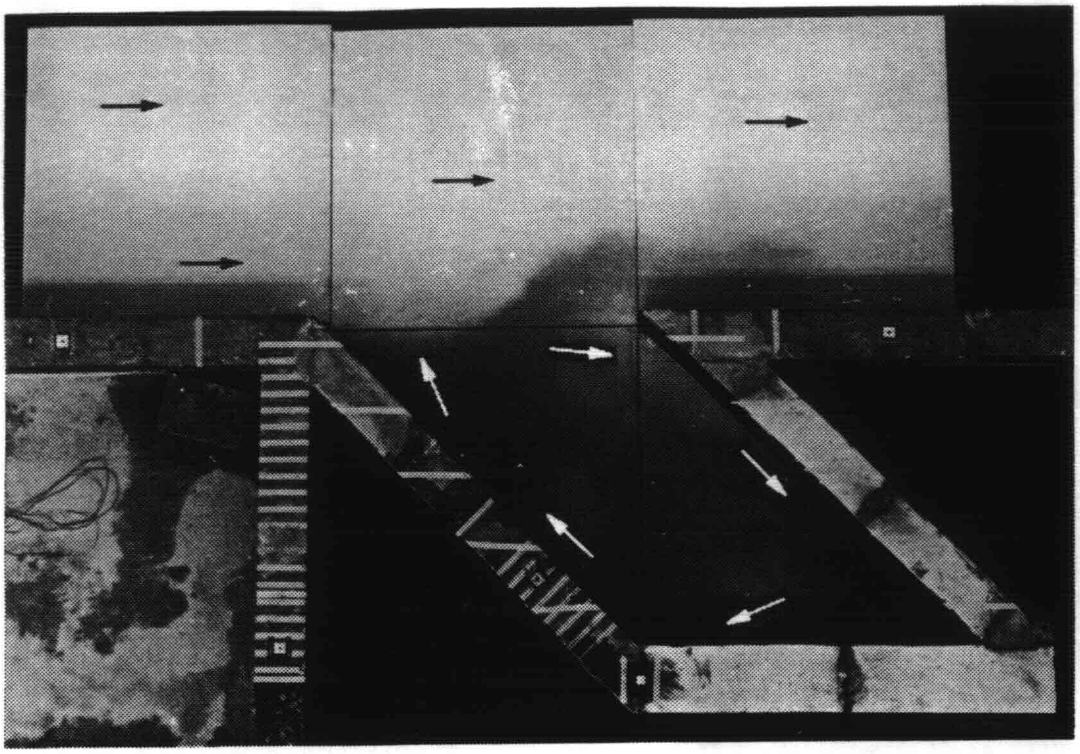

Photo 7 Exchange of dyed water from the harbor and limpid river-water at maximum current in the river (Experiment 4).

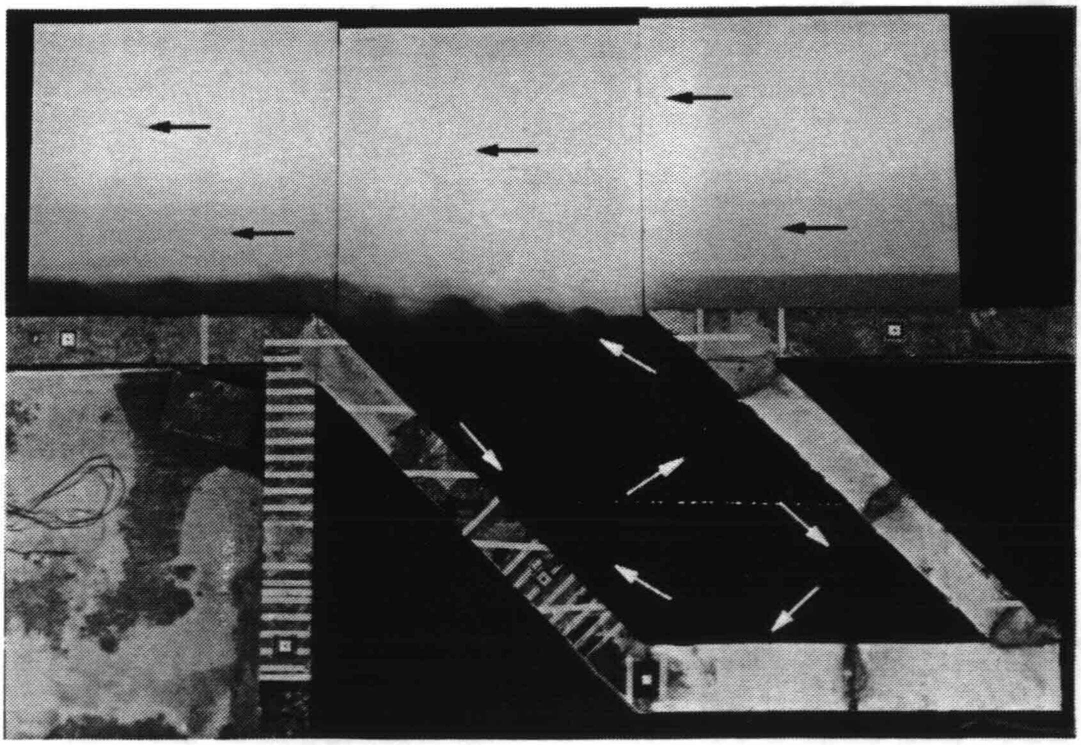

Photo 8 Exchange of dyed water from the harbor and limpid river-water at maximum current in the river (Experiment 4).